SERDP

FINAL REPORT

A Mechanistic Understanding of PFAS in Source Zones: Characterization and Control

Jennifer Field
Oregon State University

Christopher Higgins
Tissa Illangasekare
Colorado School of Mines

Stephanie Park
Jacobs

Phillip de Blanc
GSI Environmental

Konstantinos Kostarelos
University of Houston

Charles Schaefer
CDM Smith

September 2022

SERDP Project ER18-1259

REPORT DOCUMENTATION PAGE

Form Approved
OMB No. 0704-0188

1. REPORT DATE *(DD-MM-YYYY)*	2. REPORT TYPE	3. DATES COVERED *(From - To)*
9/15/2022	SERDP Final Report	8/1/2018 - 8/1/2022

4. TITLE AND SUBTITLE

A Mechanistic Understanding of PFAS in Source Zones: Characterization and Control

5a. CONTRACT NUMBER
18-C-0075

5b. GRANT NUMBER

5c. PROGRAM ELEMENT NUMBER

6. AUTHOR(S)

Jennifer Field: Oregon State University
Christopher Higgins and Tissa Illangasekare: Colorado School of Mines
Stephanie Park: Jacobs
Phillip de Blanc: GSI Environmental
Konstantinos Kostarelos: University of Houston
Charles Schaefer: CDM Smith

5d. PROJECT NUMBER
ER18-1259

5e. TASK NUMBER

5f. WORK UNIT NUMBER

7. PERFORMING ORGANIZATION NAME(S) AND ADDRESS(ES)

Oregon State University
30 Campus Way
Dept. Environmental and Molecular Toxicology
Corvallis, OR 97331

8. PERFORMING ORGANIZATION REPORT NUMBER

ER18-1259

9. SPONSORING/MONITORING AGENCY NAME(S) AND ADDRESS(ES)

Strategic Environmental Research and Development Program (SERDP)
4800 Mark Center Drive, Suite 16F16
Alexandria, VA 22350-3605

10. SPONSOR/MONITOR'S ACRONYM(S)
SERDP

11. SPONSOR/MONITOR'S REPORT NUMBER(S)
ER18-1259

12. DISTRIBUTION/AVAILABILITY STATEMENT

DISTRIBUTION STATEMENT A. Approved for public release: distribution unlimited.

13. SUPPLEMENTARY NOTES

14. ABSTRACT Retention of per- and polyfluoroalkyl substances (PFAS) is reported for soils and sediment associated with firefighter training areas (e.g., source zones) where aqueous film forming foams (AFFFs) were routinely applied during firefighter training over decades. Despite the relative water solubility of PFAS, source zones currently retain PFAS though decades have passed since the last AFFF applications. Retention of PFAS when present in complex AFFF mixtures, including successive AFFF applications, is unknown since most transport studies investigate single PFAS or a simple mixtures at low concentrations. Interactions with AFFF and nonaqueous phase liquids (e.g., Jet Fuel) is unknown but they may form thermodynamically stable phases with distinct characteristics. Discharge of chemically complex AFFFs to unsaturated soils involves PFAS interactions with the air-water interface that are not fully understood. The overall objectives of this project are to 1] identify the key PFAS and soil properties that control PFAS interaction with saturated soils when AFFF is applied at near application strength concentrations, 2] characterize the number and type of thermodynamically-stable phases that form when AFFFs are mixed with jet fuel their impact on PFAS transport, and 3] assess PFAS mobility under unsaturated zone conditions in order to identify the key hydraulic parameters and PFAS properties that control PFAS mobility and retention. Under saturated conditions, PFAS introduced as a complex AFFF were retained by clean sand and a natural C2 soil horizon under dynamic flow conditions, indicating significant adsorption, even when organic carbon and surface charge are negligible. PFAS retention was related to PFAS structure and soil properties though a machine learning-based poly-parameter quantitative structure-parameter linear regression model. PFAS retention by clean sand increases over the first three successive AFFF additions, reaching a saturation limit after four applications. Thus, sorption of PFAS is enhanced by earlier AFFF applications. Viscous Winsor Type II microemulsions (gels) form when AFFFs mix at the pore scale with Jet Fuel, a non-aqueous phase liquid (NAPL), during infiltration. Correlations between air-water partition coefficient (Kia) and chromatographic retention time indicate Kia values can be predicted from chromatographic retention times for a wide range of PFAS. A mass transfer index is required to model the correlation between immobile water and tortuosity as saturation decreases in unsaturated soils and is critical for accounting PFAS interfacial activity in unsaturated soils. Greater retention of PFAS in porous media when compared to studies on single component or simple mixtures underscores the importance of working with actual AFFF at application strength. PFAS transport is dynamic and is nearly independent of soil properties, making PFAS transport difficult to model using conventional models. The presence of viscous microemulsions may complicate PFAS recovery efforts. Future research is aimed at determining if PFAS and NAPL associate as microemulsions or as non-microemulsion mixtures at fire-fighter training sites, which is the first step toward understanding if residual NAPL acts as a sink for PFAS and thus, a potential long-term source of PFAS to groundwater. A Technology Transfer module was created to support management of PFAS source zones using stakeholder site data. Overall, the transport properties of PFAS in porous media comprised of multiple phases (air, NAPL) is significantly more complex than saturated flow. Improved empirical and conceptual models were developed that can be used to assess the transport potential of a wide variety of PFAS in the vadose zone.

15. SUBJECT TERMS PFAS, source zones, Source zone, aqueous film forming foams (AFFF), phase behavior, microemulsion, air-water partition coefficient, sorption, unsaturated transport, modeling, per- and polyfluoroalkyl substances, (PFAS), nonaqueous phase liquid

16. SECURITY CLASSIFICATION OF:			17. LIMITATION OF ABSTRACT	18. NUMBER OF PAGES	19a. NAME OF RESPONSIBLE PERSON
a. REPORT	b. ABSTRACT	c. THIS PAGE			Jennifer Field
UNCLASS	UNCLASS	UNCLASS	UNCLASS	152	19b. TELEPHONE NUMBER *(Include area code)* 541-737-2265

Table of Contents

Table of Figures

Table of Tables

Abbreviations and Acronyms

ADE	Advection-dispersion equation
AFB	Air Force Base
AFFF	Aqueous film forming foam
A_{aw}	Air-water interfacial area
BTC	Breakthrough curves
CEC	Cation exchange capacity
CMC	Critical micelle concentration
Db	Bulk density
FeOX	oxalate extractable iron
foc	Fraction of organic carbon
FTSA	Fluorotelomer sulfonate
FtTAoS	Fluorotelomer thioether amido sulfonate
HDPE	High density polyethylene
HPLC	High performance liquid chromatography
IPWR	Injected pulse width recovery
Jet A	Jet Fuel A
K_{ia}	Air-water partition coefficient
K_d	Soil: water partition coefficient
K_d *app*	Apparent soil:water partition coefficient
K_d *BTC*	Breakthrough curve soil:water partition coefficient
K_f	Freundlich sorption coefficient
K_{oc}	Organic carbon: water partition coefficient
LC-QTOF	Liquid chromatography quadrupole time of flight mass spectrometry
m.e.	Microemulsion
MilSpec	Military specification
MIM	mobile immobile method
M_R	Mass retained
MS	Mass Spectrometry
MTI	Mass transfer index
NaCl	Sodium chloride
NAPL	Non-aqueous phase liquid
OC	Organic carbon
OSU	Oregon State University
ρb	solid phase bulk density
Pe	Peclet number
pKa	Acid dissociation constant
PFAA	Perfluoroalkyl acids
PFAS	Perfluoroalkyl substances

PFBA	Perfluorobutanoate
PFBS	Perfluorobutane sulfonate
PFCA	Perfluorinated carboxylate
PFHpA	Perfluoroheptanoate
PFHpS	Perfluoroheptane sulfonate
PFHxA	Perfluorohexanoate
PFHxS	Perfluorohexane sulfonate
PFOA	Perfluorooctanoate
PFOS	Perfluorooctane sulfonate
PFPeA	Perfluoropentanoate
PFSA	Perfluoroalkyl sulfonate
ppQSPR	Poly-parameter quantitative structure-parameter
QTOF	Quadrupole time of flight
RMSE	Root mean squared error
Rf	Retardation factor
Rt	Retention time
SA_{BET}	Specific surface area
SDBS	Sodium dodecyl benzene sulfonate
SML	Surface microlayer
STW	Synthetic tap water
ΣPFAS	Sum-total PFAS
TDS	Total dissolved solids
TQD	Triple quadrupole mass spectrometer
T-FTIR	Transmission Fourier transform infrared spectroscopy
TSS	Total suspended solids

Acknowledgements

The research described in this final report was supported by the US Department of Defense, through the Strategic Environmental Research and Development program (SERDP). We thank Dr. Dorin Bodgan of AECOM for soil collection from Wurtsmith Air Force Base. Dr. Andrea Leeson and other SERDP staff are acknowledged for their assistance and support.

Sections on Task 2.1 are reprinted with permission from "Viscous Microemulsions of Aqueous Film-Forming Foam (AFFF) and Jet Fuel A Inhibit Infiltration and Subsurface Transport", Konstantinos Kostarelos, Pushpesh Sharma, Emerson Christie, Thomas Wanzek, and Jennifer Field, *Environmental Science & Technology Letters* **2021** *8* (2), 142-147, DOI: 10.1021/acs.estlett.0c00868". Copyright 2021 American Chemical Society.

Sections on Task 2.2 are reprinted with permission from "Role of Mineral-Organic Interactions in PFAS Retention by AFFF-Impacted Soil," by Thomas Wanzek, John F. Stults, Mark G. Johnson, Jennifer A. Field, and Markus Kleber, *Environmental Science & Technology* **20123** DOI: 10.1021/acs.est.2c08806. Copyright 2023 American Chemical Society.

Sections on Task 3.1 are reprinted with permission from "Uptake of Poly- and Perfluoroalkyl Substances at the Air–Water Interface," by Charles E. Schaefer, Veronika Culina, Dung Nguyen, and Jennifer Field, *Environmental Science & Technology* **2019** *53* (21), 12442-12448 DOI: 10.1021/acs.est.9b04008. Copyright 2019 American Chemical Society.

Sections on Task 3.2 and Task 3.3 are reprinted with permission from:

- "Estimation of Transport Parameters of Perfluoroalkyl Acids (PFAAs) in Unsaturated Porous Media: Critical Experimental and Modeling Improvements" by John F. Stults, Youn Jeong Choi, Charles E. Schaefer, Tissa H. Illangasekare, and Christopher P. Higgins, *Environmental Science & Technology* **2022** *56* (12), 7963-7975, DOI: 10.1021/acs.est.2c00819. Copyright 2022 American Chemical Society.
- "The Mass Transfer Index (MTI): A Semi-Empirical Approach for Quantifying Transport of Solutes in Variably Saturated Porous Media" by John Stultz, Tissa Illangasakare and Christopher P. Higgins. 2021. *Journal of Contaminant Hydrology, 242,* DOI: 10.1016/j.jconhyd.2021.103842. Copyright 2021 Elsevier.
- *Predicting* Concentration and Electrolyte Dependent Air-Water Interfacial Partitioning Parameters of PFASs Using Quantitative Structural Property Relationships (QSPRs) by John F. Stults, Y.J., Choi, C. Rockwell, C. Schaefer, D. Nguyen, D. Knappe, *T. Illangasekare, Christopher Higgins, C. Accepted.* Environ. Sci. Technol. DOI: not yet assigned.

Additional material, not yet published, will be submitted for publication to journals during the ix month embargo placed on this Final Report. At that point, the journals will hold the copyright on the remaining submitted material.

Abstract

Introduction. Retention of per- and polyfluoroalkyl substances (PFAS) is reported for soils and sediment associated with firefighter training areas (e.g., source zones) where aqueous film forming foams (AFFFs) were routinely applied during firefighter training over decades. Despite the relative water solubility of PFAS, source zones currently retain PFAS though decades have passed since the last AFFF applications. Retention of PFAS when present in complex AFFF mixtures, including successive AFFF applications, is unknown since most transport studies investigate single PFAS or a simple mixtures at low concentrations. Interactions with AFFF and nonaqueous phase liquids (e.g., Jet Fuel) is unknown, yet may form thermodynamically stable phases with distinct characteristics. Discharge of chemically complex AFFFs to unsaturated soils involves PFAS interactions with the air-water interface that are not fully understood.
Objectives. The overall objectives of this project are to 1] identify the key PFAS and soil properties that control PFAS interaction with saturated soils when AFFF is applied at near application strength concentrations, 2] characterize the number and type of thermodynamically-stable phases that form when AFFFs are mixed with jet fuel their impact on PFAS transport, and 3] assess PFAS mobility under unsaturated zone conditions in order to identify the key hydraulic parameters and PFAS properties that control PFAS mobility and retention.
Results. Under saturated conditions, PFAS introduced as a complex AFFF were retained by clean sand and a natural C2 soil horizon under dynamic flow conditions, indicating significant adsorption, even when organic carbon and surface charge are negligible. PFAS retention was related to PFAS structure and soil properties though a machine learning-based poly-parameter quantitative structure-parameter linear regression model. PFAS retention by clean sand increases over the first three successive AFFF additions, reaching a saturation limit after four applications. Thus, sorption of PFAS is enhanced by earlier AFFF applications. Viscous Winsor Type II microemulsions (gels) form when AFFFs mix at the pore scale with Jet Fuel, a non-aqueous phase liquid (NAPL), during infiltration. Under unsaturated conditions, sorption of PFAS at environmentally relevant concentrations at the air-water interface is best modeled by Freundlich models. Correlations between air-water partition coefficient (K_{ia}) and chromatographic retention time indicate K_{ia} values can be predicted from chromatographic retention times for a wide range of PFAS. A mass transfer index is required to model the correlation between immobile water and tortuosity as saturation decreases in unsaturated soils and is critical for accounting PFAS interfacial activity in unsaturated soils.
Benefits. Greater retention of PFAS in porous media when compared to studies on single component or simple mixtures underscores the importance of working with actual AFFF at application strength. PFAS transport is dynamic and is nearly independent of soil properties, making PFAS transport difficult to model using conventional models. The presence of viscous microemulsions may complicate PFAS recovery efforts. Future research is aimed at determining if PFAS and NAPL associate as microemulsions or as non-microemulsion mixtures at fire-fighter training sites, which is the first step toward understanding if residual NAPL acts as a sink for PFAS and thus, a potential long-term source of PFAS to groundwater. A Technology Transfer module was created to support management of PFAS source zones using stakeholder site data. Overall, the transport properties of PFAS in porous media comprised of multiple phases (air, NAPL) is significantly more complex than saturated flow. Improved empirical and conceptual models were developed that can be used to assess the transport potential of a wide variety of PFAS in the vadose zone.

Keywords

Source zone, aqueous film forming foams (AFFF), phase behavior, microemulsion, air-water partition coefficient, sorption, unsaturated transport, modeling, per- and polyfluoroalkyl substances, (PFAS), nonaqueous phase liquid

Executive Summary

Introduction

The overall goal of this project was to identify processes governing the retention of per- and polyfluoroalkyl substances (PFAS) in soils and sediments impacted by repeated AFFF applications during firefighter training with aqueous film forming foams (AFFF). Prior to the project, relatively little was known about PFAS transport and attenuation in source-zone soils and sediments, and why source zones act as long-term sources of PFAS. Beyond understanding the transport of anionic PFAS including perfluoroalkyl sulfonates (PFSA) and perfluoroalkyl carboxylates (PFCA), comparatively little was known about the retention and transport of other anionic, zwitterionic, and cationic PFAS. Understanding the mechanisms of PFAS retention associated the historical discharge scenarios of AFFF was needed to understand and predict PFAS release from source zones.

AFFFs are complex mixtures of PFAS,[1, 2] hydrocarbon surfactants,[3, 4] and solvents (e.g., butyl carbitol).[5, 6] Repeated use of AFFF during firefighter training, equipment 'capacity' testing, leaks and other accidental releases, along with emergency responses to aircraft crashes has led to significant AFFF releases at US military sites.[7] Limited data on the composition of AFFF indicates they contain high levels (g/L) of PFAS, of which perfluorooctane sulfonate (PFOS) and perfluorooctanoate (PFOA) are the two most well-known. Prior to this project, field data for primarily PFOS and PFOA indicated high concentrations (µg/L to mg/L) remain in groundwater and soils and sediments at fire-fighter training areas even though it can be two decades since the last AFFF application.[2, 8, 9] During execution of the present project, the US EPA reduced the Health Advisory values for PFOS and PFOA in water from 70 ng/L (70,000 ppt)[10] to 0.02 and 0.004 ppt, respectively.[11]

Earlier laboratory data indicated that zwitterionic and cationic PFAS are strongly sorbed to soils.[12-14] Since these earlier studies, an ESTCP-funded field project reported that zwitterionic and cationic PFAS have significantly lower concentrations in groundwater while more mass is retained in source-zone soils and sediments.[15-17] Given the persistence of a range of PFAS in source-zone soils and sediments, it is important to understand the potentially complex interactions that occured when PFAS infiltrated into unsaturated soils of the vadose zone and moved downward toward the saturated aquifer sediments.

A number of studies indicate good agreement between anionic PFAS sorption and soil/sediment organic matter content,[18-20] while a more recent review documents poor correlations.[21] In particular, there is a lack of correlation for the zwitterionic and cationic PFAS, which is consistent with reports for zwitterionic (nonfluorinated) pharmaceuticals.[22-24] Importantly, the soil-water partition coefficients (K_d) values for cationic and zwitterionic PFAS are 5 to 50 times greater than those of anionic PFAS of corresponding chain length. Although a single measure of organic matter

content is desirable due to its simplicity and low cost for the measurements, it does not appear sufficient to predict the transport for a wide range of PFAS. Differences in the chemical character of organic matter may result in different strengths of interactions with anionic, cationic, and zwitterionic PFAS. Because the sorption of zwitterionic/cationic PFAS could not be predicted from cation exchange capacity (CEC),[12] it is likely that a more complex set of mechanisms control their transport. We hypothesized that the key parameters that control PFAS sorption in source zones will be organic matter type and quantity, the amount and type of surface charge on mineral phases, pH, and major electrolyte composition.

Prior to the onset of this project, few studies focusing on sorption conducted PFAS transport experiments with intact AFFF, at levels representing AFFF application strengths (3 or 6% solution in water v/v), or upon multiple additions of AFFF. The impacts of the complex chemical composition of AFFF and the high (g/L) concentrations of PFAS and other organics on PFAS behavior during infiltration and transport was unknown. At AFFF application strengths, AFFF is above the mixture's critical micelle concentration (CMC), such that hemi-micelles and micelles containing PFAS could undergo sorption[25] or form layers that act like liquid crystals or gels. Viscous gels block soil pores, thus changing flow characteristics of porous media. We hypothesized that PFAS retention when applied to soil horizons as solutions of near application strength AFFF will result in fundamentally different PFAS retention when compared to experiments conducted with simple solutions at low concentration. Given these data gaps, Task 1 was to quantify changes in PFAS retention in saturated column experiments for four soil horizons that received a single application of AFFF diluted to below its CMC.

Releases of AFFF occurred both in the presence and absence of fuels since firefighters trained explicitly to put out fires with AFFF, but also tested equipment that did not involve fuels. Free-phase fuels form nonaqueous phase liquids (NAPL). However, no information was available on the phase behavior of AFFF and NAPL when mixed. Microemulsions are thermodynamically stable mixtures that incorporate both NAPL and water.[26, 27] The Winsor system was developed to describe "oil-in-water" microemulsions (Winsor Type I), "water-in-oil" microemulsions (Winsor Type II), and microemulsions that contain both oil and water (Winsor Type III). However, no information is available on the number and type of thermodynamically stable phases that form when AFFF and fuels mixed, nor on how microemulsions impact PFAS transport. We hypothesized that PFAS transport through soils/sediments is fundamentally different when AFFF is mixed with NAPL. Given these data gaps, Task 2.1 was designed to characterize the number and type of thermodynamically stable phases that form when AFFFs are mixed with jet fuel their impact on PFAS transport.

To date, no experiments have been performed to understand the impacts of multiple, successive additions of AFFF have on PFAS transport and retention. Given the historical practice of repeated AFFF applications, PFAS likely entered increasingly altered soils, potentially characterized by layers of pre-existing PFAS and other AFFF components. We hypothesized that repeated

applications of AFFF will change the retention of PFAS with successive additions. Given these data gaps, experiments were designed for Task 2 to quantify changes in PFAS retention for a sand column and a C2 horizon column that each received four successive applications of application-strength AFFF.

In water-saturated soils, the mobility of PFAS is controlled by advection, dispersion and retardation, where the latter is thought to result primarily from sorption. In the partially saturated soils of the vadose zone, factors that contribute to both mobility and retardation are much more complex. In the vadose zone, water saturation varies as a function of the capillary pressure, and advection and dispersion depend on both spatially and temporally varying water saturation. The air-water interfacial area generally decreases upon re-wetting. PFAS sorbed at the air-water interface may lead to (transient) immobilization of PFAS in the vadose zone.[28-31] However, as PFAS may reduce the air-water interfacial tension due to sorption at the air-water interface (as predicted by the Gibbs Adsorption Equation), this could also lead to an altered pressure-saturation relationship and faster infiltration through the vadose zone and thus greater transport in underlying saturated groundwater. Once the pressure-saturation-area relationship is determined under ambient (no PFAS) conditions and combined with knowledge of how PFAS sorb at the air-water interface (via independent methods like the pendant drop method), one can estimate the mass of PFAS retained at a given water content. In addition, one can estimate the PFAS mass released during an infiltration event as the air-water interface diminishes. We hypothesized that the air-water interfaces present in the pores of vadose zone soils act as preferred sorption sites for PFAS, and that retardation of PFAS at the air-water interface and subsequent release during wetting are key parameters for understanding PFAS transport in source zones.

Hypotheses

1. We hypothesized that PFAS retention when applied to soil horizons as solution of near application strength AFFF will result in fundamentally different PFAS retention of PFAS when compared to experiments conducted with simple solutions at low concentration (Task 1).

2. We hypothesized that PFAS transport through soils/sediments is fundamentally different when AFFF is mixed with NAPL and upon successive AFFF applications (Task 2).

3. We hypothesized that PFAS sorption at the air-water interface significantly impacts the phase partitioning and mobility of PFAS under vadose zone conditions (Task 2 and 3).

Objectives

The overall objectives of this project were to 1] identify the key PFAS and soil properties that control PFAS interaction with saturated soils when AFFF is applied at near application strength concentrations, 2] characterize the number and type of thermodynamically-stable phases that form

when AFFFs are mixed with jet fuel their impact on PFAS transport, 3] assess PFAS mobility under unsaturated zone conditions in order to identify the key hydraulic parameters and PFAS properties that control PFAS mobility and retention.

Technical Approach

Task 1.1 Detailed Soil and AFFF Characterization

Pristine soil was collected from Oscoda-Wurtsmith AFB, immediately adjacent from several known PFAS source zones. The mineral phase and organic matter phase were interrogated using a suite of analytical techniques in an effort to determine any and all potential PFAS retention mechanisms. Basic soil data was collected that included: total organic matter content, pH, soil particle size classes present, and ion exchange capacity (CEC). The PFAS composition of the 3M AFFF used in all experiments related to this SERDP project was determined and found to be in good agreement with the composition reported by Hao et al for the same 3M AFFF.[32] The CMC of the 3M AFFF was measured to be 60 mg/L using the pendant drop method. When AFFF was diluted to the prescribed 3 % (v/v) application rate with synthetic tap water, the 3M AFFF was well above its CMC.

Task 1.2 Saturated Soil Column Experiments

Individual soil horizons were dry packed into columns following a packing procedure detailed elsewhere generating four columns, one for each soil horizon. The packed bulk density was determined and to ensure that no PFAS were sorbed to system components, the system was flushed with methanol and no PFAS were detected in the effluent. Non-reactive tracer experiments were performed on each column to calculate residence time, effective porosity, and effective pore volume. After the no-reactive tracer experiment and prior to the start of the AFFF experiment. Fluids were delivered using an HPLC pump and effluent fractions were collected for PFAS analysis by liquid chromatography quadrupole time of flight mass spectrometry. Effluent samples were analyzed for PFAS that matched the list presented in Hao et al. for the same AFFF.[32] Soil partitioning coefficients (K_d) were calculated in each of the soil columns for the PFAS species that broke through and using two different methods: 1] using the final concentration of PFAS in the effluent divided by the concertation on the soil and 2] an equilibrium-based model fit to the individual breakthrough curves. Partitioning values from the two methods were then converted to total PFAS mass retained by multiplying with the known mass of soil in each column. To describe the PFAS mass retained, a machine learning-based poly-parameter quantitative structure-parameter (ppQSPR) linear regression model was developed. This modeling approach provided a tool to quantitatively measure the combination and relative contribution of PFAS physicochemical properties and soil properties as they related to PFAS mass retained in each soil column.

Task 2.1 Phase Behavior

Phase behavior tests were conducted using the well characterized AFFF (AFFF-1). Five additional AFFFs were evaluated including three older AFFFs with known PFAS content a newer AFFF on the current MilSpec Qualified Products List a fluorine-free AFFF. Synthetic tap water was used in experiments since potable water is used on bases for fire-fighting training and to fill emergency trucks. Jet A was purchased from municipal airport. Salinity scans were conducted Jet A, and 3% v/v AFFF-1 over a range of salinities and water-oil ratios, and AFFF concentrations. Limited phase behavior tests were conducted with the five additional AFFFs. The viscosity of the 3% AFFF-1, the Jet A, and a microemulsion generated by mixing AFFF-1 and Jet A at a 1:1 water-oil ratio were measured. Rheological measurements were performed using TA Instruments DHR-2, double-gap concentric cylinder cup at 20˚C.

Task 2.2 Saturated Column (1D flow) experiments

Four flow experiments were conducted in columns to explore the AFFF/jet fuel and microemulsion transport properties. The control case **(A)** was conducted first, using only clean, quartz sand (OK-75) where four successive applications of AFFF were used to study the potential adsorption onto relatively inert media. The successive addition experiments were also conducted with the C2 horizon soil obtained from Wurtsmith AFB. Both cases were conducted without NAPL present. Column tests were also conducted using the OK-75 sand with a single AFFF application; however, the column contained residual saturation of Jet A. Both constant flow and constant pressure expeiments were performed. Effluent was collected using a fraction collector and PFAS were measured by LC-QTOF or LC-MS/MS.

Task 3.1 PFAS Sorption at the Air-Water Interface.

Interfacial tensions of the PFAS solutions were determined using the pendant drop method[42] for various PFAS solutions with concentrations ranging from 0 (deionized water or NaCl solution only) to 100 mol m^{-3}. To directly measure PFAS uptake at the air-water interface at environmentally relevant concentration, and at levels below which accurate interfacial tensions measurements can be made, experiments were performed in cylindrical vessels filled with the desired PFAS solutions and at multiple salinities. Following equilibration, the PFAS solution was drained from the vessel and analyzed for PFAS. The PFAS sorbed at the air-water interface was determined by mass balance using the Gibbs Adsorption Equation[43,44] and fit with the Freundlich adsorption isotherm rather than the Langmuir isotherm.

Task 3.2 Unsaturated Transport Experiments

Three one-meter long columns were constructed to evaluate the transport of conservative tracers and PFAS in variably saturated porous media (sand). The rectangular cross section design was chosen to facilitate the use of x-ray absorption spectroscopy for water content measurements and

water content/electrical conductivity sensors. Water content, temperature, and electrical conductivity sensors were used to monitor the breakthrough of conservative salt tracers and ensure uniform water content along the length of the column. A single short, circular column was constructed to evaluate the movement of conservative tracers and a well-studied surfactant (sodium dodecyl benzene sulfonate - SDBS). Conservative tracers were used to determine the MTI and pore volume of the media, and SDBS was used to measure the air-water interfacial area of quasi-saturated conditions of multiple sands prior to PFAS transport experiments. Constant flow was maintained using peristaltic pumps at the inlet and outlet of the column. Two sets of PFAS mixtures were used in this study. Single component mixtures of PFOS in low ionic strength water was used in column studies with the highly ideal sandy media. The second PFAS mixture was a mixture of contaminated natural groundwaters that were highly impacted from PFAS manufacturing and from AFFF.

Breakthrough curve analysis of the long and short columns was conducted using an analytical solution of the advection dispersion equation modified to incorporate the mass transfer index (MTI). The MTI is used to correct non-dimensional time to pore volumes, thereby providing a more accurate estimation of the retardation factor and providing a simple quantification of potential transport non-idealities.

Task 3.3 Unsaturated Transport Modeling and Analysis

The MTI model developed was intended as a proof-of-concept study using an idealized sand with no mass transfer limitations or chemical retardation. The underlying hypothesis of this study was that when no mass transfer limitations are present, advective flow path tortuosity and mass transfer into and out of immobile zones will produce the same effect on the breakthrough curve. However, this hypothesis breaks down when there is rate limited exchange of solute between the mobile and immobile zones. In this case, only advective tortuosity should follow the power law type relationship described for the MTI model.

Numerical inversion of PFOS data was conducted using PEST and a modified version of HYDRUS which incorporated the MTI for steady state flow to determine the most appropriate isotherm for modeling PFAS breakthrough. The equilibrium and two site-nonequilibrium models of the Freundlich and Langmuir isotherms were fit to the PFOS BTC data with the inversion of HYDRUS described previously.

A significant amount of equilibrium K_{ia} data was collected for a wide range of PFASs. Because measuring equilibrium K_{ia} values is a time consuming and expensive process, developing quantitative structural property relationships (QSPRs) which can accurately estimate K_{ia} is of interest.

Results and Discussion

Task 1: Mechanisms of PFAS retention in Saturated Soil Systems

Task 1.1. Detailed Soil/Sediment Characterization

The soil horizons collected from Oscoda-Wurtsmith AFB were by in large characterized by high sand content (greater than 90%), low clay content (3 to 5%) and very little organic carbon (OC; maximum of 0.28%). We found 15 other soils with very similar physical and chemical characteristics (e.g. high sand content and low OC content) that also contained PFAS source zones that were near or around existing airports or military installations.

Task 1.2. Saturated Soil Column Experiments

The 34 PFAS in the 3M AFFF applied to soil horizon columns sorted into two cohorts with mass retained between 0 and ~15% for PFAS with three, four, and five fluorinated carbons and generally below 30% for all anionic PFAS with less than 8 fluorinated carbons, and complete retention was a rare exception even for those that had 8 fluorinated carbons.

In the case of zwitterionic PFAS, complete retention was the norm with a minority of instances where zwitterionic PFAS actually broke through after flowing with the equivalent of five pore volumes of water. The spread in M_R was greatest for zwitterionic PFAS with four or fewer fluorinated carbons. Zwitterions with five or more fluorinated carbons had at least 50% of their mass retained, even in the soil columns with the lowest percent OC. No mass for C6 and C7 zwitterions broke through any of the soil columns (M_R = 100%). Organic matter concentration in the soil matrix was not a predictor for the retention of anionic PFAS and clearly not the only predictor for the retention of zwitterionic PFAS.

In the absence of single value predictor for PFAS retention, a more comprehensive model was developed. Of a total of 136 sorbate-sorbent combinations assessed for their ability to describe the total capacity of the soils to retain PFAS, 14 PFAS physiochemical PFAS properties and 9 soil predictor variables result in the following model:

$$M_R = \{[0.204 * molar\ mass] + [0.318 * mass\ fluorine] + [c * nitrogens] + Z] \pm 16.2$$
$$c = \{[3.5 * FeOx] + [89.7 * \%\ OC] = 22.7\}$$
$$Z = \{[0.12 * SA_{BET}] - 146\}$$

where M_R is percent mass retained of a given PFAS molecule in the soil of interest, *molar mass* is the mass of the PFAS molecule, *mass fluorine* is the total mass of fluorine on the PFAS molecule, *nitrogens* is the number of nitrogen atoms in the PFAS molecule, *FeOx* is the amount of oxalate extractable iron (g Fe kg^{-1} soil), *%OC* is the mass percentage of organic carbon in the soil, and SA_{BET} is the specific surface area of the soil (m^2 g^{-1}).

Based on free energy calculations carried out by Xiao et al.,[13] exclusion of both cations and zwitterions *from* the aqueous phase was one of the predominant driving forces for adsorption to soil surfaces. As molar mass of the PFAS increases, the thermodynamic impetus for the molecule to be expelled from the aqueous phase increases as well,[33, 34] and nitrogen represents positively charged functional groups, thus underlining the plausibility of a mechanistic contribution of these structural PFAS features.{Nguyen, 2022 #1691;Mejia-Avendano, 2020 #1560;;Barzen-Hanson, 2017 #93} The absence of correlation between anionic PFAS and charged soil components indicates that anions do not interact electrostatically with sorbent surfaces. Thus, our interpretation is that anions migrate to any surface, not just those with organic carbon. The sorbent parameters *FeOx* and *%OC* were statistically related to the *number of PFAS nitrogens*, meaning that they influence the retention of PFAS with both positive and negative charges but not the retention of strictly anionic PFAS. This is noteworthy as Al/Fe oxides contribute positive charge at typical soil pH ranges, while well decomposed organic matter carries net negative charge and serves as a potent cation exchange medium. Thus, zwitterionic PFAS mass retained was related to percent organic carbon where no such relationship was found for anionic PFAS.

Task 2: Impact of phase behavior on PFAS transport–saturated conditions

Task 2.1-Phase behavior experiments.

Microemulsions formed, appeared viscous, and were immobile. Micelles were in the Jet A phase but not in the lower, aqueous phase, which indicates a Winsor Type II microemulsion formed. The five PFAS-based AFFFs and fluorine-free AFFF all produced viscous, Type II microemulsions when mixed with Jet A. The formation of viscous microemulsions under the range of test conditions is consistent with the fact that all MilSpec AFFFs are designed to spread on fuel surfaces and not mix.

Task 2.2. Saturated Column Tests (Multiple AFFF Applications).

Case (A and B): Repeated AFFF Applications to OK-75 Sand (Control) and C2 Horizon.

Repeated application of 3% AFFF (field-application strength) through the both porous media revealed that the adsorption behavior changed with subsequent applications of AFFF (e.g., the concentration history for subsequent applications were not the same as the initial). This observation is indicative of surfactant-surfactant adsorption, where adsorbed species from the first application serve as sorption sites for species during subsequent AFFF applications. This is a very subtle yet highly important observation with regard to the use of single component or even multi-component solutions to conduct research studies: the interactions between the AFFF components are not reflected in most studies unless actual AFFF solutions are used. The degree of mass retention (adsorption) and the degree of retardation (partitioning) correlated with longer PFAS carbon-fluorine chain length.

Case (C and D): Single AFFF Application: Constant Flow and Constant Pressure Experiments.

In the constant flow experiment where AFFF was introduced to a column containing residual Jet A, significant back pressure rapidly developed, which is indicative of a viscous microemulsion formation as the AFFF and emplaced jet fuel mixed. Based on the observation of pressure increase during constant flow rate, we concluded that a viscous phase formed in situ once the AFFF solution combines with the residual Jet A. Two mechanisms are likely 1) a viscous microemulsion phase formed that is immobile and blocking pore space, and causing injected fluids to flow through reduced flow path, or 2) the viscous phase is flowing and requires higher pressure gradient to move. In the constant pressure experiment, the flow rate decreased by half after only 1 pore volume of AFFF. Constant pressure mimics infiltration of AFFF, as could occur if a pool of AFFF formed on the surface and then encountered residual fuel in the subsurface. In situ formation of a viscous microemulsion phase stopped the flow in the constant pressure column and ended the experiment.

Task 3.1-PFAS Adsorption at the Air-Water Interface

Results from pan film testing to measure the low concentration air-water interfacial adsorption of PFASs demonstrated the K_{ia} of PFASs was concentration dependent. Under the Langmuir model conceptualization, the K_{ia} of PFASs should be concentration independent and follow a linear isotherm at these concentrations. Therefore, a Freundlich model of the IFT data was chosen as it allows for concentration dependence of K_{ia} across the full range of relevant PFAS concentrations. The Freundlich model was well correlated with PFOS and PFOA data from the pan film experiments.

Task 3.2 PFAS Unsaturated Soil Transport

The mass transfer index concept was developed as an empirical tool to explain the discrepancy between estimated and measured linear pore velocities using advective tortuosity and exchange between immobile water. The MTI value was well correlated with effective saturation and has a strong theoretical underpinning. The MTI model is summarized by the following Equations.

$$TR\frac{dC}{dt} = -\frac{q}{\theta_w}\frac{dC}{dx} + D\frac{d^2C}{dx^2}$$

$$T = b * (S_e)^n$$

The saturated conditions in the ideal sand demonstrated ideal behavior for the conservative tracers and PFOS. Quasi-saturated conservative tracer tests in the ideal sand demonstrated ideal behavior, however PFOS demonstrated significant retardation and tailing behavior. The degree of retardation was inversely correlated with concentration, suggesting a Freundlich isotherm may was appropriate for modeling PFOS air-water interfacial adsorption. Drainage based experiments with

PFOS in the same sand revealed highly non-Fickian transport behaviors under certain flow rates, saturations, and PFOS concentration.

Conservative tracer experiments in a non-ideal (<90 SiO_2, subangular grains, C_u >1.5, d_{50} < 0.250 mm) sandy media were ideal under both saturated and quasi-saturated conditions. The transport experiments with AFFF impacted groundwater showed a wide variety of behavior of PFAS in both quasi-saturated and saturated conditions. Solid phase sorption was very low or negligible for everything except some of the long chain sulfonates and carboxylates (i.e. PFOS, PFOA). Nearly all PFASs in the mixture had significant air-water interfacial adsorption, even the short chain carboxylates and ethers. Statistically significant non-equilibrium air-water interfacial partitioning was observed for the first time in these experiments.

Task 3.3 PFAS Unsaturated Transport Modeling

To demonstrate the phenomenon of advective tortuosity, we use a trigonometric mass balance on a finite fluid element to calculate the advective tortuosity in terms of linear pore velocity for a steady state system. Then, using data from a sand column experiment with rate-limited mass transfer to immobile zones (Padilla et al. 1999) it is demonstrated that the MTI model breaks down, but advective tortuosity can be calculated directly using the mobile-immobile (MIM) model.

Results of the HYDRUS inversion demonstrated that an equilibrium Freundlich model provided the best fit to the BTC inversion data for all 3 replicate columns. Further the estimated Freundlich parameters (K_f and n) values from the inversion data were consistent with the empirically determined Freundlich parameters from K_{ia} vs Concentration regression data. The consistency of these findings supports the application of a concentration dependent isotherm (e.g. Freundlich) across the full range of relevant PFAS concentration.

Structural properties of PFASs were selected based on their correlation with hydrophobicity and PFAS concentration. All possible combinations of these structural properties were fit to log(K_{ia}) data and evaluated using adjusted R^2 best fits. The QSPR models were also corrected for ionic strength and had good to very good prediction accuracy for both calibration and validation data across a full range of relevant PFAS concentrations.

Implications for Future Research and Benefits

Using a soil known to support PFAS source zones, a commercial AFFF with multiple anionic and zwitterionic PFAS species, and one-dimensional saturated column experiments, we observed significant PFAS mass retention which was best described by a multi-parameters quantitative-structure property relationship. Retention of anionic PFAS was generally low until the fluorinated chain comprised at least eight (8) fluorinated C atoms. Even more important for site managers and policy makers was the observation that for anionic PFAS, soil and sediment properties in systems with negligible organic carbon content have little relevance for their retention behavior. Instead,

the overriding control towards environmental matrices was the size of the fluorocarbon chain and the associated thermodynamic impetus to be expelled from the aqueous phase. The retention of zwitterionic PFAS was related to the PFAS molar mass and the # of N atoms incorporated in the molecule. Zwitterionic PFAS also showed significant tendencies to actually bind with environmental matrices through electrostatic mechanisms. Given the fact that the soil chosen for this investigation was a sandy matrix almost devoid of clay and with miniscule surface reactivity, we posit that we have investigated the equivalent of a best-case scenario for soil contamination with PFAS – almost any other soil matrix will retain both anionic and zwitterionic PFAS to a significantly larger extent. Finally, our research showed that the fraction of soil organic carbon present (f_{OC}) does not represent a single value predictor for retention of all PFAS in source zones[12, 35-37] and that there are other influencing variables such as the mineral phase or the quality of the organic carbon, which should also be considered. Future research is aimed at determining if PFAS and NAPL associate as microemulsions or as non-microemulsion mixtures at fire-fighter training sites, which is the first step toward understanding if residual NAPL acts as a sink for PFAS and thus, a potential long-term source of PFAS to groundwater.

This research has provided a comprehensive framework for evaluating the air-water interfacial partitioning & non-Fickian transport properties of PFASs at a laboratory scale. The improved understanding air-water interfacial partitioning & non-Fickian transport can be scaled up to numerical models and conceptual models used to evaluate the fate and transport of PFASs at field sites. Key findings of the work include: the development of a simple empirical model to evaluate the potential for non-Fickian transport to develop unsaturated porous media; non-Fickian transport can reduce the observed retention of PFASs in to the air-water interface by over 10 fold as compared to equilibrium models; the development of a quasi-saturated column method to minimize the impact of non-Fickian transport in multi-phase partitioning column studies; development of a multiparametric QSPR models to approximate the K_{ia} of PFAS under relevant environmental conditions. Future studies can build on the work presented here by studying PFAS transport under more realistic (e.g., drainage and imbibition from rainfall) conditions using the simplified empirical models for estimating non-Fickian transport and the K_{ia} of PFASs. Further work is also needed on the effects of organic carbon, competitive sorption, and multi-component solution effects on PFAS transport in the vadose zone. Validating the numerical models developed herein for field conditions can be done through controlled/well monitored lysimeter studies.

--END OF EXECUTIVE SUMMARY--

Background

The overall goal of this project was to identify processes governing the retention of per- and polyfluoroalkyl substances (PFAS) in soils and sediments impacted by repeated AFFF applications during firefighter training with aqueous film forming foams (AFFF). Prior to the project, relatively little was known about PFAS transport and attenuation in source-zone soils and sediments, and why source zones act as long-term sources of PFAS. Beyond understanding the transport of anionic PFAS including perfluoroalkyl sulfonates (PFSA) and perfluoroalkyl carboxylates (PFCA), comparatively little was known about the retention and transport of other anionic, zwitterionic, and cationic PFAS. Understanding the mechanisms of PFAS retention associated the historical discharge scenarios of AFFF was needed to understand and predict PFAS release from source zones.

AFFFs are complex mixtures of PFAS,[1, 2] hydrocarbon surfactants,[3, 4] and solvents (e.g., butyl carbitol).[5, 6] Repeated use of AFFF during firefighter training, equipment 'capacity' testing, leaks and other accidental releases, along with emergency responses to aircraft crashes has led to significant AFFF releases at US military sites.[7] Limited data on the composition of AFFF indicates they contain high levels (g/L) of PFAS, of which perfluorooctane sulfonate (PFOS) and perfluorooctanoate (PFOA) are the two most well-known. Prior to this project, field data for primarily PFOS and PFOA indicated high concentrations (µg/L to mg/L) remain in groundwater and soils and sediments at fire-fighter training areas even though can be two decades since the last AFFF application.[2, 8, 9] During execution of the present project, the US EPA reduced the Health Advisory values for PFOS and PFOA in water from 70 ng/L (70,000 ppt)[10] to 0.02 and 0.004 ppt, respectively.[11]

Earlier laboratory data indicated that zwitterionic and cationic PFAS are strongly sorbed to soils.[12-14] Since these earlier studies, an ESTCP-funded field project reported that zwitterionic and cationic PFAS have significantly lower concentrations in groundwater while more mass is retained in source-zone soils and sediments.[15-17] Given the persistence of a range of PFAS in source-zone soils and sediments, it is important to understand the potentially complex interactions that occurred when PFAS infiltrated into unsaturated soils of the vadose zone and moved downward toward the saturated aquifer sediments.

A number of studies indicate good agreement between anionic PFAS sorption and soil/sediment organic matter content,[18-20] while a more recent review documents poor correlations.[21] In particular, there is a lack of correlation for the zwitterionic and cationic PFAS, which is consistent with reports for zwitterionic (nonfluorinated) pharmaceuticals.[22-24] Importantly, the soil-water partition coefficients (K_d) values for cationic and zwitterionic PFAS are 5 to 50 times greater than those of anionic PFAS of corresponding chain length. Although a single measure of organic matter content is desirable due to its simplicity and low cost for the measurements, it does not appear sufficient to predict the transport for a wide range of PFAS. Differences in the chemical character

of organic matter may result in different strengths of interactions with anionic, cationic, and zwitterionic PFAS. Because the sorption of zwitterionic/cationic PFAS could not be predicted from cation exchange capacity (CEC),[12] it is likely that a more complex set of mechanisms control their transport. We hypothesized that the key parameters that control PFAS sorption in source zones will be organic matter type and quantity, the amount and type of surface charge on mineral phases, pH, and major electrolyte composition.

Prior to the onset of this project, few studies focusing on sorption conducted PFAS transport experiments with intact AFFF, at levels representing AFFF application strengths (3 or 6% solution in water v/v), or upon multiple additions of AFFF. The impacts of the complex chemical composition of AFFF and the high (g/L) concentrations of PFAS and other organics on PFAS behavior during infiltration and transport was unknown. At AFFF application strengths, AFFF is above the mixture's critical micelle concentration (CMC), such that hemi-micelles and micelles containing PFAS could undergo sorption[25] or form layers that act like liquid crystals or gels. Viscous gels block soil pores, thus changing flow characteristics of porous media. We hypothesized that PFAS retention when applied to soil horizons as solutions of near application strength AFFF will result in fundamentally different PFAS retention when compared to experiments conducted with simple solutions at low concentration. Given these data gaps, Task 1 was to quantify changes in PFAS retention in saturated column experiments for four soil horizons that received a single application of AFFF diluted to below its CMC.

Releases of AFFF occurred both in the presence and absence of fuels since firefighters trained explicitly to put out fires with AFFF, but also tested equipment that did not involve fuels. Free-phase fuels form nonaqueous phase liquids (NAPL). However, no information was available on the phase behavior of AFFF and NAPL when mixed. Microemulsions are thermodynamically stable mixtures that incorporate both NAPL and water.[26, 27] The Winsor system (Figure 1: Winsor Type microemulsions.) was developed to describe "oil-in-water" microemulsions (Winsor Type I), "water-in-oil" microemulsions (Winsor Type II), and microemulsions that contain both oil and water (Winsor Type III). However, no information is available on the number and type of thermodynamically stable phases that form when AFFF and fuels mixed, nor on how microemulsions impact PFAS transport. We hypothesized that PFAS transport through soils/sediments is fundamentally different when AFFF is mixed with NAPL. Given these data gaps, Task 2.1 was designed to characterize the number and type of thermodynamically stable phases that form when AFFFs are mixed with jet fuel their impact on PFAS transport.

To date, no experiments have been performed to understand the impacts of multiple, successive additions of AFFF have on PFAS transport and retention. Given the historical practice of repeated AFFF applications, PFAS likely entered increasingly altered soils, potentially characterized by layers of pre-existing PFAS and other AFFF components. We hypothesized that repeated applications of AFFF will change the retention of PFAS with successive additions. Given these data gaps, experiments were designed for Task 2 to quantify changes in PFAS retention for a sand

column and a C2 horizon column that each received four successive applications of application-strength AFFF.

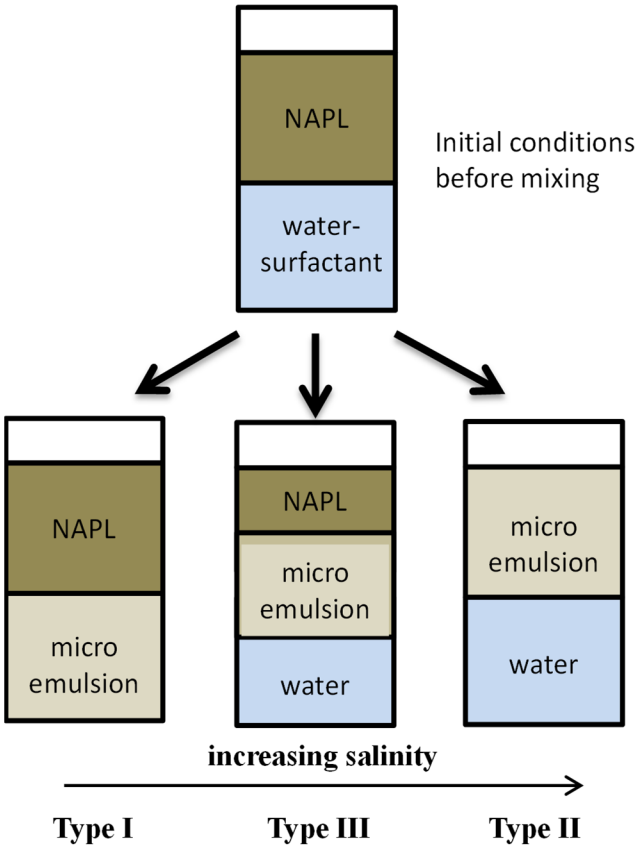

Figure 1: Winsor Type microemulsions.

In water-saturated soils, the mobility of PFAS is controlled by advection, dispersion and retardation, where the latter is thought to result primarily from sorption. In the partially saturated soils of the vadose zone, factors that contribute to both mobility and retardation are much more complex. In the vadose zone, water saturation varies as a function of the capillary pressure, and advection and dispersion depend on both spatially and temporally varying water saturation. The air-water interfacial area generally decreases upon re-wetting. PFAS sorbed at the air-water interface may lead to (transient) immobilization of PFAS in the vadose zone.[28-31] However, as PFAS may reduce the air-water interfacial tension due to sorption at the air-water interface (as predicted by the Gibbs Adsorption Equation), this could also lead to an altered pressure-saturation relationship and faster infiltration through the vadose zone and thus greater transport in underlying saturated groundwater. Once the pressure-saturation-area relationship is determined under ambient (no PFAS) conditions and combined with knowledge of how PFAS sorb at the air-water

interface (via independent methods like the pendant drop method), one can estimate the mass of PFAS retained at a given water content. In addition, one can estimate the PFAS mass released during an infiltration event as the air-water interface diminishes. We hypothesized that the air-water interfaces present in the pores of vadose zone soils act as preferred sorption sites for PFAS, and that retardation of PFAS at the air-water interface and subsequent release during wetting are key parameters for understanding PFAS transport in source zones.

Objectives

The overall objectives of this project were to:

1] identify the key PFAS and soil properties that control PFAS interaction with saturated soils when AFFF is applied at near application strength concentrations,

2] characterize the number and type of thermodynamically stable phases that form when AFFFs are mixed with jet fuel their impact on PFAS transport,

3] assess PFAS mobility under unsaturated zone conditions in order to identify the key hydraulic parameters and PFAS properties that control PFAS mobility and retention.

Methods and Materials

Task 1: Mechanisms of PFAS retention in Saturated Soil Systems

Task 1.1. Detailed Soil/Sediment Characterization

Chemicals for both Task 1.1 and 1.2, unless noted otherwise, were of reagent grade purchased from Fisher Scientific. For PFAS quantification, analytical standards, both native (50) and isotopically labelled (33), were purchased from Wellington Laboratories Inc. (Guelph, ON, Canada).

Soil Collection and Characterization

Four PFAS-free subsurface soil horizons were collected from Oscoda-Wurtsmith Air force base (AFB) in Michigan (Figure 2). The sampled horizons included the E, B, C1, and C2 horizons from a soil with the National Resource Conservation Service taxonomic class: *Isotic, frigid Typic Udipsamments*. The topmost horizon (the A horizon) was not included in the study. After sampling, soil was transferred into sampling bags (4 L polyethylene bags), placed in coolers, and shipped to Oregon State University. Upon receipt, the soil was stored at 4 °C. Analyses were conducted by either the Oregon State University Soil Health Lab or at Oregon State University OSU. Along with basic soil properties (e.g., pH and % organic carbon), the following detailed physiochemical soil characteristics were measured:

- Total functional groups present on the soil organic carbon were characterized using Thermo Scientific Nicolet iS50 Transmission FTIR (T-FTIR) (Thermo Fisher Scientific, Waltham, MA)
- Surficial functional groups were characterizes using photo-acoustic FTIR MTEC Model 300 photo-acoustic detector (MTEC Photoacoustics, Inc, Oakland, CA) attached to the same Nicolet iS50 FTIR instrument.
- Particle surface area was measured using Brunauer-Emmett-Teller N2 method (BET N2) on a NOVA 2000e Gas Sorption System (Boynton Beach, FL)
- Mineral composition was determined via x-ray diffraction using a Rigaku Ultima IV X-Ray Diffractometer (Rigaku Americas Corporation, The Woodlands, TX)

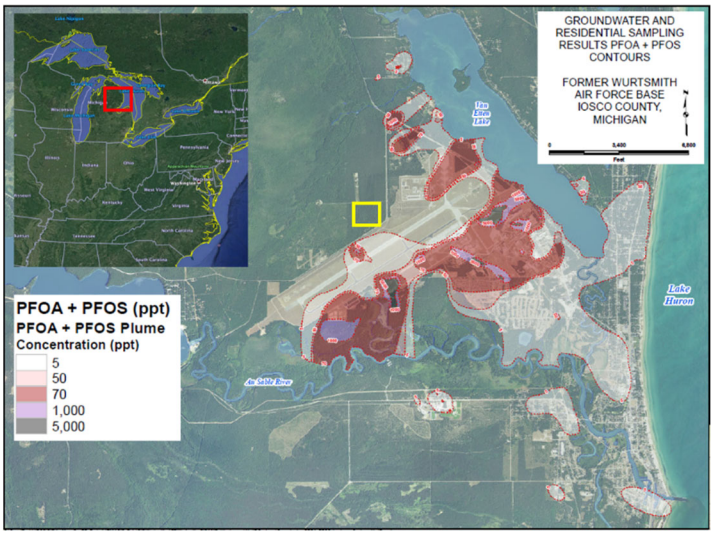

Figure 2: Soil sampling location (yellow box) at former Air Force Base.

Task 1.2. Saturated Soil Column Experiments

Soil Column Design and Packing

Individual soil horizons were dry packed into columns that were 10 cm long and 2.25 cm in diameter following a packing procedure detailed elsewhere generating four columns, one for each soil horizon.[1, 2] Prior to packing, the soils were air dried and sieved to a particle size of ≤ 2mm. Replicate columns (n = 3) were packed using the same method but with 30/40 grade quartz sand (Accusand, Ottowa, MN) to serve as both replication and control columns. The columns were constructed of 1 cm sections of rigid, polyvinyl chloride tubing (effective soil column length = 10 cm and i.d. = 2.125 cm). Sections were stacked and held together using heat-shrink tubing to allow for destructive sampling of the columns at the end of the experiments. Both ends were capped with mesh flow distributors and custom frit (to allow for tubing connections). The packed bulk density (Db) for E, B, C1, and C2 columns were 1.70, 1.63, 1.72, and 1.76 g cm^{-3} respectively. The average

packed Db for the Accusand columns was 1.74 ± 0.02 g cm^{-3}. To ensure that no PFAS were sorbing to the system components, after four test experiments were conducted, the system was flushed with methanol and no PFAS were detected in the effluent (data not shown).

Soil Column Pack Characterization

Synthetic tap water (STW) with a total electrolyte concentration of 0.02 mM (pH 7.2) was made and used as the aqueous phase for all experiments and in non-reactive tracer (NRT) experiments in this study. Briefly, the STW was prepared using ultra-pure deionized water (Millipore) and low concentrations of analytical grade mono- and divalent electrolytes and metals, purchased from either Sigma Aldrich (St. Louis, MO, USA) or Fisher Scientific (Waltham, MA, USA), with component details described elsewhere.[3]

A non-reactive tracer experiment was conducted on each column individually prior to the start of the PFAS application experiment to calculate residence time, effective porosity, and effective pore volume. The column was oriented vertically and first saturated with ~ 10 pore volumes of deionized water (flow rate = 0.1 mL/min) in an upward flow direction to remove any entrapped air following a similar method outlined by Brusseau et al.[4] Synthetic tap water was then applied from the top down and the change in electrical conductivity (EC) was measured using an inline EC electrode (flow rate = 1 ml/min). Once the EC reached steady state, the column was flushed with DI water to determine the decreasing side of the breakthrough curve (BTC). It was assumed that hydrodynamic properties of the soil packs did not change over the relatively short-duration and low flow rate experiments.[5] After the no-reactive tracer experiment and prior to the start of the AFFF experiment, each column was flushed with ~5 pore volumes of STW. The STW was used as the no-reactive tracer such that soil sorption sites were not complexed with a salt or other contaminants not used in the experiments.

Column Flow Conditions.

All fluid delivery (either STW or AFFF) was performed using an Agilent 1100 HPLC pump and effluent fractions from the PFAS application experiments were collected using a Spectrum CF-2 fraction collector (Spectrum Chromatography, Houston, TX). A mean pore water velocity of ~0.24 m/day (volumetric flow rate of ~0.064 ml/min) through the column was chosen for the PFAS experiments so as to replicate that of the natural groundwater recharge rate at Oscoda-Wurtsmith AFB (between 0.09 and 0.25 m/day).[6] Each column received 0.5 pore volumes of AFFF, diluted below the critical micelle concentration (CMC). The measurement of the CMC for the AFFF as a whole is detailed elsewhere.[3] A minimum of ~100 ml of effluent (in 2 mL fractions), or six to eight pore volumes, was collected from each column in 15 ml polypropylene tubes

AFFF Characterization and Sample Analysis.

The AFFF used in the column experiments was first characterized by liquid chromatography quadrupole time of flight mass spectrometry (LC-QTOF) (SCIEX, Framingham, MA) by injecting 100 µL of sample onto an orthogonal LC system (Agilent 1260 HPLC, Santa Clara, CA).[7] AFFF samples were analyzed in both negative and positive electrospray ionization (ESI- and ESI+ respectively) modes. The identified PFAS were cross-referenced against a detailed analysis done by Hao et al. (listed as AFFF-1 therein).[8] Criteria regarding mass errors, isotope ratios, and library matching for target and suspect screening which were used to confirm PFAS identifications can be found in Nickerson et al.[9] Thirty-four major PFAS (12 anionic and 22 zwitterionic) were identified in the applied AFFF. On a mass basis zwitterionic PFAS made up about 60% of the total fluorinated mass where anionic PFAS contributed about 40%.

The PFAS in the applied AFFF and column effluent samples were quantified using isotope dilution and analyzed using an Agilent 1100 HPLC (Santa Clara, CA) coupled with triple quadrupole mass spectrometer (TQD) (Waters Corporation, Milford, MA). The TQD was operated simultaneously in both negative and positive electrospray ionization modes and controlled by MassLynx (version 4.1). PFAS for which there was no matched standards were semi-quantified by assuming an equal molar response to a related analyte.[7, 9]

Quality Control/Assurance.

Internal continuing calibration quality control standards were analyzed every 10 samples and required to fall within 70 – 130% of the expected value. An external, third party reference standard (Absolute Standards, Hamden, CT) was analyzed at the beginning of every analytical sequence and also required to fall within 70 – 130% of the expected values. Accuracy of the measurement of each PFAS (calculated as relative standard deviation) during each analytical run was measured by including at least one replicate set of samples (n = 4). Replicate Accusand columns (n = 3) were generated and used to determine accuracy of experimental procedures and analytical results.

Formation of ppQSPR Model.

To describe the mass retained (M_R) of PFAS a machine learning-based poly-parameter quantitative structure-parameter (ppQSPR) linear regression model was developed. This modeling approach provided a tool to quantitatively measure the combination and relative contribution of PFAS physicochemical properties and soil properties as they related to PFAS M_R in each soil column.

First, models using all possible combinations of PFAS physiochemical parameters were generated (22,802 models in total). We determined that a three parameter model sufficiently described the data without over-parameterizing/over-fitting the data by comparison of the adjusted R-squared values for all PFAS parameter models against the number of parameters included in the model.

Second, the coefficients for each included parameter and the intercept in the selected PFAS-parameter only model were then analyzed against the soil properties for each horizon to generalize the model for variable soil properties. The resulting and final model (PFAS parameters + soil properties; equations 1.3 – 1.5) was selected using goodness of fit against data from all of the four soil horizons, evaluated using adjusted R-squared values and root mean squared error (RMSE) analysis of the metadata.[10] The final model was externally validated against data from the average of the three replicate Accusand columns. Results from the external validation test indicated that the model described the mass retained with acceptable accuracy based on similar root mean squared error values to the original ppQSPR model. Co-variance of all potential model parameters was tested and related parameters were not included in final model iterations. The final model is presented in the Results section (equations 1.3 – 1.5).

Data Analysis Using Equilibrium Model

Soil partitioning coefficients (K_d) were calculated in each of the soil columns for the PFAS species that broke through and using two different methods (equations 1.1 and 1.2 below). First, an apparent K_d ($K_{d,\,app}$) was calculated using the final concentration of PFAS in the effluent divided by the concertation on the soil (calculated by subtracting the amount of mass input from the total mass in effluent samples, equation 1.1).

$$K_{d,app} = \frac{[soil]}{[aqueous]} \tag{1.1}$$

The second method used an equilibrium-based model fit to the individual breakthrough curves (BTC; herein referred to as $K_{d,BTC}$). To do this we fit the BTCs with an exact analytical solution to an advection-dispersion equation (ADE) of finite duration.[11] The column-based calculation assumes that sorption in the system is: linear, reversible, mono-layer, and, crucially, and under equilibrium conditions in an advection-dominated system.[12] Violations of any of these assumptions can significantly decrease confidence in the resulting $K_{d,\,BTC}$ estimations, indicate that other sorption processes/mechanisms (e.g. electrostatic interactions and not strict hydrophobic partitioning) are active, or nullify the approach altogether.[12-14] A violation of any one of these assumptions may also suggests that other sorption mechanisms, other than a hydrophobic exclusion mechanism driven by the fluorinated tail, may be active.[12, 15, 16] Analysis of the BTC for each PFAS generated the Peclet (Pe) number, retention time (R_t,), and predicted injection pulse width. The retardation factor (R_f) for a given PFAS was calculated from the ADE-derived R_t, and ultimately used to calculate $K_{d,\,BTC}$ using equation 1.2

$$R_f = 1 + K_{d,BTC}\left(\frac{Db}{n}\right) \tag{1.2}$$

where *Db* is packed column bulk density and *n* is porosity. Confidence in the K_d values derived from the ADE generated parameters for each PFAS from each soil column were evaluated using the following criteria: 1) comparison of the time of the actual injected pulse width to predicted pulse width and calculating the percent injected pulse width recovery (IPWR). The IPWR can be used to assess the fit of the ADE to a given BTC.[17, 18] The IPWR was between 70% to 130% (the same range used for continuing calibration quality control samples) and 2) screening for Pe number > 10, which indicates rapid equilibrium in an advection-dominated system.[12, 13]

A $K_{d, BTC}$ value calculated from non-symmetrical, long-tailing BTC with an IPWR outside of the 70% to 130% range and a Pe number < 10 was not counted as valid.[12, 14] A long-tailing, non-symmetrical BTC is not well captured by a one-domain ADE[13, 14] and a Pe number < 10 indicates increased dispersive forces. Values in these ranges for IPRW and Pe number is also potentially a sign of non-equilibrium/non-linear sorption or effects of other non-Fickian processes which also cannot be quantified by the ADE.[12, 19] Partitioning values from the two methods were then converted to total PFAS mass retained by multiplying with the known mass of soil in each column. Partitioning coefficient results for both methods from example PFAS are presented in the Results and Discussion section.

Task 2: Impact of phase behavior on PFAS transport–saturated conditions

Task 2.1. AFFF Phase Behavior

The phase behavior experiments were conducted using an AFFF that was collected from actual AFFF dispensing equipment on an Air Force Base military base and used as a model AFFF for both phase behavior and flow experiments. AFFF-1 was chemically characterized by OSU and found to contain 9.5 g/L PFOS (Table 1: AFFF manufacturer, year of manufacture, primary PFAS 'active ingredient concentration, and hydrocarbon surfactant classes (qualitative)(Table 1) and other PFAS produced by electrofluorination chemistry, which is consistent with a Type 3 (3M) Military Specification (MilSpec) AFFF. Five additional AFFFs (Table 1) were evaluated including three older AFFFs with known PFAS content (1989 and 2001 3M Lightwater and fluorotelomer-based Chemguard 2010), and the newer 2018 Chemguard AFFF, which is on the current MilSpec Qualified Products List.[3] The 2018 Chemguard was not characterized for its PFAS content but was manufactured to meet the 2017 MilSpec that limited the PFOS and PFOA (C8) content and is likely is comprised of fluorotelomer-based PFAS.[4] The fifth AFFF (Solberg RF-6 Re-Healing) was included since there is great interest in fluorine-free AFFF but was not chemically characterized.

Synthetic tap water was used in experiments since potable water is used on bases for fire-fighting training and to fill emergency trucks. Jet Fuel A (Jet A) was purchased from municipal airport. The sand used in flow experiments was OK-75 sand (US Silica, 99.8 wt.% quartz) and soil obtained from the Wurtsmith AFB and subsequently categorized (OSU) as the C2 horizon. All

project teams agreed to use a synthetic tap water that could be re-created and lead to comparable results among the teams, and could also be re-created by researchers seeking to duplicate our work in the future. The pH of the synthetic tap water was maintained between 7.6 to 7.8 by adding minimal quantity of a 1% v/v hydrochloric acid solution. Each batch of synthetic tap water was stored for only 1 week and, if not utilized within 1-week, a new batch was prepared.

For the salinity scans, synthetic tap water was combined with a stock solution of sodium chloride (NaCl) to yield a desired NaCl concentration. In the phase behavior testing, when synthetic tap water was used, it was labelled as 0% NaCl from the perspective that no additional salt(s) were added to the tap water. When creating serial dilutions of the AFFF-1, conductivity measurements of the solutions were plotted and followed a linear trend. The conductivity measurements were verified using liquid chromatography equipped with a light scattering detector, indicating that a bulk measurement could be made if the composition of the solution were not relevant. This observation could be useful for field applications where a rapid method may be desired as a screening tool.

Salinity scans were conducted with Jet A and 3% v/v AFFF-1 over a range of salinity between 0 to 4 wt.% NaCl and water-oil ratios of 1:1, 3:1, and 9:1. Aqueous phases (synthetic tap water or NaCl solutions) are added to 5-mL pipettes that were first heat-sealed at the bottom to achieve a target salinity between 0 to 4 wt.% NaCl while the AFFF-1 concentration was fixed at 3 % v/v. A volume of AFFF-1 and Jet A was added to the pipettes to achieve water-oil ratios of 1:1, 3:1, and 9:1. Pipettes were then heat-sealed from the top and shaken by hand vigorously for 30 s before being allowed to equilibrate at 20˚C and constant pressure. All pipettes were allowed to equilibrate for weeks and examined daily. No significant heat transfer to the Jet A and AFFF-1 solution was confirmed by an infrared thermometer, which indicated that ambient temperature (20°C ± 2°C) was maintained during the heat-sealing process.

The presence of micelles was determined by shining a laser light through each of the resulting phases. Micelles, being nano-sized colloids, scatter light (Tyndall effect) and the laser beam becomes visible within the phase, while the absence of a visible laser beam in a phase indicates the absence of micelles.[6-8] A second set of salinity scans was performed, using the same procedures, with AFFF-1 at concentrations of 1.5, 0.75, to 0.375 vol.%, (representative of an improperly diluted formulation) over a salinity range from 0 to 1 wt.% NaCl, but the water-oil ratio was fixed at 1:1. No pre-foamed AFFF-1 was used in the second set of tests.

Limited phase behavior tests were conducted with the five additional AFFFs (see Table 1). Sets of 5-mL pipettes were prepared with AFFF solution and Jet A using the same procedures described above, except they were limited to 1:1 water-oil ratio and 0% NaCl only. These tests included variations of the procedures, namely: a) no mixing (replicating conditions at ground surface), b) vigorous mixing, c) pre-foaming the AFFF, and d) changing the order of AFFF and Jet A addition.

In addition, all tests and variations (a) - (d) were repeated for these five AFFFs using larger 15-mL tubes. This complementary set of tests conducted using 15-mL plastic centrifuge tubes to study the effect of larger cross-sectional area on the phase behavior of the fluids: the 15-mL tubes had a cross–sectional area that is 9 times greater than that of the thinner, 5-mL pipettes and thus add less energy to the solutions when mixed.

Table 1: AFFF manufacturer, year of manufacture, primary PFAS 'active ingredient concentration, and hydrocarbon surfactant classes (qualitative)

AFFF	year	primary PFAS concentration
AFFF-1	unknown	9,500 mg/L PFOS*
3M Lightwater	1989	15,000 mg/L PFOS[1]
3M Lightwater	2001	7,900 mg/L PFOS[1]
Chemguard 2010	2010	6,100 mg/L FtTAoS[1]
Chemguard 2018	2018	not analyzed
Solberg RF-6	2018	not analyzed

Critical Micelle Concentration of AFFF-1.

The CMC of AFFF-1 was measured to be 60 mg/L using the pendant drop method (DataPhysics OCA 15EC). When AFFF-1 was diluted to the prescribed 3 % v/v dilution (3 parts per hundred or approximately 30 g/L) with synthetic tap water, AFFF-1 was well above its CMC.

Foam stability.

The foaming properties of AFFF-1 were explored with and without Jet A. Briefly, 10-mL volume of AFFF-1 was loaded into a custom apparatus then air was injected at 0.034 mPa for 30 s and foam height decay was determined with time**.** A custom polyacrylamide column (0.95 cm inner diameter by 30.5 cm) based on Singh[9] was built to determine bulk foam height decay with time. A 10-µm aluminum sparging frit at the bottom of the column helped distribute the gas phase during tests. A 10-mL volume of AFFF-1 was loaded into the apparatus then air was injected at 0.034 mPa for 30 s. Foam height decay with time was determined by reading the upper height level h_u and the lower height level h_l after each time step to calculate the foam height h_n at the n^{th} time step of the test using the expression $h_n=h_u-h_l$. Foam heights were normalized by dividing all values with the initial height h_o. AFFF-1 foam stability was also tested with the presence of Jet A using

the same method to study its effect on the foam stability, where 10 ml of AFFF-1 and 1 ml of Jet A were added before foaming.

Rheological measurements.

The viscosity of the 3% AFFF-1, the Jet A, and a microemulsion generated by mixing AFFF-1 and Jet A at a 1:1 water-oil ratio were measured. Rheological measurements were performed using TA Instruments DHR-2, double-gap concentric cylinder cup at 20˚C. Since viscosity can be a function of shear rate, the shear rate was varied from 0.1 s^{-1} to 100 s^{-1}. The viscosity of 3% AFFF-1, Jet A, and a microemulsion generated by mixing AFFF-1 and Jet A at a 1:1 water-oil ratio, were measured by placing each fluid in a cylindrical cup suspended in a liquid reservoir and measuring the torsion required to rotate the cup.[8] The viscosity of the microemulsion was measured after equilibrating for only 10 min and again after equilibrating for 1 week. The longer equilibration time was examined to determine if the rheology of the microemulsion remained constant as it infiltrates into the subsurface.

Column (1D flow) experiments.

Four flow experiments were conducted to explore the AFFF/jet fuel and microemulsion transport properties. The control case (A) was conducted first, using only clean, quartz sand (OK-75), no clay or organic matter, where repeated applications of AFFF-1 were used to study the potential adsorption onto relatively inert media. The second case (B) was similar to the first, but using C2 horizon soil obtained from a clean area at the Wurtsmith AFB to compare adsorption onto media obtained at a site (note: analysis of the Wurtsmith AFB soil was conducted by OSU–see Task 1.1). Both cases were conducted without NAPL present. The next two cases (C) and (D) were conducted using the OK-75 sand, however, the preparation steps also created a residual saturation of Jet A in the soil pores prior to application of AFFF-1. The AFFF-1 was not applied in repeated doses, but rather a continuous injection where two flow schemes were employed: (C) constant flow rate, where mixing energy is constant, and (D) constant pressure, where mixing energy varies directly with the resulting flow rate. The preparation steps for all four cases are similar and as follows.
A glass chromatography column (Kimble-Kontes Chromoflex, Fisher Scientific) with 2.5-cm diameter and 15-cm length was used for the dynamic flow experiments. An HPLC pump was used to deliver fluid to the column with capability to pump at constant pressure or constant rate as desired. Multiple floating piston accumulators were used to contain fluids (3% AFFF-1, Jet A, synthetic tap water). A water circulator (Thermo Scientific ISOTEMP 6200) was used to maintain 20 ˚C. Pressure transducers (Omega PX-26) were used to measure the pressure drop between the inlet and outlet of the column. The set-up was oriented vertically and designed to have a flow direction either downward or upwards, depending upon the fluid flow, and ensure a gravity-stable displacement (Figure 3). Produced fluid samples were collected using a fraction collector (ISCO Retriever 500) in 15-ml plastic centrifugal tubes. Gravimetric measurements are used to determine the porosity of the sand pack and are confirmed by conducting tracer tests.

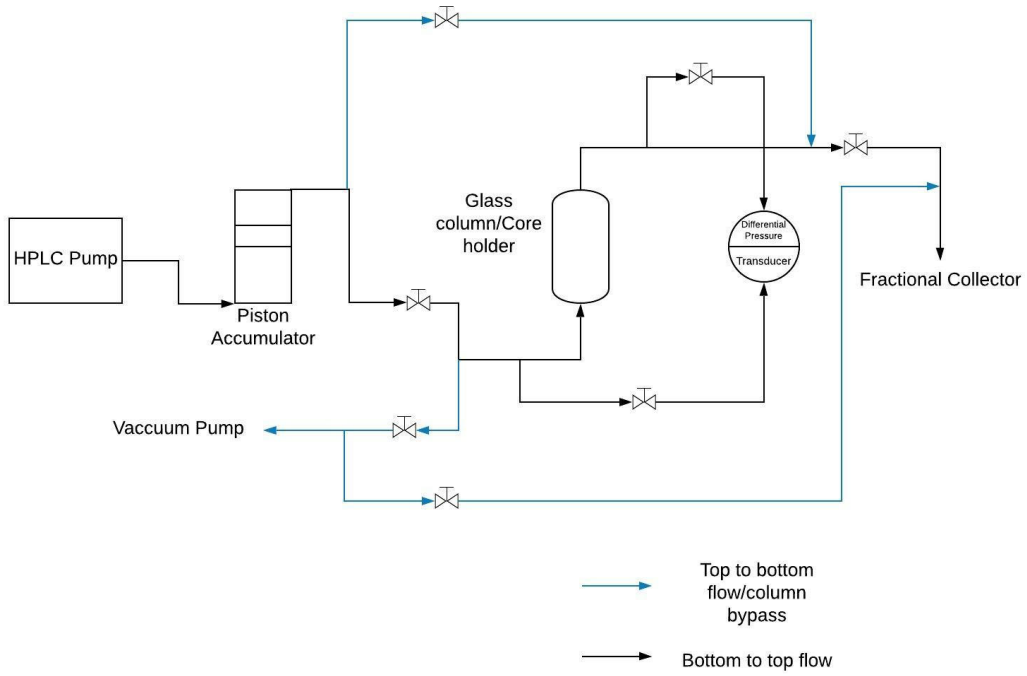

Figure 3: Flow diagram for flow experiments; blue colored arrows highlight the downward flow loop.

After characterizing the porous media (porosity, permeability), AFFF-1 injections began for cases (A) and (B). The two cases (C) and (D) included steps to achieve residual Jet A saturation prior to introducing the AFFF-1. Jet A was injected into the water–saturated column downward to achieve a gravity–stable displacement of water until residual water saturation was achieved (*i.e.*, tap water was no longer observed at the outlet). The injection flow rate was increased to ensure that all moveable water was produced. The sandpack was then waterflooded with tap water (upwards for gravity-stable displacement) to achieve residual oil saturation. Waterflooding was continued with increased flow rates until no jet fuel was produced to ensure the sandpack was at residual oil phase saturation, mimicking the natural occurrence of contamination.

Flow rate for saturated column conditions.

To establish the flow rates for the saturated column, OSU and the University of Houston considered reports published by the United States Geological Survey published in 1983 and 1995 specifically describing the hydraulic conditions of the Oscosda-Wurtsmith area.[12,13] Under saturated conditions, the local hydraulic gradient, moving west to east, supports a groundwater recharge rate between 0.3 ft/day to 0.8 ft/day. Thus, using Darcy's law and the Kozeny-Carmen equation, we computed a flow rate that would yield a flux or linear velocity on the same order of

magnitude as that found in the literature—the flow rate used achieved a flux of 1 ft/day for the saturated column experiments to closely resemble the natural recharge rates.

Task 2.2. Saturated Column Tests.

Case (A): Repeated AFFF Applications to OK-75 Sand (Control).

The first series of column tests was performed with a sandpack of OK-75 sand (>99% quartz) (Figure 4). The dynamic properties of the column including porosity, pore volume, and permeability (Table 2) were determined; the pore volume was measured gravimetrically and confirmed by means of a tracer test (Figure 5).

Table 2: Dynamic properties of the column, quartz sand (US Silica OK75)

porosity	34%
pore volume	83 ml
permeability	10 darcy

Four injections of 3% AFFF solution, each of a fixed volume less than 0.5 pore volumes (termed a "slug"), was injected into the saturated porous media followed by synthetic tap water. This experiment was intended to be the control for future tests to study the AFFF adsorption on an inert media, however, the results from this test were surprising and insightful. Some retardation and adsorption onto the quartz sand was measured for each of the four AFFF injections. In all cases, the adsorption was significantly higher than that measured in static tests that were conducted prior to the dynamic flow experiments (approximately 0.007 mg/g). The concentration history and more details on the chemical analyses of the effluent samples collected from this test are reported below. Note that the conductivity measurements were not expected to provide detailed information with respect to specific PFAS compounds but was measured to understand whether it could be useful as a bulk measurements or screening tool after observing the linear response to AFFF concentration during Task 2.1.

Figure 4: Experimental setup for 1-D flow experiments. A homogeneous sand pack of either US Silica OK-75 sand or C2 horizon field-obtained sand was used.

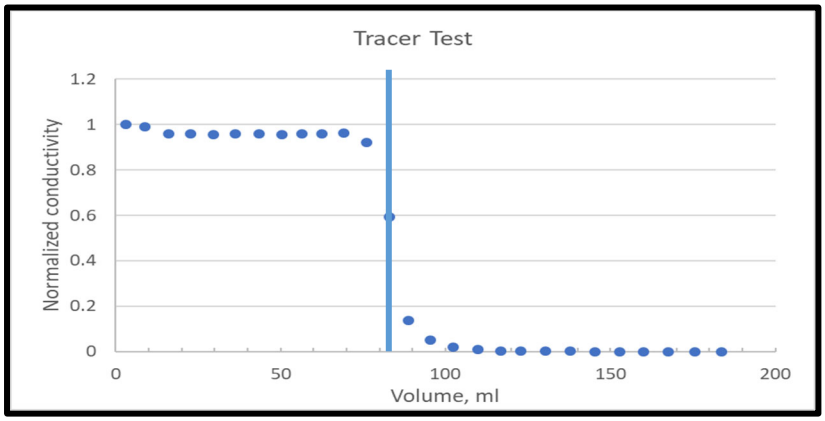

Figure 5: Tracer test to determine pore volume and porosity of OK-75 sand pack.

Case (B): Repeated AFFF Applications to C2 Soil Horizon.

A second series of column tests was prepared using the C2 soil horizon. PFAS retention and retardation was determined during four successive applications of 3% AFFF-1 (recommended dilution for firefighting). The C2 horizon soil is composed of 96.5 wt.% quartz sand with 3.2 wt.% silt, 0.3 wt.% clay, cation exchange capacity 3.8 $cmol_c/kg$, and only 0.04 wt% organic matter. The properties of the pack are listed in Table 12, where a tracer test using isopropyl alcohol was conducted to measure the pore volume (Figure 20). Note that the pressure drop across the C2 horizon sandpack was extremely low and thus the permeability cannot be reported accurately.

Case (C): Single AFFF Application: Constant Flow.

We conducted a dynamic flow experiment to explore the potential for developing a microemulsion phase within porous media (OK-75 Sand) and the effect on AFFF retention. This test was designed to have a residual jet fuel saturation before injection the AFFF. The properties of the media are reported below in Table 3. The porosity was measured by two methods, yielding 31.1% (gravimetric) and 32% (volumetric). A constant flow of 1 ft/day (0.3 m/d) was used for AFFF-1 injection while pressure drop across the sand pack was monitored.

Table 3: Properties of the porous media used for the constant flow and constant pressure column experiments.

parameter	constant flow (Case C) (0.3 m/d)	constant pressure (Case D) (0.5 mPa)
porosity (vol.%)	31.4	35
residual water saturation (vol.%)	70.2	64
residual Jet A saturation (vol.%)	23.8	31.5
permeability, absolute (m^2)	3.4×10^{-12}	30.6×10^{-12}

Case (D): Single AFFF Application: Constant Pressure.

A 4th column test to explore the possibility of viscous phases being formed *in-situ*, similar to Case (C), but conducted using a constant pressure instead of constant flow rate. In this column experiment, the AFFF solution was injected at a constant pressure of 0.5 MPa (72 psig) and the resulting flow rate was measured.

Task 3: PFAS Transport under Unsaturated Conditions and Modeling

Task 3.1: PFAS Adsorption at the Air-Water Interface

Perfluorooctanoic acid (PFOA, perfluoroheptanoic acid (PFHpA), perfluorohexanoic acid (PFHxA), perfluoropentanoic acid (PFPeA), perfluorobutanoic acid (PFBA), perfluorooctanesulfonic acid potassium salt (PFOS), perfluorohexanesulfonic acid potassium salt (PFHxS), perfluorobutanesulfonic acid (PFBS), all at ≥96% purity, were purchased from Sigma-Aldrich. 6:2 fluorotelomer thioether amido sulfonate (FtTAoS) was obtained from a commercial source material sold under the trade name Lodyne. The Lodyne formulation consists of approximately 45% 6:2 FtTAoS, with the balance consisting primarily of water (38%) and

hexylene glycol (15%).[1] The 6:2 FtTAoS is a main component in Ansul AFFF.[2] Solutions of the individual PFAS or equimolar mixtures of the perfluoroalkyl acids (PFAAs), or PFOS with FtTAoS, were prepared in deionized water with 0.01 M NaCl. Additional solutions were prepared in the absence of salt, or with 0.001 M NaCl.

Groundwater from Wurtsmith Air Force Base, collected nearby an AFFF-impacted source area, was used in one set of air-water interfacial adsorption experiments. Groundwater parameters are provided in Table 4, and PFAS concentrations in the groundwater are provided in Table 5.

Table 4: Characteristics of the Wurtsmith groundwater

Parameter	(mg/L)
Fluoride	<0.2
Chloride	0.63
Nitrite as N	0.23
Sulfate as SO4	1.9
Bromide	<0.2
Nitrate as N	<0.2
Chlorate	<0.2
Phosphate as ortho-P	<0.2
Alkalinity as $CaCO_3$	500
Hardness as $CaCO_3$	540
Chemical Oxygen Demand	200
Total Organic Carbon	38
Total Suspended Solids (TSS)	110
Turbidity	170 NTU

Table 5: PFAS concentrations in the Wurtsmith groundwater

PFAS	Concentration (µg/L)
PFOA	19
PFHxS	54
PFOS	1100
FHxSA	1100
MeFOSAA	280
6:2 FTS	94
8:2 FTS	450
6:2 $FTSO_2PrAd$-DiMeEtS	75
8:2 $FTSO_2PrAd$-DiMeEtS	990
TAmPr-FHxSA	8.6

Interfacial Tension Experiments

Interfacial tensions of the PFAS solutions were determined using the pendant drop method.[3] A Biolin Scientific Theta Lite tensiometer was used to measure the surface tension of the various PFAS solutions, at concentrations ranging from 0 (deionized water or NaCl solution only) to 100

mol m^{-3}. Interfacial tension measurements were performed in triplicate for each concentration and solution.

Film Experiments

To directly measure PFAS uptake at the air-water interface at environmentally relevant concentration, and at levels below which accurate interfacial tensions measurements can be made, experiments were performed in high density polyethylene (HDPE) cylindrical vessels with a 25 cm diameter and 4 cm deep. The film experimental system is shown in Figure 6. A hole was drilled in the bottom of the vessel and fitted with a threaded coupler and a luer-lok valve to facilitate drainage of the PFAS solutions.

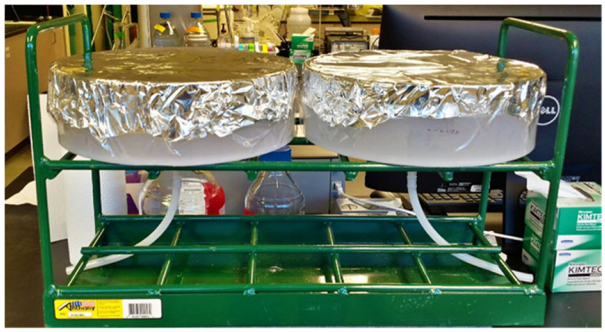

PFAS-spiked water equilibrated in HDPE pans

PFAS measured in bulk water (via drained water), then in bulk water + air-water interface (via collection of water film)

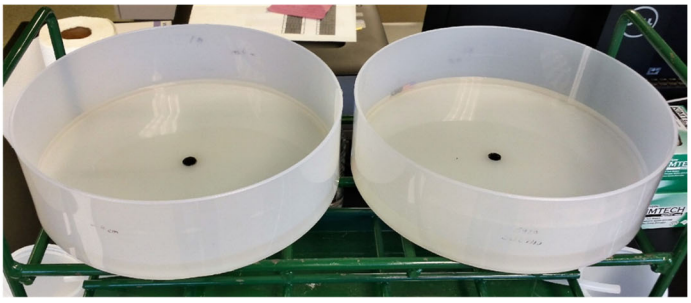

Figure 6: Film experiments to measure PFAS adsorption at the air-water interface.

The vessels initially were filled with approximately 2.2 L of the desired PFAS solution. The solutions were covered with aluminum foil to limit water evaporation, and equilibrated in the vessels for 3 days at approximately 20 °C. Following equilibration, the PFAS solution was drained from the vessel so that only a water film (approximately 0.5 cm in depth, and a volume of approximately 300 mL) remained in the vessel. Both the solution that was drained from the vessel, and the film in the vessel (collected by pouring the film from the vessel), were collected in HDPE bottles and sent to SGS-AXYS Analytical Services, Ltd in Canada for analysis of PFAAs. Experiments were performed with PFOS only, with an equimolar mixture of PFAAs, and with

PFOS + FtTAoS. PFOS-only experiments also were performed in the presence of various NaCl concentrations, and with the Wurtsmith groundwater.

The PFAS sorbed at the air-water interface was determined by mass balance as follows:

$$\Gamma = \frac{M_f - CV}{A} \qquad \text{Eq. 3.1}$$

where Γ is the moles PFAS sorbed at the air-water interface per unit area (mol m^{-2}), M_f is the molar mass of PFAS in the collected film (mol), C is the PFAS concentration in the aqueous phase measured in the water collected from the drained sample (mol m^{-3}), V is the volume of water in the film (m^3), and A is the air-water interfacial area in the vessel (m^2). All experiments were performed in at least duplicate. Experiments performed using a 6-day equilibration time (both drained water and film analyzed at 6 days) showed no additional PFAS interfacial sorption than those performed at 3 days.

To verify that any PFOS adsorption to the HDPE could be neglected, parallel experiments were performed in HDPE tubes (20 cm long, 1 cm diam.) filled with PFAS solution and capped on either end to limit air-water interfaces. Following 4 days equilibration, no measurable decreases in PFOS aqueous concentrations (compared to that in the initial aqueous solution before filling the tubes) were observed, indicating that any sorption to HDPE could be neglected.

Determination of PFAS Uptake at the Air-Water Interface

In the presence of background ions, the molar mass sorbed at the air-water interface is related to the air-water interfacial tension, assuming ideal solutions in the aqueous phase, by the following form of the Gibbs Adsorption Equation:[4,5]

$$\Gamma = \frac{-1}{RT}\frac{\partial \sigma}{\partial ln[C_T]} \qquad \text{Eq. 3.2}$$

$$C_T = C\,(C + C_s) \qquad \text{Eq. 3.3}$$

where σ is the measured air-water interfacial tension (mN m^{-1}), C_T is the square of the mean ionic activity ([mol m^{-3}]^2), C_s is the concentration of background NaCl (mol m^{-3}), R is the gas constant (8310 mJ mol^{-1} K^{-1}), and T is the temperature (293K). For dilute solutions well below the critical micelle concentrations and below monolayer coverage at the air-water interface (which was the case for the work performed herein), a theoretical basis has been derived showing that interfacial sorption takes the form of the Freundlich model,[6,7] where

$$\Gamma = k(C_T)^n \qquad \text{Eq. 3.4}$$

where k and n are constants. Combining Eqs. 3.2 through 3.4 and integrating, the interfacial tension can be described as a function of the PFAS and background NaCl concentrations:

$$\sigma = \sigma_0 - RTk\frac{C_T^n}{n} \quad \text{Eq. 3.5}$$

where σ_0 is the air-water interfacial tension in absence of PFAS. For a system with a mixture of PFAS and assuming dilute ideal behavior at the interface and in bulk solution, the interfacial sorption of the mixture can be predicted based on single component data (Eqs. 3.4 and 3.5) for N number of PFAS as follows: [8]

$$\Gamma = \sum_{i=1}^{N} k_i C_{T,i}^{n_i} \quad \text{Eq. 3.6}$$

where k_i and n_i are obtained from the single component interfacial tension experiments for PFAS component i (Eq. 3.5), and Γ in the mixed system refers to the total PFAS sorbed at the interface.

Employing a similar approach to that used for deriving Eqs. 3.4 and 3.5, but using the Langmuir adsorption isotherm, a form of the Szyszkowski Equation can also be used to relate the decrease in air-water interfacial to PFAS surface adsorption: [4,9]

$$\Gamma = = \frac{\Gamma_m \alpha C_T}{1+\alpha C_T} \quad \text{Eq. 3.7}$$

$$\sigma = \sigma_0 - RT\Gamma_m ln[1 + \alpha C_T] \quad \text{Eq. 3.8}$$

where Γ_m is the interfacial sorption capacity (mol m^{-2}) and α is the adsorption affinity coefficient ($[m^3\ mol^{-1}]^2$). Eqs. 7 and 8 assume that the Langmuir isotherm, rather than the Freundlich isotherm, is appropriate for describing PFAS adsorption at the air-water interface.

To describe PFAS partitioning between the bulk aqueous phase and the air water interface at a given aqueous concentration, the following constant is defined: [10]

$$k_{aw} = \frac{\Gamma}{C} \quad \text{Eq. 3.9}$$

where k_{aw} is the air-water interfacial sorption coefficient (m).

Task 3.2: PFAS Unsaturated Soil Transport

Three one-meter long columns with five by seven centimeter rectangular cross sections were constructed to evaluate the transport of conservative tracers and PFAS in variably saturated porous

media. The one-meter long column design was chosen to increase the residence time of PFAS and promote unit gradient conditions throughout the unsaturated soil columns. The rectangular cross section design was chosen to facilitate the use of x-ray absorption spectroscopy and water content/electrical conductivity sensors. METER 5TE water content, temperature, and electrical conductivity sensors were strategically placed 10 cm from the top, the center, and 10 cm from the bottom of the column. The sensors recorded measurements every 5 min and were used to monitor the breakthrough of conservative salt tracers and ensure uniform water content along the length of the column. All experiments were conducted under ambient temperatures (25 ± 3 °C) to ensure environmentally relevant transport conditions were observed. Constant, steady flow was maintained using peristaltic pumps and the inlet and outlets of the columns.

A single 15.6 cm long column with a diameter of 2.5 cm was constructed to evaluate the movement of conservative tracers and a well-studied surfactant (sodium dodecyl benzene sulfonate - SDBS). The small column was monitored by conductivity sensors at the outflow and had constant flow maintained using peristaltic pumps at the inlet and outlet of the column. The purpose of the small columns was to obtain baseline transport information (e.g., air-water interfacial areas of quasi-saturated conditions) for the sands in this study prior to long column PFAS testing.

Two types of sand were used to evaluate the transport of PFAS in porous media. The first was a highly uniform (C_u < 1.5), medium grained (0.5 mm > d_{50} > 0.250), ideal sand (> 99.6 % silicon dioxide) with rounded grains. Sands of this nature are known to be highly ideal under saturated conditions, with negligible interparticle or intraparticle diffusion limited transport domains, otherwise referred to as non-Fickian transport. The high silica purity also ensured negligible solid phase sorption was present in the system. This ideal sand was used for to evaluate the transport properties of a single component PFAS mixture (PFOS) in highly idealized conditions. The second sand used was a non-uniform (C_u >1.9), fine grained (0.25 mm > d_{50} > 0.125), non-ideal sand (<90% SiO_2) with sub-angular grains. The lower degree of uniformity, surface roughness, and smaller grain sizes promotes the formation of diffusion limited immobile domains, otherwise referred to as non-Fickian transport, in saturated and unsaturated conditions. The lower degree of silica purity also promotes the sorption of PFAS to the solid phase. This non-ideal sand was chosen to observe the transport of a single component PFAS under more realistic conditions.

Two sets of PFAS mixtures were used in this study. Single component mixtures of PFOS in low ionic strength ($8.0 * 10^{-5}$ M) water was used in column studies with the highly ideal sandy media. These studies were conducted as a baseline to examine the air-water interfacial partitioning of well-known PFAS under ideal and non-ideal saturation conditions. The second PFAS mixture was a mixture of contaminated natural groundwaters that were highly impacted from PFAS manufacturing and from AFFF. This natural groundwater mixture had an ionic strength of 0.0036 M, and was well characterized prior to receiving the groundwater. A synthetic groundwater mixture was prepared which mimicked the ionic composition of the groundwater. The synthetic

groundwater was applied prior to the PFAS injection into the column and afterwards until the end of the experiment to endure no differential transport behavior occurred due to reductions in ionic strength.

Column Methods

The conservative tracer used for all transport experiments was 0.01 M NaCl. Sodium chloride is well known to be a conservative tracer in most sandy media and showed no solid phase retention in batch testing. A well-studied surfactant, SDBS, was used to determine the air-water interfacial area of quasi-saturated conditions in small column studies. SDBS is known to have a K_{ia} of 0.00304 cm when present in 0.01M NaCl at a concentration of 0.1M.[17,18] The conservative tracers, SDBS, and PFOS/PFAS mixtures were applied to the top of the column at a known concentration for a finite period of time. A form of the ADE modified to account for a pulse of finite duration was used to fit the BTC data in order to solve for the retardation factor and account for conservation of mass. All BTCs are presented in terms of pore volumes determined by through conservative tracer tests.

X-ray System

Through careful experimentation by controlling and accurately measuring saturation along the test column and thorough literature review, we found these physical transport parameters are directly correlated with the porous media properties, the degree of saturation, and the flow velocity of the wetting phase. This new technique is a significant contribution to the parametrization of transport of solutes in the unsaturated zone, and will give us more confidence to when measuring multi-phase partitioning of PFAS. Experiments were conducted in a specially fabricated Plexiglas soil column (Figure 7). As designed, this setup allowed us to dynamically monitor the water saturation along the length of the column, the transport of the dissolved chemical along the length of the column, and the breakthrough at the end of the column. The test setup consisted of the following components: (1) A 1.1 m long, 7cm wide, and 5 cm thick rectangular column mounted on a platform of traversing x-ray system, (2) a traversing x-ray system that consists of an x-ray source and a detector mounted across the soil sample (3) an outflow line that can be used to sample the effluent. All the experimental techniques needed to generate high temporal and spatial resolution data have been developed in our past and ongoing research. The x-ray attenuation system works on the Beer-Lambert relation between intensities of photons entering and leaving the sample that can be used to measure the path lengths of different materials attenuating the photons. In a two-phase system, the wetting and non-wetting fluid saturations can be estimated using the path lengths, In the case of unsaturated soils, the method allows for the measurement of water and air saturations.

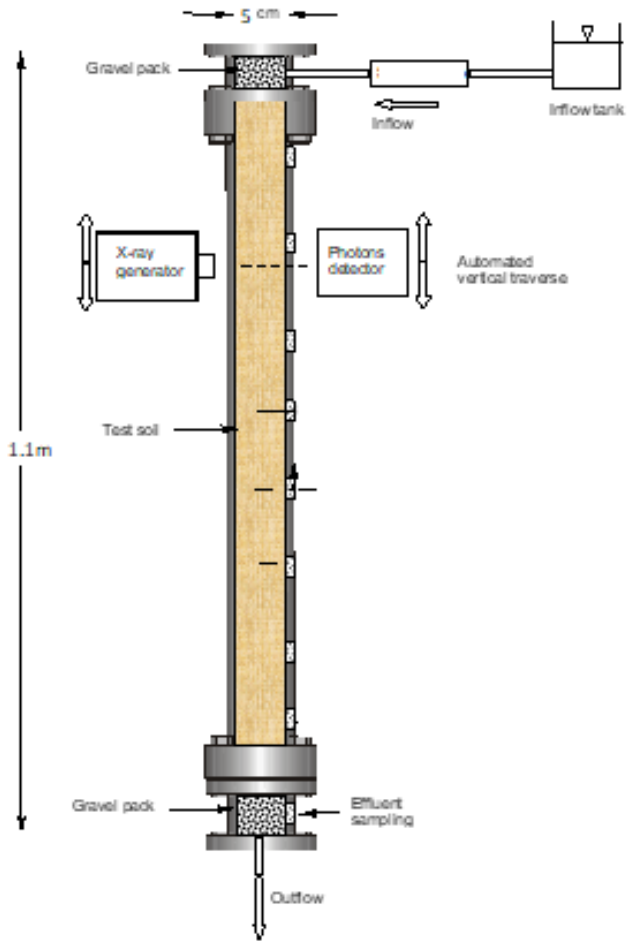

Figure 7: Setup consists of a long column with controlled flow and soil war content monitored by x-ray attenuation.

Results from the x-ray absorbance system and the 5TE soil moisture sensors show that we are able to precisely control the flow and degree of saturation in the 0.35mm sand for several days at a time. The x-ray system gives high spatial resolution measurements in the soil column while the 5TE moisture sensors give high temporal resolution measurements of conductivity, temperature, and water content. This allows us to confirm the soil columns have both uniform water content and steady state flow, validating the steady-state and equilibrium assumptions used in preliminary models. An image X-ray scans of three different soil columns is presented in Figure 8.

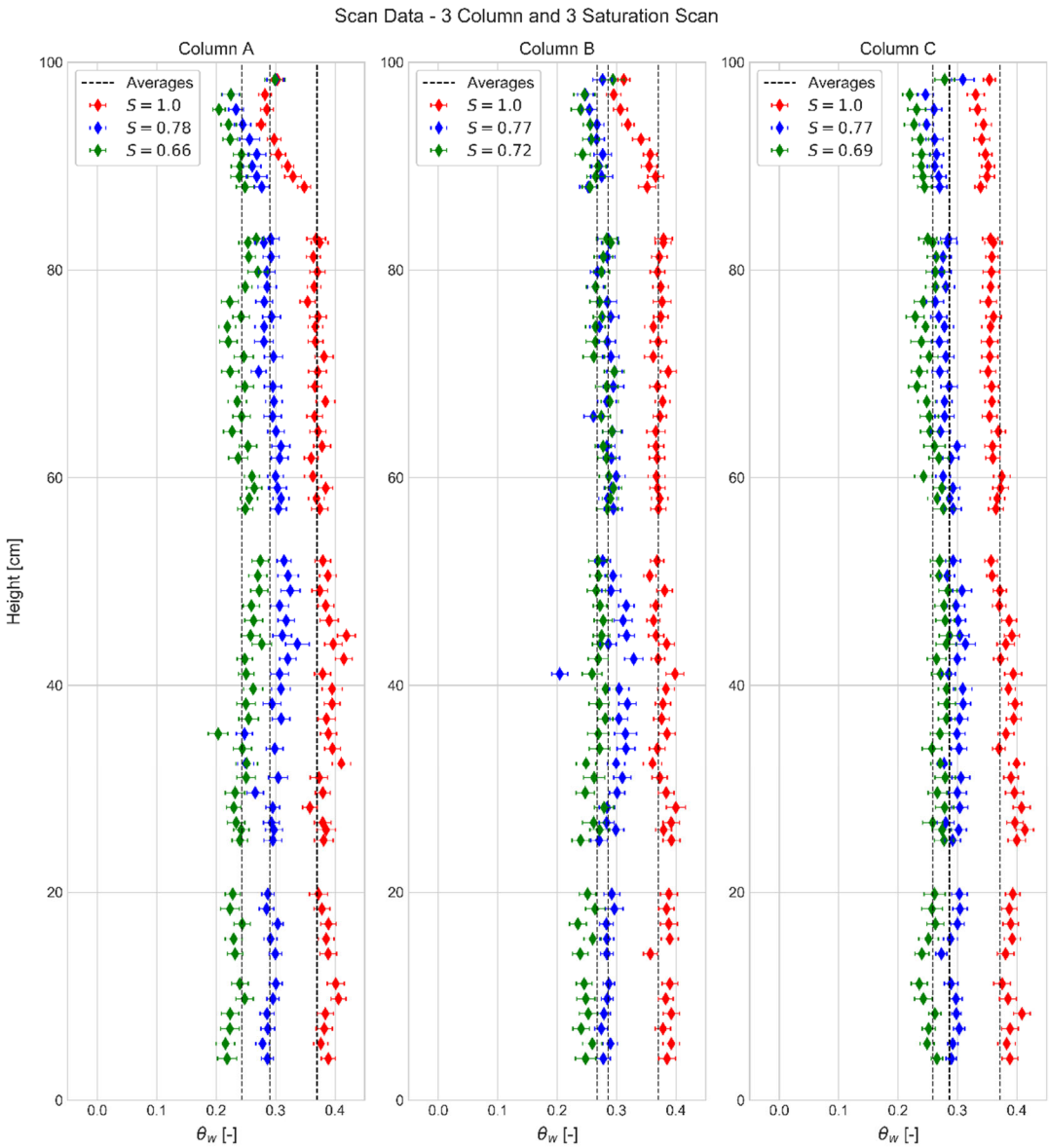

Figure 8: X-ray attenuation observations of water content during for three columns during three different conservative tracer experiments conducted at high, medium, and low saturations respectively.

Breakthrough Curve Analysis

All breakthrough curve analysis of the long and short columns was conducted using an analytical solution of the ADE modified to incorporate the mass transfer index (MTI). The MTI is used to correct non-dimensional time to pore volumes, thereby providing a more accurate estimation of the retardation factor and providing a simple quantification of potential transport non-idealities.

The MTI modified ADE is presented in Equation 3.11, dimensional analytical solutions are presented in Stults et al. 2021: [19]

$$TR\frac{\partial C_{aq}}{\partial t} = -v\frac{\partial C_{aq}}{\partial x} + D\frac{\partial^2 C_{aq}}{\partial x^2} \quad \text{(Eq. 3.11)}$$

where T is the Mass Transfer Index (MTI), R is the retardation factor, C_{aq} is the aqueous phase concentration of solute, t is time, v is the measured linear pore velocity, x is the longitudinal length along the column, and D is the macroscopic coefficient of dispersion. Any solution of the ADE for step function input can be easily modified to a pulse of finite duration using the principle of linear superposition as demonstrated in Runkel 1996.[20] The column- and experiment-specific tracer-based MTI values and PFOS R values were determined by fitting the BTCs using a non-dimensional form of the ADE to solve for R and Peclet number.[19,21,22] This is the mathematical foundation for the method of moments for calculating R.[21,22] The concepts behind the MTI formulation of the ADE is developed below. The correlation between the retardation factors and multi-phase partitioning (solid phase and air-water interface) were calculated using the correlation in Equation 2 as presented in Brusseau 2018,[23] which was determined from breakthrough curve analysis using an non-dimensional form of the MTI modified ADE presented in Equation 3.12:[19]

$$R = 1 + \frac{K_d \rho_b}{\theta_w} + \frac{K_{ia} A_{aw}}{\theta_w} \quad \text{(Eq. 3.12)}$$

where K_d is the solid phase partitioning parameter, ρ_b is the solid phase bulk density, θ_w is the measured water content of the media, K_{ia} is the equilibrium air-water interfacial partitioning parameter, and A_{aw} is the air-water interfacial area of the unsaturated conditions.

Air-water interfacial areas of the quasi-saturated conditions were calculated using the retardation factor for SDBS, as the K_{ia} of SDBS is well known for the experimental conditions in this study. No information is available on the air-water interfacial areas of quasi-saturated conditions to the best of our knowledge. A linear relationship between saturation and air-water interfacial area has been demonstrated for high end saturation of primary drainage conditions.[24–27] A variation on this linear relationship is presented in Equation 3.13, and was proposed for applicability at the various quasi-saturations in this media using the small column experiments:

$$A_{aw} = A_{aw,max-q}(1 - S) \quad \text{(Eq. 3.13)}$$

where A_{aw} is the air-water interfacial area of quasi-saturation, $A_{aw,max-q}$ is the theoretical maximum interfacial-area of quasi-saturation, and S is the degree of saturation as a fraction of the measured water content (θ_w) over the total porosity (ϕ) of the media at quasi-saturation conditions. The air

water interfacial areas of drainage conditions were estimated using previously published grain size correlations. The correlation used is presented in Equation 3.14:

$$A_{aw} = \frac{3.9}{(d_{50})^{1.2}}(1 - S) \qquad \text{(Eq. 3.14)}$$

where the d_{50} is the median grain diameter in cm.

Task 3.3: PFAS Unsaturated Transport Modeling

Calculating Advective Flow Path Tortuosity Using the MTI Concept & Mobile-Immobile Model (MIM)

The MTI model developed was intended as a proof-of-concept study using an idealized sand with no mass transfer limitations or chemical retardation. The underlying hypothesis of this study was that when no mass transfer limitations are present, advective flow path tortuosity and mass transfer into and out of immobile zones will produce the same effect on the breakthrough curve. Therefore, in sands with mass transfer limitations, it is possible the T value will no longer follow a well correlated power law type relationship with effective saturation. However, when mass transfer limitations are present, we can use the Mobile Immobile Model (MIM) to directly calculate the mass transfer rate and mobile volume fraction. This information allows us to calculate the advective tortuosity for the media, which should follow a similar inverse power law type relationship. A key citation, Padilla et al.[33] performed a similar study to ours in an idealized sand with mass transfer limitations. The data from Padilla et al. can be used to demonstrate how the concepts from the MTI model can be scaled into a larger and more robust model.

Herein, we first demonstrate the concept of advective flow path using a simple mass balance on a finite fluid element. To satisfy the conditions of mass balance for a steady state system, the average linear water velocity must be equal to the Darcy flux divided by the mobile water content. However, under experimental conditions, we note this relationship between Darcy flux and water content is often incorrect, and use the concept of "effective porosity" to account for this discrepancy. To satisfy the conditions of this mass balance, we must recall that the macroscopic conception of linear pore-velocity determined by the moment method only accounts for flux in the direction normal to the plane of 1-D flow. Therefore, the conditions of mass balance can be satisfied when we consider that the water flux in a system is not necessarily normal to the plane of 1-D advective flux. A simple trigonometric relationship is developed in Figure 9 to calculate advective tortuosity and satisfy mass balance.

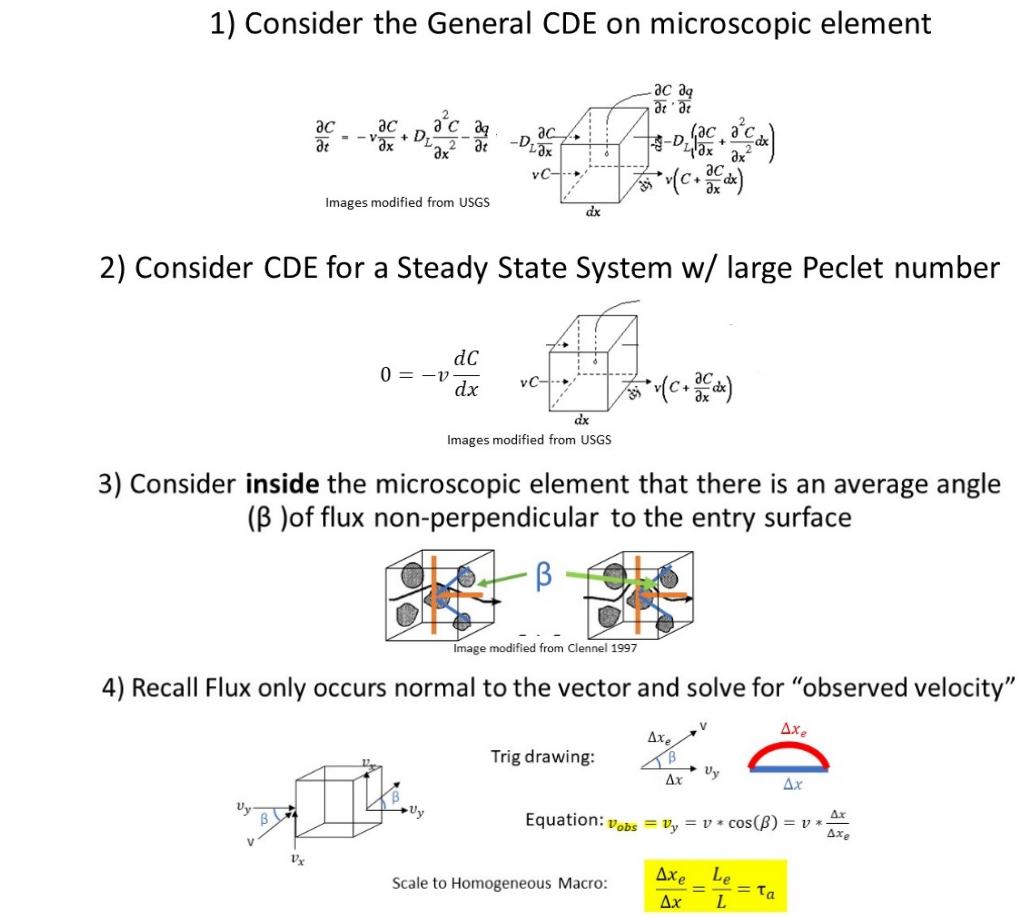

Figure 9: Mass balance on a finite fluid element for calculating advective tortuosity.

Under equilibrium conditions, instantaneous solute mass transfer into immobile zones has the same effect on the BTC (delaying the predicted emergence of the BTC) as advective tortuosity. If solute exchange effects are minimal and the tortuosity of the mobile phase is small, one might actually observe early emergence of the solute plume under equilibrium conditions. Table 1 of Padilla et al. (1999) was used to calculate the MTI (*T*) values for all the 16 experiments in the study at varying degrees of effective saturation. This was done by simply taking the ratio of the predicted velocity (Padilla et al. 1999, column 4 – table 1) to the moment velocity (Padilla et al. 1999, column 8 table 1). Equation 3.19 presents the calculation for the MTI (*T)* based on the advective tortuosity concept established here and main concepts established in the above:

$$T = \frac{L_e}{L} = \frac{t_{actual}}{t_{pred}} = \frac{v_{pred}}{v_{moment}} = b * (S_e)^n \qquad \text{(Eq. 3.19)}$$

While the MTI (T) calculation is valid for a system without mass transfer limitations, this

relationship is not expected to hold for systems with mass transfer limitations. However, based on the concepts developed in the MTI theory, it should be possible to separate the effects solute mass transfer in and out of immobile zones from that of advective tortuosity when mass transfer limitations are present. Padilla et al. 1999 is an excellent study to test this hypothesis, because they observed mass transfer limitations in their sand used the MIM to calculate the mobile water fraction/mass transfer coefficient. To calculate advective tortuosity using the MIM model we simply take the predicted pore velocity (Padilla et al. 1999, column 8 table 1), divide it by the fraction of the water content which is mobile in pore space (Padilla et al. 1999, Table 2 – column 6). This is done because in the original prediction of the linear pore velocity (Padilla et al. 1999, column 8 table 1) it was assumed all pore space is mobile. Next, the modified predicted velocity was divided by the macroscopic velocity predicted by the MIM to get the advective tortuosity. The equation for modifying the predicted velocity from MIM results is presented in Equation 3.20, and the calculation for advective tortuosity is presented in Equation 3.21:

$$v_{pred,MIM} = \frac{q}{f_{mobile} * \theta_w} = \frac{v_{pred}}{f_{mobile}} \quad \text{(Eq. 3.20)}$$

$$\tau_a = \frac{v_{pred}}{f_{mobile}} \left(\frac{1}{v_{MIM}}\right) = b_a * (S_e)^{n_a} \quad \text{(Eq. 3.21)}$$

Inversion of Non-Equilibrium HYDRUS Models

The Equations for the Retardation Factor for the Freundlich/Linear Isotherm and the Langmuir/Linear isotherm requires setting the multi-phase partitioning retardation factors for each case equal. Because the K_d for sand in these experiments was calculated to be negligible within a 95% confidence interval, the solid phase partitioning parameter was removed from all sides of the Retardation Factor equation. The resulting equivalence of all three isotherms are presented in Equations 3.22a-b respectively, and was used as an empirical method of evaluating the appropriateness of the Langmuir model and Freundlich regressions. The linearity of the low concentration Langmuir Isotherm is evident in Equation 3.22a-b, as the denominator has the following limit $\lim_{C_{aq} \to 0} \left(1 + \eta C_{aq}\right)^2 = 1$:

$$R_{linear} = 1 + \frac{K_{ia} A_{aw}}{\theta_w} = \begin{cases} R_{Freundlich} = 1 + \frac{n K_f (C_{aq})^{n-1} A_{aw}}{\theta_w} \\ R_{Langmuir} = 1 + \frac{q_{max} \eta A_{aw}}{(1+\eta C_{aq})^2 \theta_w} \end{cases} \quad \text{(Eq. 3.22a)}$$

$$K_{ia} = \begin{cases} nK_f C^{n-1}, Freundlich \\ \frac{q_{max}\eta}{(1+\eta C_{aq})^2}, Langmuir \end{cases} \quad \text{(Eq. 3.22b)}$$

where R_{linear} is the linear isotherm retardation factor, $R_{Freundlich}$ is the Freundlich Retardation factor, R_{lang} is the Langmuir isotherm Retardation Factor, K_{ia} is the linear isotherm air-water interfacial

partitioning parameter, A_{aw} is the air-water interfacial area, θ_w is the water content of the porous media, n is the exponent of the Freundlich isotherm, K_f is Freundlich air-water interfacial partitioning parameter, q_{max} is the maximum surface site sorption parameter of the Langmuir isotherm, η is the non-linear adjustment parameter of the Langmuir isotherm, and C_{aq} is the aqueous concentration. The Equations 3.22a-b were used in both the equilibrium and non-equilibrium transport equations available in HYDRUS, modified to incorporate the MTI. Equations 3.23a-b are the non-equilibrium transport equations as adapted from Van Genuchten et al. 1976: [46]

$$\left(1+\frac{fA_{aw}K_{ia}}{\theta_w}\right)\frac{\partial C_{aq}}{\partial t}=-\frac{v}{T}\frac{\partial C_{aq}}{\partial x}+\frac{D_m}{T}\frac{\partial^2 C_{aq}}{\partial x^2}-\frac{\alpha A_{Aw}}{\theta_w}\left[(1-f)K_{ia}C_{aq}-C_s\right] \quad \text{(Eq. 3.23a)}$$

$$\frac{\partial C_s}{\partial t}=\alpha\left[(1-f)K_{ia}C_{aq}-C_s\right] \quad \text{(Eq. 3.23b)}$$

where T is the Mass Transfer Index (MTI),[19] R is the generalized retardation factor term, Pe is the Peclet Number defined as the ratio of the measured linear pore velocity times the characteristic length scale over the MTI modified macroscopic coefficient of dispersion $\left(\frac{vL}{D}\right)$, L is the characteristic length scale, v is the macroscopic linear pore velocity, D_m is the MTI modified macroscopic coefficient of dispersion,[19] t is measured time, q is the measured Darcy Flux, θ_w is the measured water content, C_{aq} is the aqueous concentration of the solute, f is the fraction of equilibrium sorption sites, α is the rate limited air-water interfacial partitioning parameter, K_{ia} is the air-water interfacial partitioning parameter, and C_s is the concentration of rate-limited sorbed solute at the air water interface. K_{ia} in Equations 3.23a-b can be substituted for the Freundlich or Langmuir isotherms using the relationships developed in Equations 3.22a-b.

Empirical Evaluation of non-Equilibrium Partitioning Using Apparent Partitioning Coefficients

Because rate-limited partitioning was present some of the systems evaluated, equilibrium K_d or K_{ia} values determined from the standard Retardation factor are not necessarily valid. The standard retardation factor equation can be modified slightly to incorporate the 'apparent' partitioning parameter. The apparent partitioning parameter suggests this is merely what is calculated using the equilibrium ADE, and may be an underestimation of the equilibrium partitioning value. This modified Retardation factor equation is presented in Equation 3.24:

$$R=1+\frac{K_{d,app}\rho_b}{\theta_w}+\frac{K_{ia,app}A_{aw}}{\theta_w} \quad \text{(Eq. 3.24)}$$

where R is the retardation factor, $K_{d,app}$ is the apparent solid phase sorption parameter, ρ_b is the bulk density of the solid phase, θ_w is the measured water content of the system, $K_{ia,app}$ is the apparent air-water interfacial partitioning coefficient, and A_{aw} is the specific air-water interfacial area. Note

that $K_{d,app}$ and $K_{ia,app}$ are equal to K_d and K_{ia} under equilibrium conditions but are significantly less than K_d and K_{ia} when rate-limited partitioning is present. The 95% confidence interval of the measured R, $K_{d,app}$ and $K_{ia,app}$ values are calculated using the average and standard deviation of values from replicate experiments with identical conditions (i.e. flow rate). Air water interfacial areas of the quasi-saturated condition were fitted to saturation using the Equation S.1 correlation and calculated retardation factor from Equation 3.24 as successfully demonstrated in a Stults et al. 2022.[72]

The modified form of the 1-D ADE incorporating the non-equilibrium retardation factor was used to estimate the estimate the MTI[19] and residence time of conservative tracer data and estimate the retardation of PFAS in this system.[72] The conversion of non-dimensional time to pore volumes using the MTI is presented in Equation 3.25a, the non-dimensional analytical solution to the 1-D MTI modified ADE for step function input is presented in Equation 3.25b:

$$PV = \frac{Non-Dimensional\ Time}{T} = \frac{q*t}{\theta_w*L}\left(\frac{1}{T}\right) \quad \text{(Eq. 3.25a)}$$

$$\frac{C_{aq}}{C_{aq,0}}(PV, Pe, R) = 0.5 * \left[erfc\left(\frac{R-PV}{sqrt\left(\frac{4*R*PV}{Pe}\right)}\right) + \exp(Pe)\, erfc\left(\frac{R+PV}{sqrt\left(\frac{4*R*PV}{Pe}\right)}\right)\right] \quad \text{(Eq. 3.25b)}$$

where T is the MTI, , PV is pore volumes, Non-dimensional time is the ratio of Darcy flux and real time over water content and longitudinal length $\left(\frac{q*t}{\theta_w*L}\right)$, v is the measured linear pore velocity (i.e. length divided by conservative tracer residence time), Pe $\left(Pe = \frac{q}{\theta_w*T}\frac{L}{D} = \frac{vL}{D}\right)$ is the Peclet number defined as the ratio of the measured linear pore velocity (v). As the flow was steady, the solution of the ADE for step function input (i.e. Equation 3.25b) can be easily modified to a pulse of finite duration using the principle of linear superposition as demonstrated in Runkel 1996[20] and our prior publications.[19,72]

To date, only Lyu et al. 2018[10] examined the change in $K_{ia,app}$ as a function of linear pore velocity. Analysis of Lyu et al. 2018[10] data demonstrates that the $K_{ia,app}$ of measured by the authors could be well-fit using and exponential regression utilizing the equilibrium K_{ia}, the linear pore velocity, and a single fitting parameter. This empirical correlation is presented in Equation 3.26:

$$K_{ia,app} = K_{ia} * \exp\,(v * -a) \quad \text{(Eq. 3.26)}$$

where, v is the measured linear pore velocity and a is the empirical fitting parameter. This empirical fitting parameter is appropriate because it is well-demonstrated that higher linear pore velocities are associated with lower residences time and result in lower measured Retardation coefficients. The empirical function presented in Equation 3.26 satisfies this requirement. Further, the empirical

correlation satisfies the limiting conditions of low linear pore velocities (i.e. $\lim_{v\to 0} K_{ia,app}(v) = K_{ia}$) and high linear pore velocities (i.e. $\lim_{v\to \infty} K_{ia,app}(v) = 0$).

Python-Based Machine Learning Tools

The Sci-Kit Learn[79] poly parameter linear regression module was used to fit the $\log_{10}(K_{ia})$ data to eight PFAS characteristics related to hydrophobicity and concentration (Table 19, results below), some of which were specific to these experiments (Molar Volume, Total Chain Number, Longest Chain Number, Longest Fluorinated Chain Number, C18 Retention Time, in minutes the ΔG_0 and $K_{iw,0}$ as estimated in Le et al. 2021[80], and log base 10 of the concentration in ng/L). These parameters were correlated with equilibrium air-water interfacial partitioning values. All possible combinations (246 combinations in total) of the eight parameters were tested as ppQSPRs for quantifying K_{ia} from physiochemical characteristics of PFAS. Because over-parameterization is a concern when developing multi-parametric relationships, adjusted R^2 analysis was used to ensure that the models were not over specified. Standard correlation analysis (R^2) and variable appearance rates were used to select the most appropriate models for quantifying air-water interfacial partitioning of PFAS from their physicochemical characteristics. The same process was repeated for non-equilibrium data to determine what physicochemical characteristics contribute to non-equilibrium air-water interfacial partitioning

Results and Discussion

Task 1: Mechanisms of PFAS retention in Saturated Soil Systems

Task 1.1. Detailed Soil/Sediment Characterization

Soil characterization and extent

The soil horizons collected from Oscoda-Wurtsmith AFB were by in large characterized by high sand content (greater than 90%), low clay content (3 to 5%) and very little organic carbon (OC; maximum of 0.28%). Complete soil characterization results are presented in Table 6. In an effort to find similar soils to the one collected from the Oscoda-Wurtsmith AFB, a non-exhaustive search was done using publicly available soil survey data. As a result of this search we found 15 other soils with very similar physical and chemical characteristics (e.g. high sand content and low OC content) that also contained PFAS source zones that were near or around existing airports or military installations (Table 7). These locations may be PFAS source zones at which results generated in Task 1.2 could be applied.

Table 6: Physical and chemical properties of the four soil horizons used in this study

Horizon	Dominant Mineral Type[a]	CEC[b]	OC	N	FeOx[c]	Sand	Silt	Clay	Surface area[d]	Dominant OC functional group[e]
		cmol kg^{-1}	%	%	g kg^{-1}	%	%	%	m^2 g^{-1}	
E	Quartz	0.81	0.15	0.001	4.6	95.2	1.3	3.5	1.4	C-H
B	Quartz	1.71	0.28	0.008	7.6	93.4	1.7	5	2.6	C-H
C1	Quartz	0.60	0.05	0.002	1.3	96.5	0.3	3.2	0.9	C-H
C2	Quartz	0.38	0.01	0	1.0	96.5	0.3	3.2	0.7	C-H

[a]Measured using x-ray diffraction analysis
[b]CEC: cation exchange capacity
[c]FeOX: oxalate extractable iron oxide content
[d]Specific surface areas were measured using the Brunauer-Emmett-Teller (BET N_2) method
[e]Measured via T-FTIR and PA-FTIR spectroscopy; OC mainly characterized by aliphatic-type (C-H stretching) functional groups

Table 7: Locations identified with similar soil properties to Oscoda-Wurtsmith soil and known PFAS contamination

Location	**State**
Eielson	AK
Elmendorf	AK
Robins	GA
Vandenbug	CA
Eglin	FL
Saufley Field	FL
Tyndall	FL
Fort Kamehameha	HI
Lakehurst	NJ
Wright-Patterson	OH
Portland International Airport	OR
Grand Prairie Armed Forces Reserve Complex	TX
Hill	UT
Fairchild	WA
Fort McCoy	WI

Task 1.2. Saturated Soil Column Experiments

Molecular cohorts of PFAS in AFFF.

When surveyed for commonalities in retention behavior, the 34 PFAS were found to loosely sort into two large molecular cohorts (Figure 10). Across the four soil horizons examined, mass retained (M_R) was between 0 and ~15% for PFAS with three, four, and five fluorinated carbons and generally below 30% for all anionic PFAS with less than 8 fluorinated carbons, and complete (= 100%) retention was a rare exception even for those that had 8 fluorinated carbons (Figure 10).

The opposite applied to the cohort of PFAS with additional, positively charged functional groups (often designated "zwitterions" as per community convention). In the case of zwitterionic PFAS, complete retention was the norm (Figure 10) with a minority of instances where zwitterionic PFAS actually broke through after flowing with the equivalent of five pore volumes of water. The spread in M_R was greatest for zwitterionic PFAS with four or fewer fluorinated carbons. Zwitterions with five or more fluorinated carbons had at least 50% of their mass retained, even in the soil columns with the lowest percent OC. No mass for C6 and C7 zwitterions broke through any of the soil columns (M_R = 100%). Organic matter concentration in the soil matrix was not a predictor for the retention of anionic PFAS and clearly not the only predictor for the retention of zwitterionic PFAS.

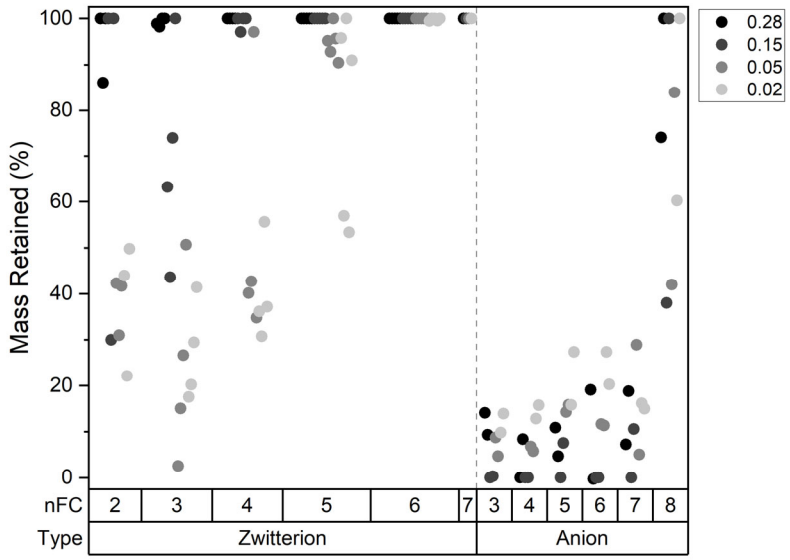

Figure 10: Mass retained for all PFAS/soil combinations (n = 136).
Mass retained data (y-axis) are organized by PFAS type (x-axis 1: zwitterions; left panel and anions; right panel) and number of fluorinated carbons (nFC) (x-axis 2). Gray scale indicates carbon concentration in

soil material, spanning the range from 0.28% to 0.02% with darker shades indicating higher C-concentrations.

Model Results and Validation.

With the absence of a single value predictor for PFAS retention, the development of a more comprehensive model was indicated. PFAS structure - soil property relationships were established for a total of 136 sorbate-sorbent combinations (34 PFAS × 4 soil horizons) and assessed for their ability to describe the total capacity of a soil of interest to retain a given PFAS molecule. This resulted in the downselection from n = 14 PFAS physiochemical and n = 9 soil predictor variables and eventually yielded the following model:

$$M_R = \{[0.204 * molar\ mass] + [0.318 * mass\ fluorine] + [c * nitrogens] + Z] \pm 16.2 \quad (1.3)$$

$$c = \{[3.5 * FeOx] + [89.7 * \%\ OC] = 22.7\} \quad (1.4)$$

$$Z = \{[0.12 * SA_{BET}] - 146\} \quad (1.5)$$

where M_R is percent mass retained of a given PFAS molecule in the soil of interest, *molar mass* is the mass of the PFAS molecule, *mass fluorine* is the total mass of fluorine on the PFAS molecule, *nitrogens* is the number of nitrogen atoms in the PFAS molecule, *FeOx* is the amount of oxalate extractable iron (g Fe kg^{-1} soil), *%OC* is the mass percentage of organic carbon in the soil, and SA_{BET} is the specific surface area of the soil (m^2 g^{-1}).

Among the downselected predictor variables (Table 8), the parameters *molar mass* and *number of nitrogens* (r^2 values of 0.51 and 0.5, respectively) dominated, but carried insufficient individual power to enable satisfactory predictions. Accordingly, consideration of the parameters: mass fluorine, *OC, FeOx* and SA_{BET} was necessary to maximize the predictive power of the model.

Table 8: Power of individual QSPR model parameters as predictors for M_R, evaluating 34 PFAS across four soil columns

		r^2	p-value
PFAS physiochemical parameters	molar mass	0.51	p<0.001
	mass fluorine	0.02	p>0.05
	number nitrogens	0.5	p<0.001
Soil properties	Organic Carbon (OC)	0.16	p<0.001
	Oxalate extractable Iron (Fe_o)	0.05	p<0.01
	Surface Area (SA_{BET})	0.05	p<0.05

	ppQSPR (combination of all variables)	0.84	p<0.001

Model predictions

Satisfactory model performance can be demonstrated by plotting actual, measured M_R as a function of predicted M_R. Figure 11 shows this plot, with the four soil horizons labeled individually.

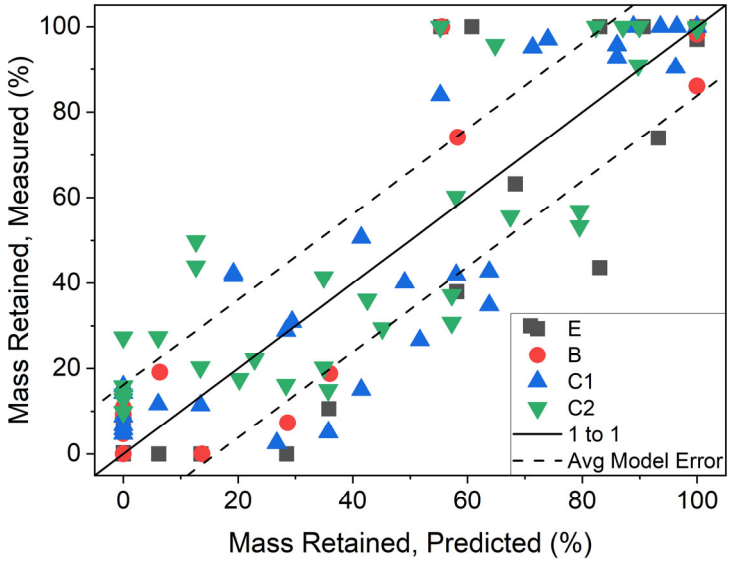

Figure 11: Actual, measured M_R plotted as a function of model prediction (M_R predicted).
Solid line represents M_R predicted = M_R measured, dashed lines indicate average error

The fact that horizon data do not cluster in certain locations of the plot validates the choice of predictor variables and confirms the general applicability of the model. Similar plots were constructed using molar mass and number of nitrogens as predictor variables, illustrating the individual weight of these variables as shown in Table 8. Doing so confirmed two basic tenets of PFAS retention: M_R will increase with molar mass, similar to Brusseau et al.[20] who observed increased partitioning at the air-water interface with increasing molar volume and with the frequency of N-containing groups.[15, 21] The latter observation can be further emphasized by examining two PFAS that have similar molar mass, but differ in N content: PFHpS (no nitrogen, molar mass = 450 g/mol) showed an average M_R across four different soil materials of 12.4%, while SPrAmPr-FPrSA (2 nitrogens, molar mass = 456 g/mol had an average M_R of 57.5%, almost four times as high.

Model Validation

Subsequently, the model was subjected to an external validation test, i.e., a material that had not been part of initial model development. To do so, the AFFF mixture was applied to n = 3 columns filled with Accusand and mass retention data collected for all 34 PFAS. Model performance was assessed through the parameters RMSE and coefficient of determination (r^2) and found to be satisfactory (Table 9).

Table 9: Root mean squared error (RMSE) and r^2 of ppQSPR model (internal validation) and external validation test to assess model performance.

	ppQSPR model (Internal)		Accusand columns (External)	
	R^2	RMSE	R^2	RMSE
All (anions+zwitterions)	0.84[a]	16.2	0.74[a]	17.8
Anions only		17.9		21.8
Zwitterions only		15.1		15.5

[a] $p < 0.001$

In a second external validation step, we took advantage of a recent study by Adamson et al.[22] who used a comprehensive hydrological modeling approach to assess the mass of PFOS retained by the soil underlying the fire training area at a naval air station. These authors calculated that after decades of exposure to AFFF, that soil still contained 40 kg of PFOS. Using publicly available soil data (https://websoilsurvey.nrcs.usda.gov) for that site, our ppQSPR model predicted that the soil would be able to retain 47.8 kg of PFOS, which is well within a margin of error of the estimate by Adamson et al.

Mechanistic considerations and plausibility of underlying assumptions

Based on free energy calculations carried out by Xiao et al.,[16] exclusion of both cations and zwitterions *from* the aqueous phase was one of the predominant driving forces for adsorption to soil surfaces. As molar mass of the PFAS increases, the thermodynamic impetus for the molecule to be expelled from the aqueous phase increases as well,[23, 24] and nitrogen represents positively charged functional groups, thus underlining the plausibility of a mechanistic contribution of these structural PFAS features.[15, 25, 26] This may apply to anions as well since Xiao et al.[16] found that both anionic and zwitterionic PFAS of the same perfluorinated carbon chain length had similar degrees of hydrophobicity. However, it is important to note the observed absence of correlation between anionic PFAS and charged soil components, suggesting that anions do not interact electrostatically with sorbent surfaces. Others have reported similar findings. For instance, Xiao et al.[16] reported that the electrostatic potential of zwitterions was several orders of magnitude higher than that of anions, leaving anions with a reduced capacity to interact electrostatically.

Using a batch study, Nguyen et al.[27] found that anion sorption was best described by a combination of %OC, silt+clay content, and micropore volume. Two of these three variables describe the amount of potential reaction space or surfaces in the soil more so than the characteristics of those surfaces (i.e. don't describe charge but how much space is available). This is in agreement with our interpretation that anions will migrate to any surface. Shafique et al.[28] found that hydrophobic exclusion was strong enough to aggregate anionic PFAS on apolar siloxane patches on the surface of silica grains. They also found that physical reorientation of the molecule was sufficient to overcome any electrostatic repulsion encountered by the head group and surface silanol groups.

Our modeling activity led to the finding that sorbent parameters *FeOx* and *%OC* were statistically related to the *number of nitrogens* parameter, meaning that they influence the retention of PFAS with both positive and negative charges but not the retention of strictly anionic PFAS. This is noteworthy as Al/Fe oxides contribute positive charge at typical soil pH ranges, while well decomposed organic matter carries net negative charge and serves as a potent cation exchange medium. Several considerations may help to constrain underlying mechanisms. For instance, charges on PFAS-zwitterions are more shielded from the electron-withdrawing F-tail by other interspaced molecules so their charges may be stronger than the negative charge on anionic PFAS. Nitrogen containing PFAS also have a hydrocarbon arm in their head group which, in contrast to the highly lipophobic fluorocarbon chain, should impart some capacity to engage in Van der Waals type interactions with hydrophobic soil components. This may contribute to the fact that zwitterion mass retained was related to percent organic carbon where no such relationship was found for anionic PFAS.

Xiao et al.[16] also hypothesized that size-exclusion and 'pore-entrapment' of PFAS may be an important retention mechanism in some size classes of soil pores. They suggested that this phenomena may be caused when PFAS are aggregated and form hemi-micelles or complete micelles. It is also plausible that when PFAS are sorbed beyond a mono-layer that a similar 'clogging' of soil pores may occur as a function of perfluorinated chain length[29] or overall molecular size.[20]

Equilibrium Sorption Mechanism

Organic carbon was tested as the sole predictor variable to describe PFAS mass retained (based on equation 1.6) using the soil partitioning coefficients derived from analysis of individual BTCs using the equilibrium model and evaluated using the criteria listed in the Methods section. The resulting K_d values were calculated using the two methods described in equations 1.1 and 1.2 and used to calculate PFAS mass retained. Breakthrough curves for two example PFAS (PFBA and PFOA) are shown in Figure 12. The equilibrium model was a good fit for C7 and shorter anions from all columns, save for PFOS, which is similar to other applications of an equilibrium model to short chain PFAS retention or breakthrough.[15, 30]

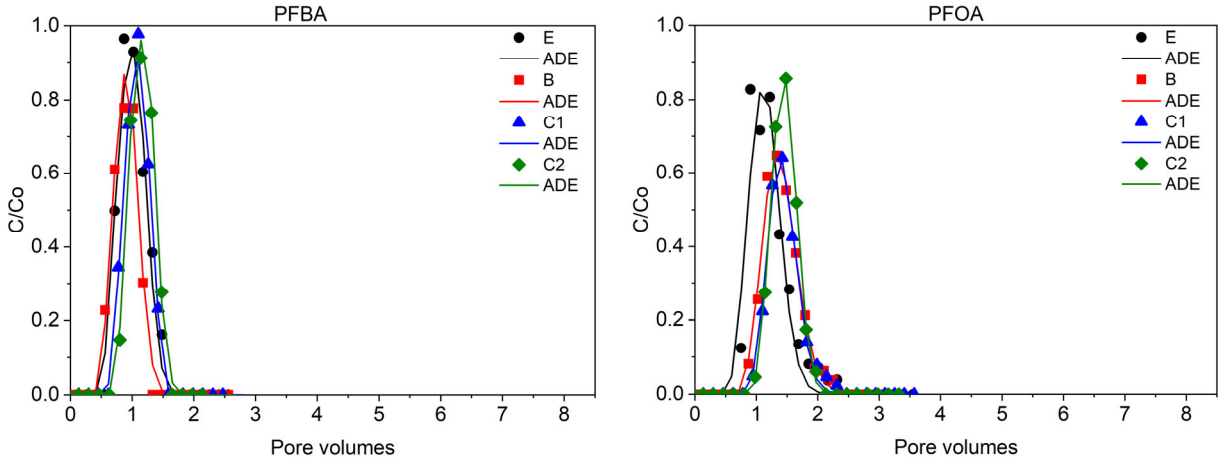

Figure 12: Breakthrough curves (BTCs) for PFBA (left) and PFOA (right) and the respective curve-fitting using the modified advection-dispersion equation (ADE) are shown.

PFAS concentration data are expressed as a fraction of the original applied concentration (C/Co; y-axis) and the number of pore volumes flowed (x-axis). Measured C/Co data points from all four soil horizon columns are shown as filled shapes (E: black circles, B: red squares, C1: blue triangles, and C2: green diamonds) and the respective ADE curve-fittings (solid lines).

With a few exceptions, M_R calculated from the BTC-derived parameters was always below that of the measured values in all soil horizons for both PFAS (Figure 13). A comparison of the average percent difference between the two methods to calculate M_R revealed that they were both in decent agreement for the E and B horizons (1.7% and 7.5% average percent difference respectively) with greater deviation in the C1 and C2 horizons (10.1% and 14.4% average percent difference respectively). Both methods show a decrease in M_R from the B to E horizons (OC decreases from 0.28% to 0.15%), however M_R shows a significant increase from the E to C1 horizons, followed by a decrease in the C2 horizon. Overall, the M_R values from both methods do not follow a trend with decreasing OC in all four soil columns as would be expected if OC were the only mechanism driving retention.

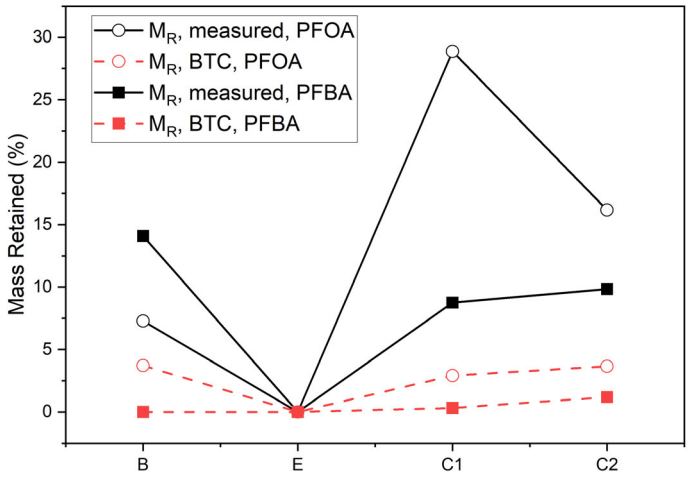

Figure 13: Comparison of two methods to determine PFAS mass retained (y-axis) as a function of soil column organized in order of decreasing organic carbon content from left to right (x-axis, B to C2).

Measured PFAS mass retained (M_R, measured; y-axis, black lines), and mass retained calculated from the fitting of the advection dispersion equation to the breakthrough curve (M_R, BTC; red dotted lines) for PFBA and PFOA. Both M_R values are compared for PFBA (closed squares) and PFOA (open circles).

Several generalizable insights were generated by our investigation of 34 PFAS from an industrial AFFF product. In terms of PFAS molecular properties, it became apparent that it is useful to distinguish between multi-ionic, amphoteric PFAS (zwitterions) and anionic PFAS when considering the propensity for retention in a soil. Among the latter group, retention is generally low until the fluorinated chain comprises at least eight (8) fluorinated C atoms. Even more important for site managers and policy makers is the observation that for anionic PFAS, soil and sediment properties from systems with little to no organic carbon or clay content have little relevance for their retention behavior. For these compounds, the overriding control on their behavior towards environmental matrices is the size of the fluorocarbon chain and the associated thermodynamic impetus to be expelled from the aqueous phase.

The situation is different for multi-ionic PFAS. For the species represented in our AFFF formulation, molar mass and the number of N atoms incorporated were the dominant molecular controls, but these substances also showed significant tendencies to actually bind with environmental matrices. Given the fact that the soil chosen for this investigation was a sandy matrix almost devoid of clay and with miniscule surface reactivity, we posit that we have been investigating the equivalent of a worst-case scenario for soil contamination with PFAS- almost any other soil matrix will retain multi-ionic PFAS to a significantly larger extent.

Finally, our research showed that the fraction of soil organic carbon present (f_{OC}) does not represent a single value predictor for retention of all PFAS in source zones[26, 27, 31, 32] and that there are other influencing variables such as the mineral phase[33, 34] or the quality of the organic carbon, which

should also be considered.[35, 36] This observation is particularly relevant given the widespread practice to derive retention characteristics from K_d values estimated from organic matter properties:

$$K_d = K_{oc}\, x\, f_{oc} \tag{1.6}$$

where K_{oc} is the organic carbon partitioning coefficient and f_{oc} is the fraction of soil organic carbon present.

Task 2: Impact of phase behavior on PFAS transport–saturated conditions

Task 2.1-Phase behavior experiments.

Microemulsions formed and appeared viscous as evidenced by the opacity or inability to view pipette gradations through liquid (Figure 14 and Figure 15). The microemulsions were immobile within the 5 mL pipettes when rotated or inverted, which also indicated that the microemulsion was viscous. Laser light appeared in the upper phase (Jet A), indicating the presence of micelles, but did not appear when shone through the lower, aqueous phase, which indicating absence of micelles. For all salinities, water-to-oil ratios, and AFFF-1 concentrations, a Winsor Type II microemulsion formed in the upper (Figure 14 and Figure 15), with the exception of the pre-foamed AFFF-1 which did not collapse to form a liquid and, hence, did not form a microemulsion. A Winsor Type II is a water-in-oil microemulsion in which surfactants and water reside within the oil phase.[14,15] The absence of micelles in the aqueous phase is due to the surfactant moving to the upper microemulsion phase, which is consistent with the observations of Meng et al.[16] who measured a higher concentration of PFOS in emulsions with hexane and octanol than in the aqueous phase.[27]

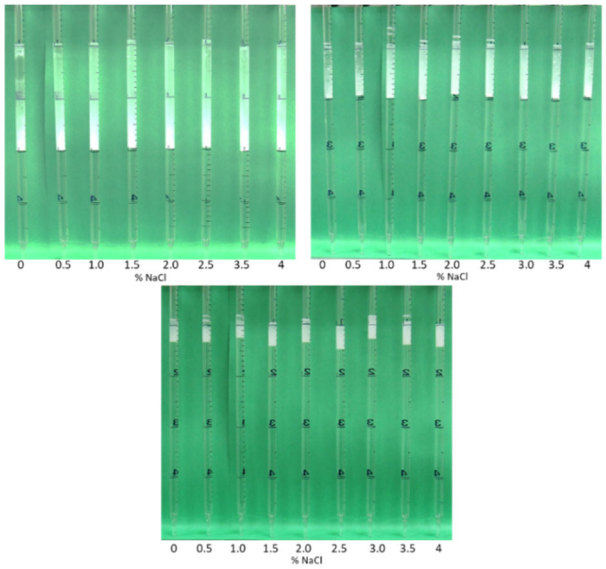

Figure 14: Viscous microemulsions (white upper phase) for Jet A and 3 % v/v AFFF-1 mixed for all salinities (0-4% NaCL) at 20˚C and for all water-oil ratio from 1 (top left,), 3 (top right), and 9 (bottom).

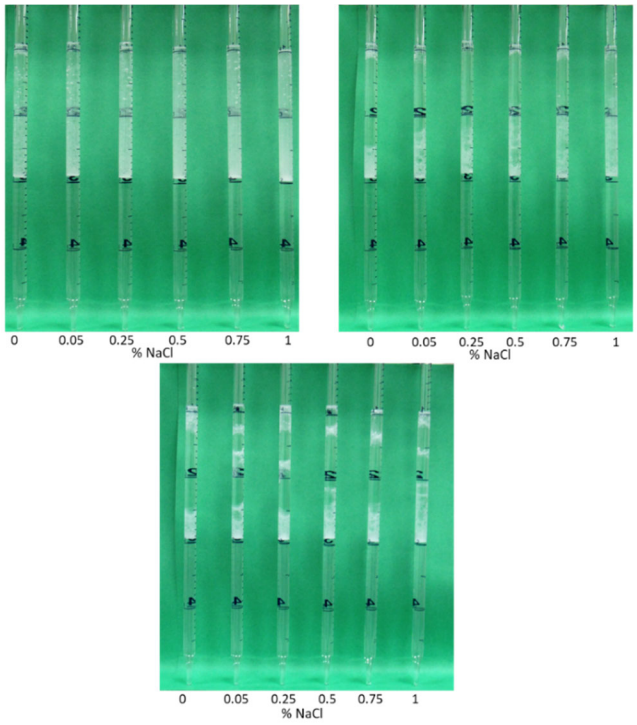

Figure 15: Viscous microemulsion (white upper phase) for Jet A at a water-to-oil ratio of 1 with AFFF-1 concentrations of 1.5 % (top right), 0.75 % (top right), and 0.375 % (bottom).

The five PFAS-based AFFFs and fluorine-free AFFF all produced viscous, Type II microemulsions (upper phase) when adequately mixed with Jet A in 5 mL pipettes, indicating that the phase behavior was not unique to AFFF-1 (data not shown). In the case of the pre-foamed AFFF, the foam not collapse to form a liquid and, hence, did not form a microemulsion. The order which the fluids were added to the pipettes and the tubes in all the testing did not play a role in forming microemulsion. Larger diameter tubes introduce less shear and mixing energy when shaken so that Type II microemulsions were not apparent using the larger 15-mL tubes. Thus, microemulsion formation is a function of cross-sectional area and indicates that microemulsions will occur within smaller pore spaces during infiltration of AFFF in the presence of Jet A where the mixing energy is higher. The formation of viscous microemulsions under the range of test conditions is consistent with the fact that all MilSpec AFFFs are designed to spread on fuel surfaces and not mix.[8,17,18] It is not coincidental that all MilSpec AFFFs form microemulsions formed irrespective of ionic strength (Figure 1 and S2) or AFFF concentration since MilSpec AFFFs must reach performance specifications even when used with seawater or the AFFF is diluted to only to half strength.[8]

The effects of scale, confinement, and mixing energy were also illustrative: microemulsion formation and the appearance of a viscous phase required adequate mixing energy, and smaller container size, respectively. Agitation of 3 %v/v AFFF solution and Jet A was required to form microemulsions for all AFFF solutions using smaller, 5-mL sealed pipettes. Without agitation of the sealed pipette, microemulsion—and consequently a viscous phase—was not observed using either the 5–mL pipettes, nor was it observed after shaking the 15–mL centrifuge tubes. Similarly, without agitation, neither the liquid nor the pre–foamed AFFF formed a microemulsion using either 5-mL and 15 mL sizes. When shaken, Winsor Type II microemulsions formed in the smaller size 5-mL pipettes as a separate, opaque phase, for all five additional AFFFs tested, which includes older and current AFFF formulations as well as the fluorine free AFFF.

Density–based mixing of liquids was observed when Jet A was added first followed by pre–foamed AFFF during foam drainage, but the short duration of mixing between the two phases due to a density gradient did not provide sufficient mixing energy to create a visible microemulsion. Other than the minor mixing due to density gradient, the order in which the fluids were added to the pipette did not play a role in formation of a microemulsion. These results indicate that, during application of AFFF foam to a pool of Jet A at the surface, it is unlikely that a viscous phase would be observed above ground. After foam drainage and infiltration of the AFFF liquid, mixing and microemulsion formation likely occurred in the presence of co-discharged or pre-existing Jet A residing in subsurface pore spaces. The dynamic flow experiments (C) and (D) were designed to explore this possibility further.

Foam stability tests.

Foam generated from using AFFF-1 gave a height of 12.7 cm and was stable for more than 3 weeks (Table 10). In the presence of Jet A, foam height was reduced 24% (9.6 cm; Table 10). The presence of an oleic phase (e.g., Jet A) is known to suppress foam generated from hydrocarbon surfactants.[19] The foams were quite stabile as indicated by no change in height for at least 3 weeks (Table 10). The stability of AFFF foam is long-lasting, leading to the potential for overland transport and surface water contamination.

Table 10: Foam height and duration.

observations	3% AFFF-1	3% AFFF-1
Jet A added	no Jet A	1 mL Jet A
foam height (cm)	12.7	9.6
duration	stable for 3 weeks	stable for more than 3 weeks

Rheological measurements.

Because AFFF and Jet A formed a viscous microemulsion, the rheological properties of the microemulsion, 3% AFFF-1, and Jet A were measured individually. The viscosities of the microemulsions measured immediately upon mixing and after equilibration for weeks were significantly higher than Jet A and 3% AFFF-1 solution at low shear rates (Figure 16). Jet A, 3% AFFF-1 solution, and microemulsion all exhibited shear–thinning (pseudo-plastic) behavior. High shear rates that result in lower fluid viscosity are achieved when AFFF is applied at high flow rates during firefighting. However, such flow rates can only be achieved using pumps such that high shear rates are not attained during infiltration of AFFF into porous media. The rheology profile (Figure 16) indicates that for lower shear rates, which occur under natural hydrologic gradients, AFFF microemulsions become viscous, and therefore less mobile in porous media. The rheological measurements confirm the formation of a viscous microemulsion phase when adequate mixing energy is provided. The phase behavior and rheology experiments indicate that microemulsions will form when sufficient energy for mixing AFFF and Jet A fuel occurs above ground (*e.g.*, during firefighting) or at low shear rates during infiltration after cessation of firefighting activities.

When viewing Figure 16, note that the graph is a log scale. The viscosity of the m.e. was significantly higher than either Jet fuel or AFFF solution for the low shear rates (10^{-1} s^{-1} to 1 s^{-1}): the m.e. was viscosity was 180% to nearly 500% higher than the viscosity of the jet fuel for all but 1 of 21 measurements. Low shear rates are of interest, since they correlate with low interstitial velocities that reflect the infiltration of fluids from surface impoundments. When compared to the AFFF solution alone, the m.e. viscosity was from 775% to 2,700% higher than that of the AFFF solution alone.

The importance of knowing the rheology of the m.e. is significant. The transport properties are greatly affected by several parameters, and viscosity is perhaps the most significant. High viscosity liquids travel more slowly through porous media compared to low viscosity fluids when the same driving force or gradient is applied. The gradient for the infiltration of fluids is usually gravity alone. Gravity is usually the gradient for flow through the shallow subsurface as well: the rate is inversely proportional to the viscosity, all other parameters being equal. Similarly, if flow rates are kept equal, a commensurate increase in pressure is required when fluid viscosity is increased.

There is an important implication for sites where there is a potential for AFFF to have combined with jet fuel: the resulting microemulsion could be highly viscous and travel much slower through the shallow subsurface. Numerical simulations that do not account for the viscosity effect will likely underestimate the transport of AFFF if it has combined with a hydrocarbon. Since jet fuel was often used in firefighting training, or the potential for a jet fuel release to the subsurface may have occurred in the same vicinity as firefighting training, this potential scenario should be given serious consideration.

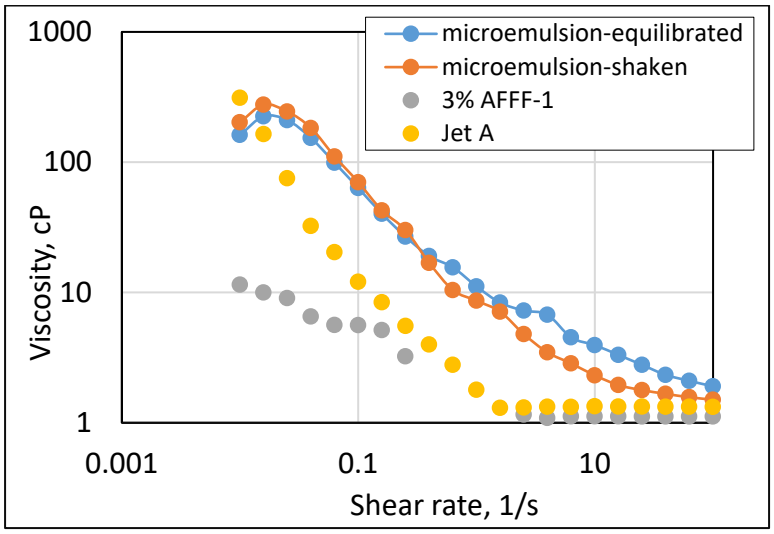

Figure 16: Viscosity of 3% AFFF-1 only, Jet A only, and microemulsion formed with AFFF-1 and Jet A equilibrated both for 10 min and for several weeks.

Task 2.2. Saturated Column Tests (Multiple AFFF Applications).

Case (A): Repeated AFFF Applications to OK-75 Sand (Control).

The concentration history of anionic and zwitterionic PFAS compounds are presented in Figure 7 and the mass retained are reported in aggregate for the two classes of PFAS compounds, anionic

and zwitterionic, in Table 5. It appears that zwitterions are retained to a higher degree than anions.

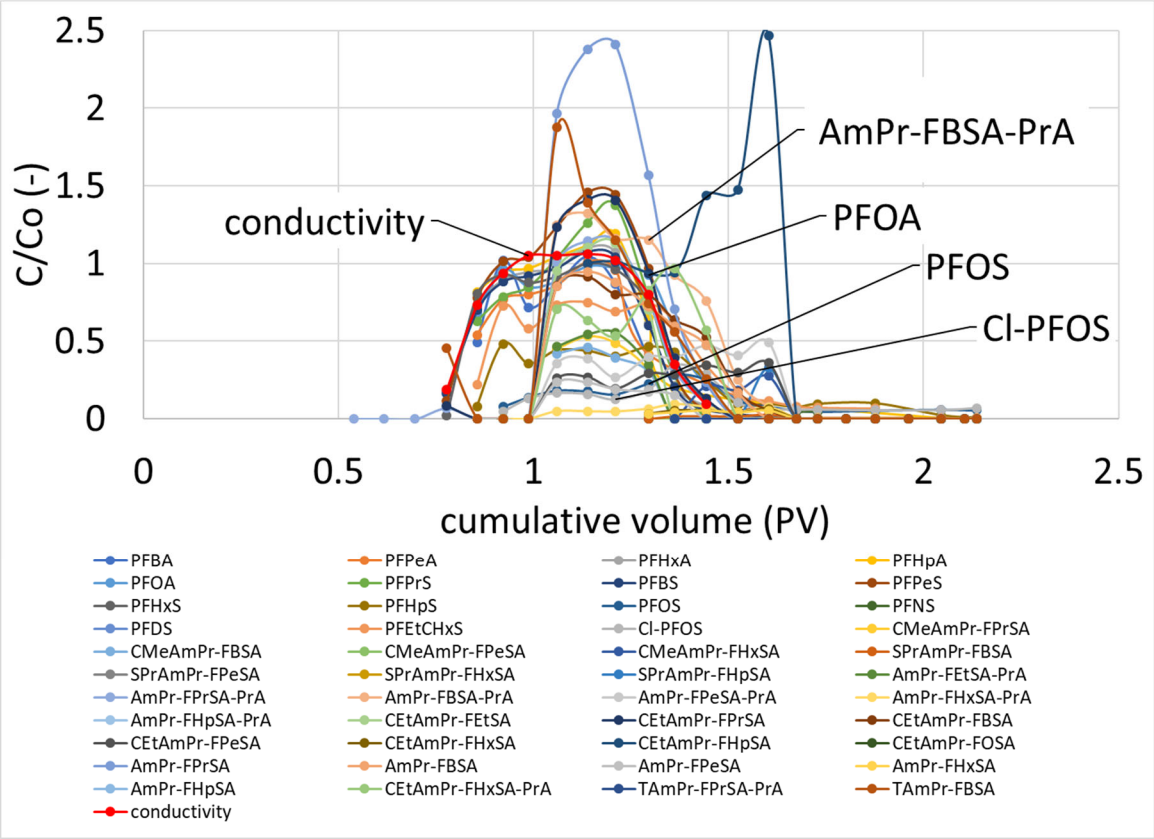

Figure 17: normalized concentration history of anionic and zwitterionic PFAS after 1 'slug' (injection) of AFFF through OK-75 sand. Note the degree of retention (adsorption) and retardation (partitioning) of several compounds.

Table 11: Mass of PFAS retained after each of four injections into a sandpack of OK-75 sand, no NAPL. The mass retained is expressed as a fraction of the mass injected.

classification (head charge)	**mass retained (%) as fraction of mass injected**			
	1st injection	**2nd injection**	**3rd injection**	**4th injection**
anions	54.6	59.5	65.4	53.4
zwitterions	81.7	64.1	76.6	68.2
total	61.2	60.6	68.0	57.0

The concentration history for the initial application of AFFF through a relatively inert porous media shows two behaviors important to note. First, a high degree of adsorption is observed for many compounds and appears correlated with higher degree of hydrophobicity. The degree of adsorption is much greater than expected for media with relatively low surface charge. The concentration history also shows some partitioning of PFAS compounds which can be observed by a retardation in the concentration profile in Figure 17.

Repeated application of AFFF-1 through the same porous media revealed that the adsorption behavior changed with subsequent applications of AFFF–*i.e.*, the concentration history for subsequent applications were not the same as the initial. This observation is indicative of surfactant-surfactant adsorption, where adsorbed species from the first application serve as sorption sites for species during subsequent AFFF applications. This is a very subtle yet highly important observation with regard to the use of single component or even multi-component solutions to conduct research studies: the interactions between the AFFF components are not reflected in most studies unless actual AFFF solutions are used.

The results from repeated are best presented as qualitative comparisons between specific compounds for the four AFFF applications. Figure 18 compares a pair of compounds having the same functional group but differing in terms of their carbon-fluorine (C-F) tail length. The degree of mass retention (adsorption) and the degree of retardation (partitioning) appear correlated with longer C-F chain length. Figure 19 compares pairs of compounds having the same C-F tail length but differing in terms of functional group, showing the effect that functional group on adsorption and retardation where the more hydrophobic compounds are correlated with higher degree of retention and retardation.

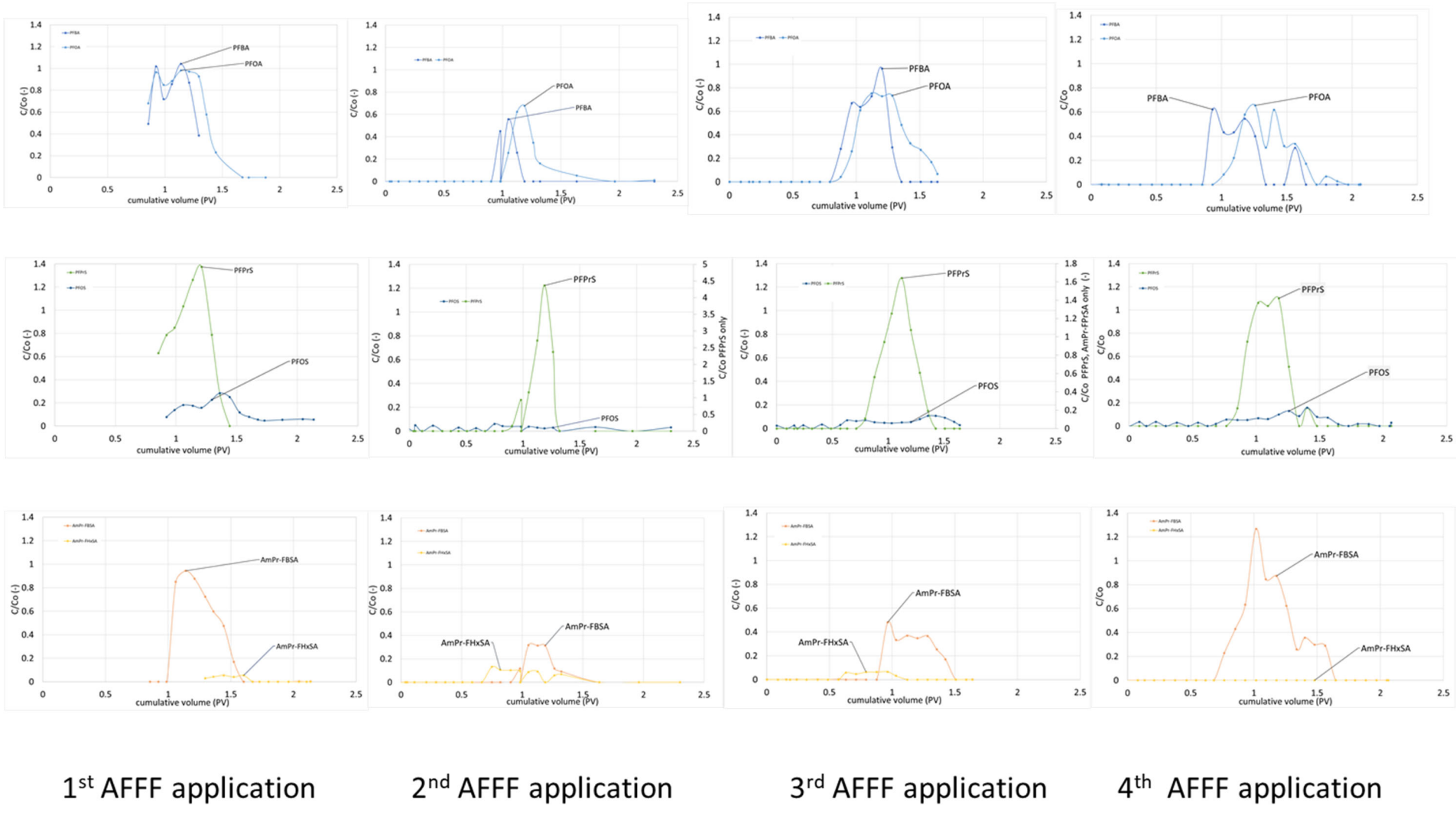

Figure 18: Four applications of AFFF-1 where chain length is compared keeping the functional group constant

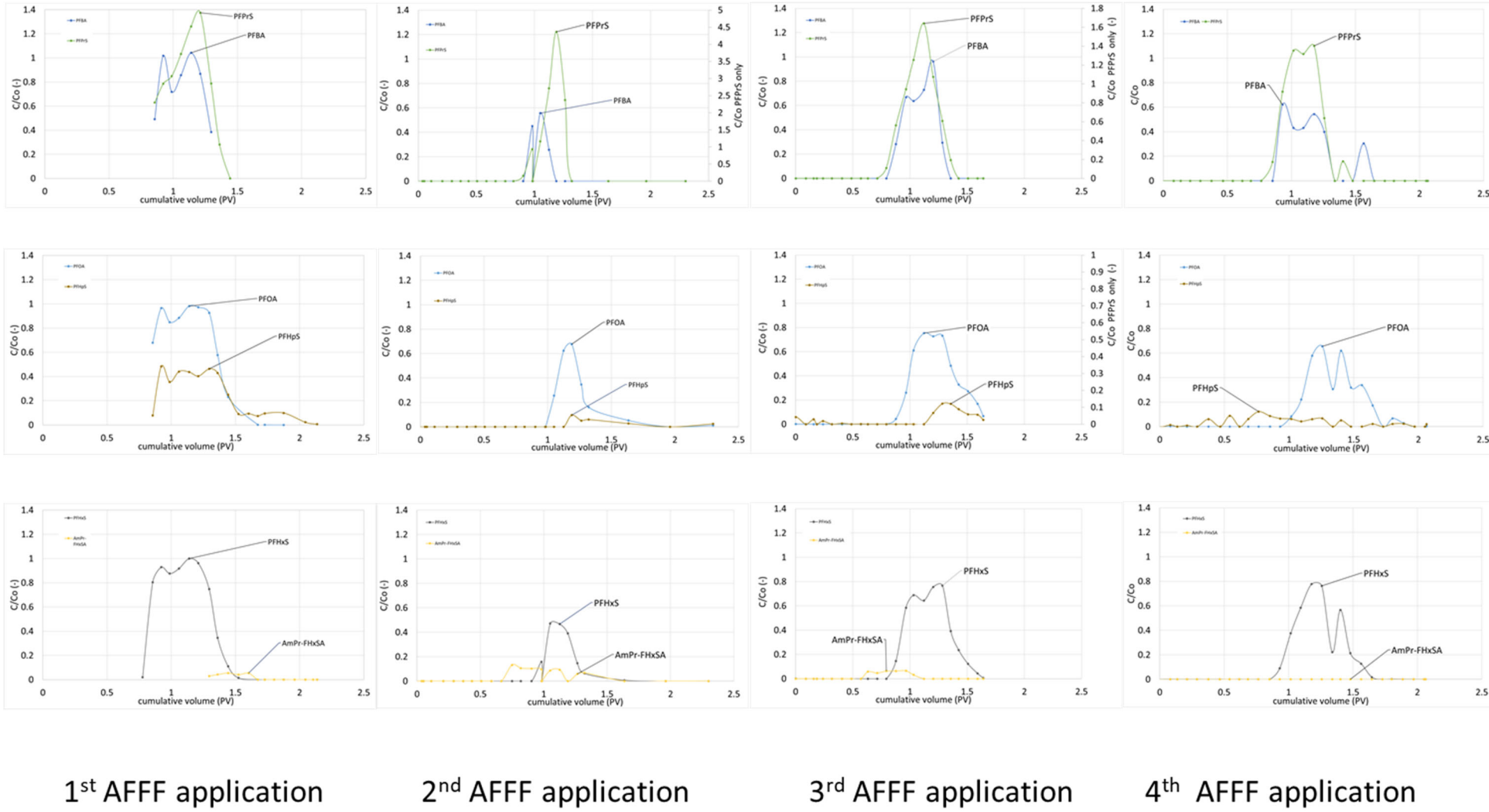

Figure 19: Four applications of AFFF comparing functional group, keeping chain length constant.

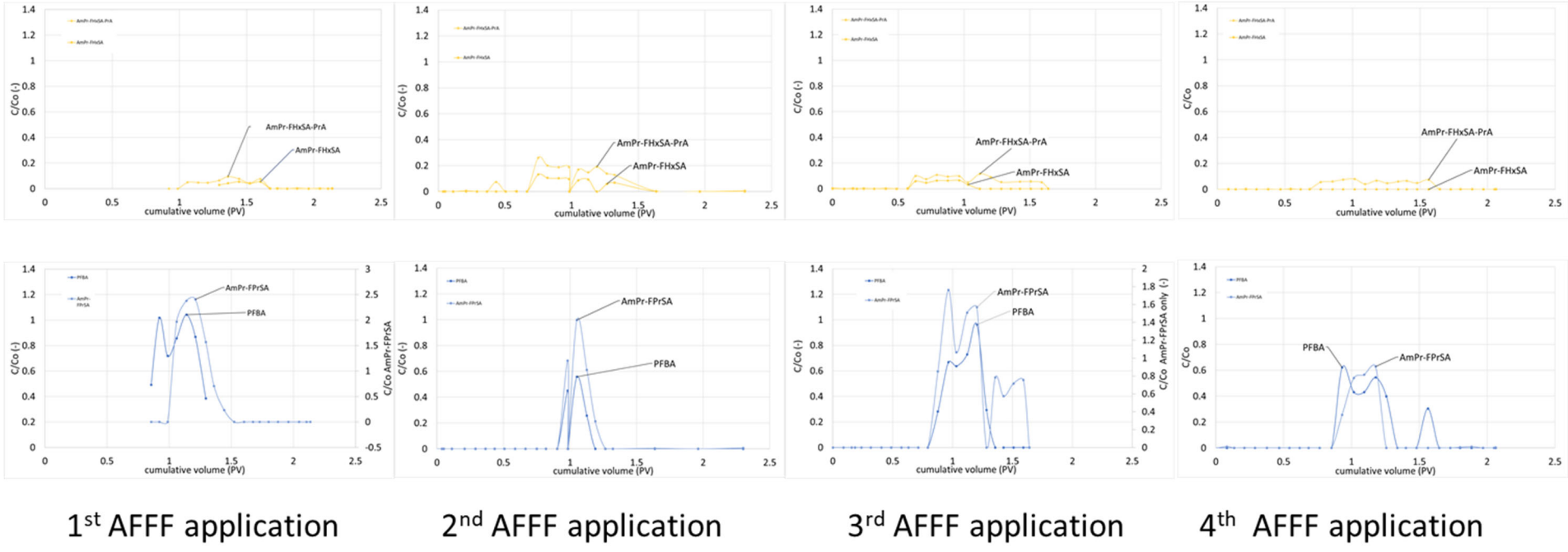

Figure 19 (continued)

Case (B): Repeated AFFF Applications to C2 Soil Horizon.

For these two tests (Case A and Case B), mass balance between injected and produced fluids indicate a degree of retardation and adsorption. Note that our static adsorption tests for this soil was on the order of 0.03 mg/g. Furthermore, the repeated applications revealed that the adsorption behavior changed with subsequent applications of AFFF. This observation is indicative of surfactant-surfactant adsorption, where adsorbed species from the first application serve as sorption sites for species during subsequent AFFF applications.

Table 12: Dynamic properties of the C2 soil horizon

porosity	38%
pore volume	103.9 ml
permeability	>10 darcy

The behavior observed was unlike commonly observed adsorption behavior where a mass balance between inflow and outflow is used to estimate the degree of adsorption. Instead, the behavior reflects partitioning phenomena where nearly all mass injected is subsequently produced—albeit retarded. In addition, some compounds were adsorbed to very high degree where nearly all the injected mass was retained. Table 13 presents the retention after each of the four injections grouped by classification as well as overall. The retained mass of anionics decreased with each application of AFFF. The same is observed for the zwitterionics, with zwitterion retention slightly higher than anionics for the first of the four injections and it appears that some retained zwitterionics were de-sorbed during the last stage. Figure 21 also indicates that the PFAS retention onto the media may have reach a saturation limit after the four injections of approximately 0.5 pore volume each.

The results from repeated applications of AFFF-1 through the field-obtained soil are strikingly similar to the results from repeated applications of the same AFFF though OK75 sand. While the amount of clay and organic carbon within the C2 horizon soil is low, it is interesting to note the similar behavior. Figure 22 presents the results qualitatively by comparing the anionic and zwitterionic compounds for the four applications in a series of graphs. It is clear that similar trends are observed that confirm the observations made when using a relatively inert media, OK-75 sand. A quantitative result was made by computing the mass retained for selected anionic and zwitterionic species. All samples before and after 1 pore volume were chemically analyzed to capture the details of the curve representing the breakthrough of the AFFF application. Alternate samples were chemically analyzed at the earliest and latest stages of the arrival. In computing the mass, data was imputed for cases where a sample was not analyzed by using the average of the previous and subsequent sample to ensure that the computation accounted for all mass produced. In addition, the limit of detection value was used for each PFAS when no signal was detected

during chemical analyses. This approach may yield a slight under-estimate of mass retained, however, we found that the mass retained for most compounds were only a fraction of 1 percent with some as much as 6% lower when using the imputed data compared to results computed not imputing data.

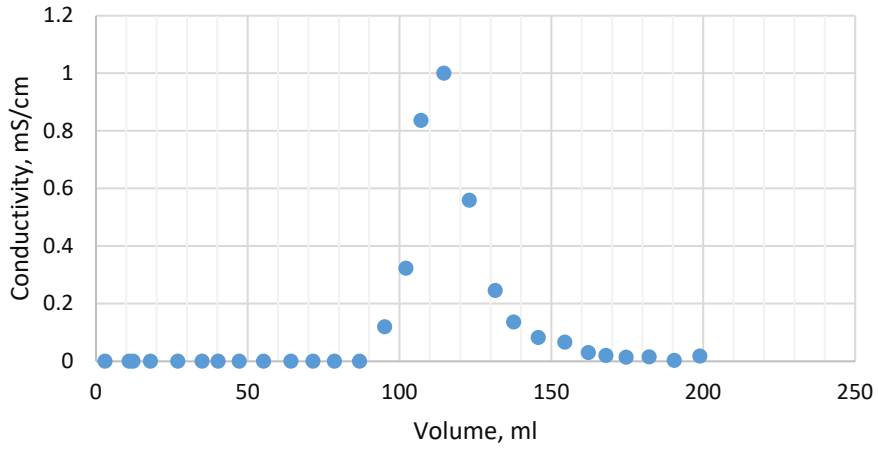

Figure 20: Tracer test - Wurtsmith soil C2 horizon

Table 13**:** Mass of PFAS retained after each of four injections into a sandpack of field-obtained soil (C2 horizont, Wurtsmith AFB): 96.5 wt.% sand with 3.2 wt.% silt, 0.3 wt.% clay, cation exchange capacity 3.8 $cmol_c/kg$, 0.04 wt.% orgranic matter, no NAPL. The mass retained is expressed as a fracion of the mass injected.

Classification (head charge)	**mass retained (%) as fraction of mass injected**			
	1st injection	**2nd injection**	**3rd injection**	**4rh injection**
anions	77.6	56.9	52.9	39.4
zwitterions	88.8	55.4	54.0	-38.8*
total	83.2	56.1	53.5	1.4

Figure 21: PFAS mass retained after each AFFF-1 application, by classification and total.

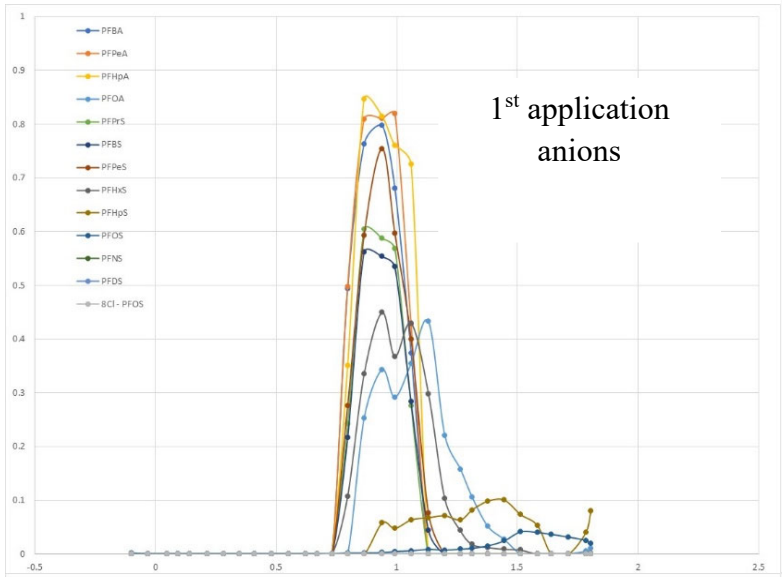

1st application anions

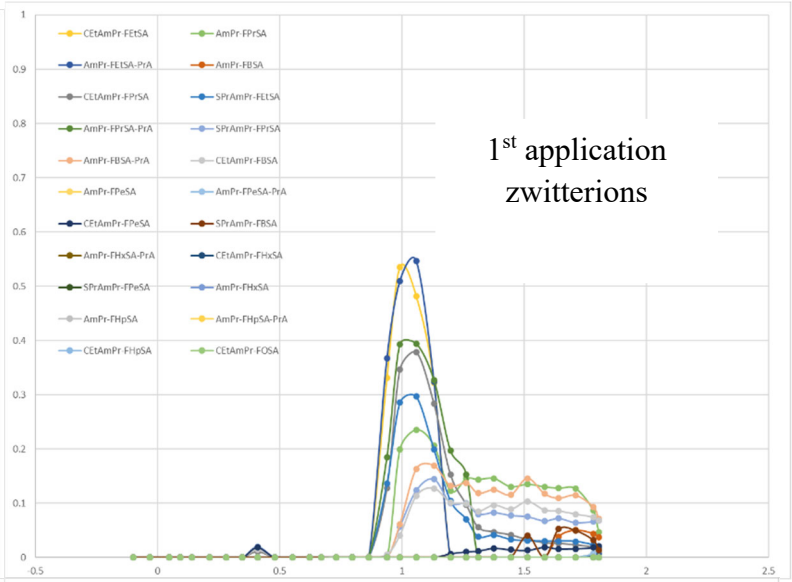

1st application zwitterions

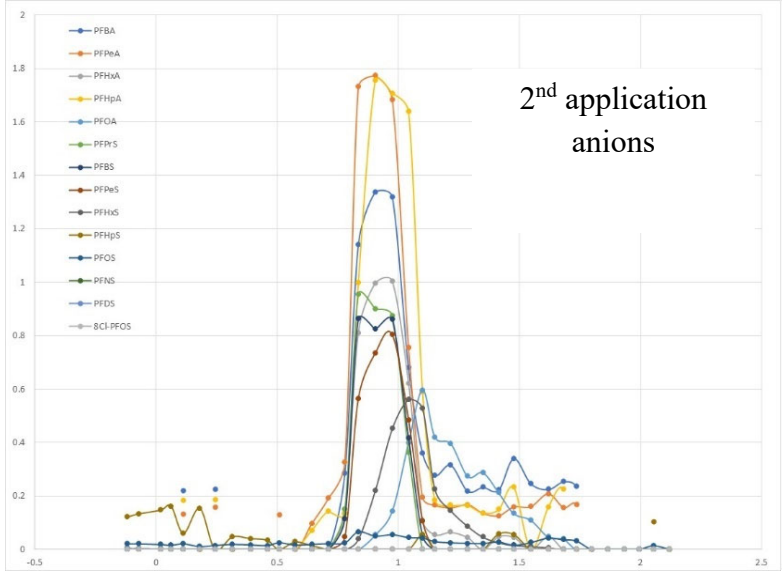

2nd application anions

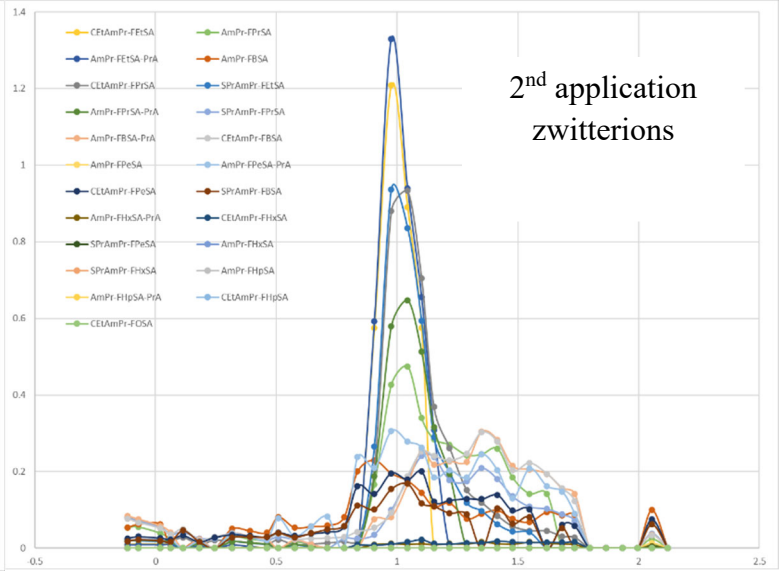

2nd application zwitterions

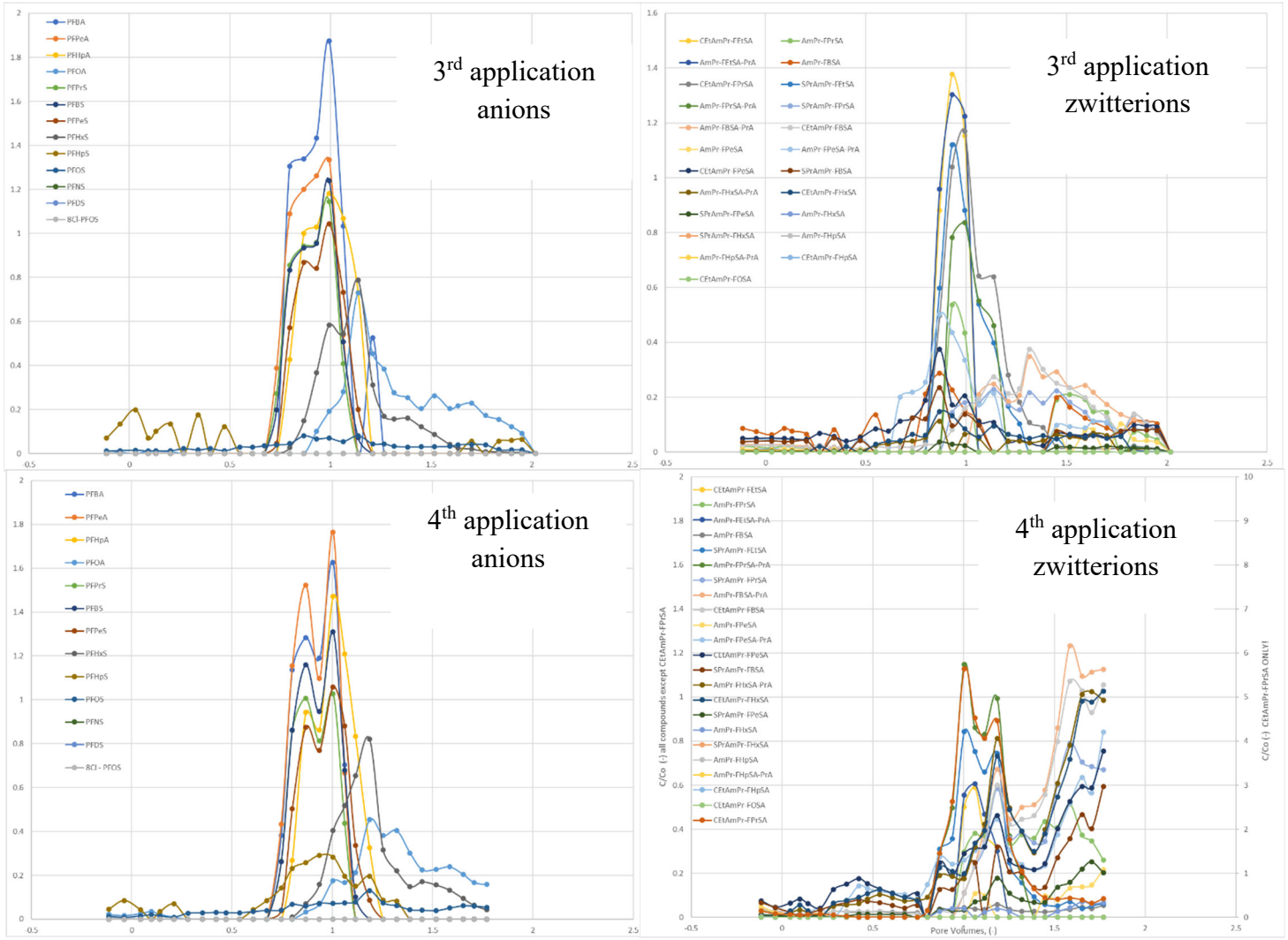

Figure 22: (this and preceding page): Concentration history showing C/Co versus pore volumes of throughput from four applications of AFFF-1 to a field-obtained soil, C2 horizon containing relatively low amount of clay and organic carbon. Note that the scale of the y-axis, C/Co, was changed after the first application of AFFF, and the 4th application showing zwitterions uses two axes.

Case (C): Single AFFF Application: Constant Flow.

This flow experiment indicated the rapid development of significant back pressure, which is indicative of a viscous microemulsion formation as the AFFF and emplaced jet fuel mixed. The pressure measured during the constant flow rate injection of AFFF solution is shown below in Figure 23. We note that the maximum pressure drop measured for the control experiment – where the same sand and packing method was used with the same AFFF injection but without the presence of jet fuel – was only 0.061 psig, while the values presented in Figure 23 rose 0.1 psig to above 10 psig. Based on the observation of pressure increase during constant flow rate, we concluded that a viscous phase is forming once the AFFF solution combines with the resident hydrocarbon.

Two mechanisms for this result are either *pore blocking* or *viscosity–based pressure increase*: either 1) a viscous microemulsion phase formed that is immobile and blocking pore space, and causing injected fluids to flow through reduced flow path, or 2) the viscous phase is flowing and requires higher pressure gradient to move. Based on our preliminary screening of the effluent samples using laser scattering, and the phase behavior observations indicating formation of a Winsor Type II microemulsion, we believe our results indicate microemulsion formation *in-situ.* We did not observe highly viscous phase in collected effluent and believe the first mechanism is more likely, but cannot determine conclusively unless the collected effluent are chemically analyzed.

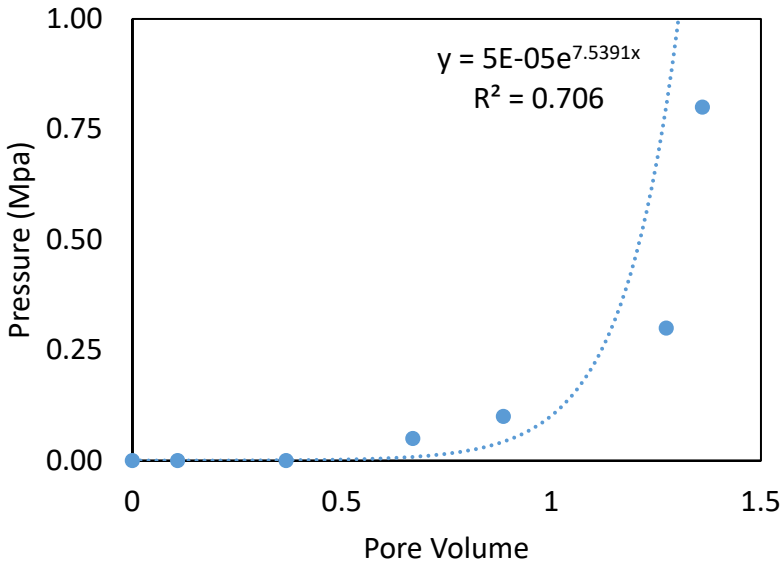

Figure 23: Pressure drop measured during constant flow injection at 0.3 m/day in OK-75 column of 23.8% residual Jet A saturation.
The increase in pressure indicates a viscous phase formed.

Case (D): Single AFFF Application: Constant Pressure.

The flow rate was initially measured to be 4.2 ft/day and decreased by half after only 1 pore volume of AFFF-1 flowed into the OK-75 sandpack, half again with the second pore volume of AFFF, and was reduced by a factor of nearly 10 after 6 pore volumes when the flow was measured only 0.27 ft/day before flow stopped completely (Figure 24). This scenario was intended to mimic the infiltration of AFFF, as could occur if a pool of AFFF formed on the surface, that may encounter a fuel within the subsurface, such as is found when a fuel leak occurs or fuel used for training unintentionally infiltrates the subsurface. The results show that the infiltrating AFFF solution can combine with the fuel within the subsurface and form a viscous phase, halting the transport of AFFF.

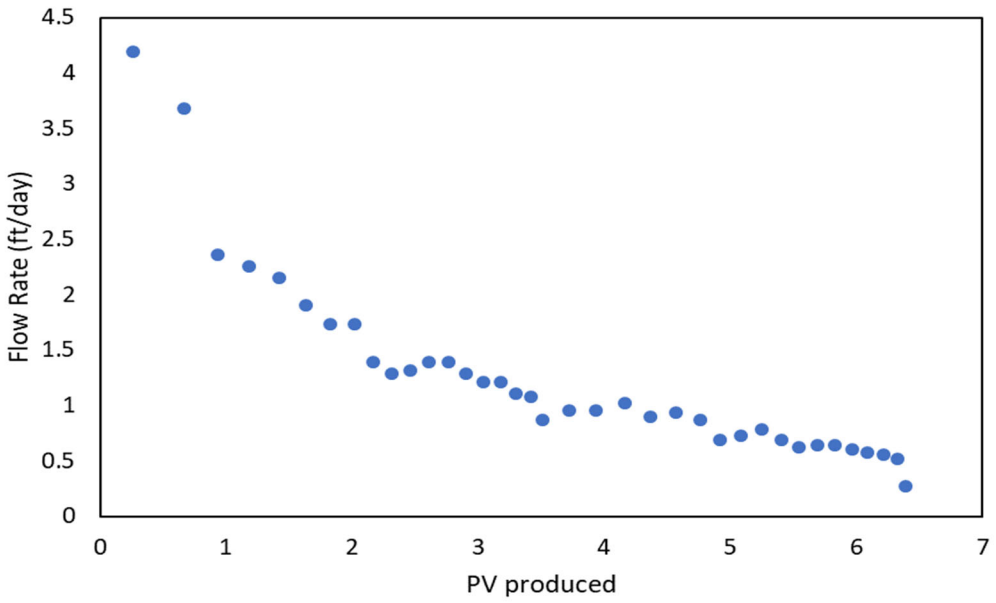

Figure 24: Flow rate (linear velocity) measured during constant pressure injection of 0.5 MPa in OK-75 column at 31.5% residual Jet A saturation.
The decrease in flow rate indicates a viscous phase formed.

Both column experiments (C) and (D) confirmed the observations of the phase behavior experiments—that AFFF solution is creating a viscous phase in presence of oleic phase and that there are strong implications on the transport phenomena within the subsurface environment. These observations have not been reported in the literature and consequently have not been well studied.

In one case, a constant flow rate was used while the resulting pressure was measured during AFFF injection (Note: in that test, pressure increased from below 0.1 psig to over 100 psig). In the other test, AFFF solution was injected at a constant pressure (0.5 MPa or 72 psig) and the resulting flow rate was measured (Note: flux was initially 4.2 ft/day and decreased to 0.27 ft/day before flow stopped completely).

Task 3: PFAS Transport under Unsaturated Conditions and Modeling

Task 3.1-PFAS Adsorption at the Air-Water Interface

Interfacial Tension

Interfacial tension measurements for the perfluorinated carboxylates and perfluorinated sulfonates are shown in Figure 25 and Figure 26, respectively. Figure 26 also shows results for FtTAoS, an equimolar mix of the eight PFAAs used in this study, and an equimolar mix of PFOS + FtTAoS. Interfacial tension measurements of PFOS at differing NaCl concentrations are shown in Figure 27. The lines in all the figures represent regression of Eq. 3.5 to the data, where k and n were used as fitting parameters. Regression parameters are provided in Table 14. Results show that the interfacial tension data were well described by Eq. 3.5, with R^2 values ≥0.98. Results also show that, consistent with the results of others,[9,11–13] interfacial uptake is greater for the longer chained perfluorinated compounds than the shorter-chained perfluorinated compounds. When comparing PFHpA to PFHxS, which both have the same perfluorinated chain length, the interfacial tension curves are nearly identical, indicating that the head group impact is less than the perfluorinated chain length impact. The data in Figure 25 and Figure 26 also indicate that the PFAS used in this study were below the critical micelle concentration and monolayer coverage at the air-water interface, as decreases in interfacial tension were observed with increasing PFAS concentration up to the highest concentrations examined.

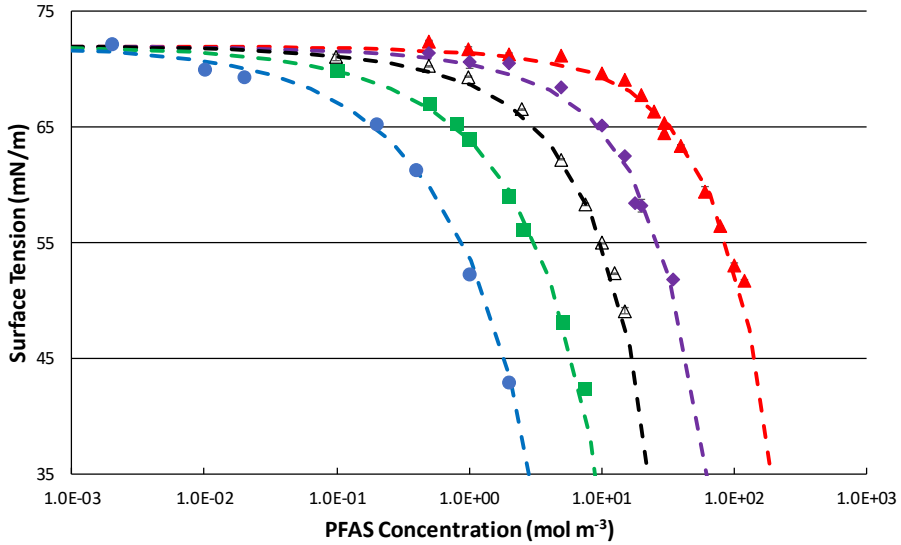

Figure 25: Interfacial tension as a function of PFAS concentrations for the perfluorinated carboxylates. The background salt concentration was 0.01 M NaCl.

Symbols represent the average of triplicate samples. Error bars represent the 95% confidence intervals (error bars typically smaller than the data symbol). Dashed lines represent regression of Eq. 3.5 to the data. ● = PFOA, ■ = PFHpA, △ = PFHxA, ◆ = PFPeA, ▲ = PFBA

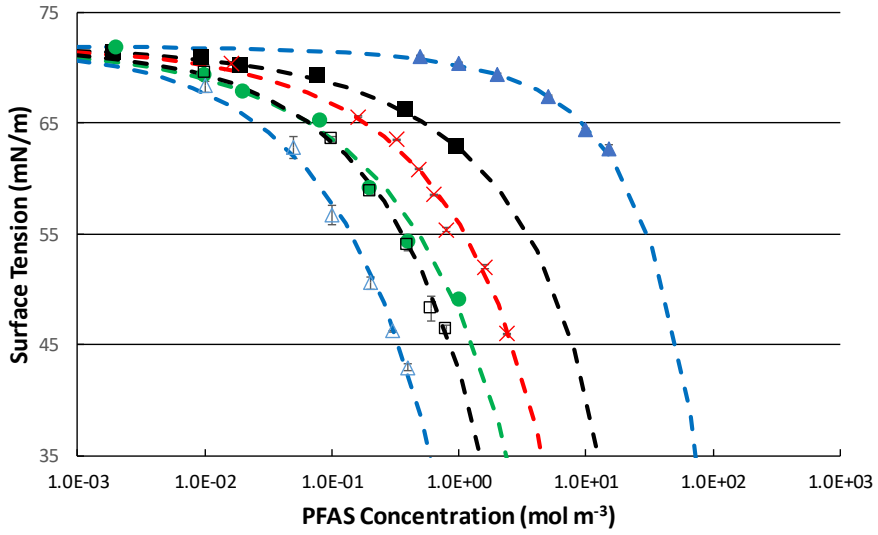

Figure 26: Interfacial tension as a function of PFAS concentrations for the perfluorinated sulfonates.

FtTAoS, an equimolar PFAA mixture, and an equimolar PFOS: FtTAoS mixture. For mixtures, the total PFAS concentrations are plotted. The background salt concentration was 0.01 M NaCl.

Symbols represent the average of triplicate samples. Error bars represent the 95% confidence intervals (error bars typically smaller than the data symbol). Dashed lines represent regression of Eq. 3.5 to the data. △ = FtTAoS, □ = PFOS: FtTAoS mix, ● = PFOS, X = PFAA mix, ■ = PFHxS, ▲ = PFBS

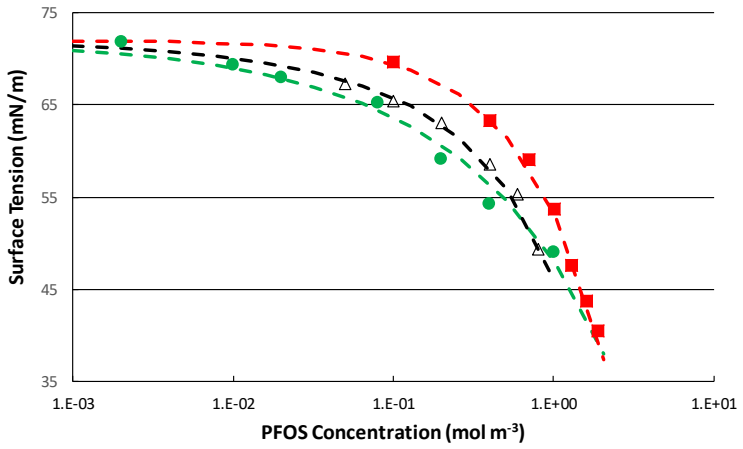

Figure 27: Interfacial tension as a function of PFOS concentrations for varying background NaCl concentrations.

Dashed lines represent regression of Eq. 3.5 to the data. ● = 0.01 M NaCl, △ = 0.001M NaCl, ■ = deionized water

Table 14: Regressed Freundlich parameters (Eq. 3.5) to the interfacial tension data.

± values indicate the 95% confidence intervals.

PFAS System	NaCl (M)	k	n	R^2
PFBA	0.01	$4.0 \pm 0.4 \times 10^{-8}$	0.49 ± 0.04	0.99
PFPeA	0.01	$9.9 \pm 0.4 \times 10^{-8}$	0.52 ± 0.08	0.98
PFHxA	0.01	$2.0 \pm 0.3 \times 10^{-7}$	0.56 ± 0.04	0.99
PFHpA	0.01	$4.9 \pm 0.3 \times 10^{-7}$	0.55 ± 0.03	0.99
PFOA	0.01	$1.1 \pm 0.1 \times 10^{-6}$	0.56 ± 0.06	0.99
PFBS	0.01	$1.1 \pm 0.2 \times 10^{-7}$	0.48 ± 0.05	0.99
PFHxS	0.01	$5.8 \pm 0.3 \times 10^{-7}$	0.45 ± 0.07	0.98
PFOS	0.01	$1.5 \pm 0.2 \times 10^{-6}$	0.44 ± 0.08	0.98
Equimolar PFAA mix[1]	0.01	$1.0 \pm 0.1 \times 10^{-6}$	0.47 ± 0.06	0.98
PFOS	0	$3.3 \pm 0.2 \times 10^{-6}$	0.43 ± 0.08	0.99
PFOS	0.001	$3.7 \pm 0.6 \times 10^{-6}$	0.49 ± 0.07	0.99
PFOS	1	$4.9 \pm 1.0 \times 10^{-6}$	0.51 ± 0.12	0.98
FtTAoS	0.01	$3.0 \pm 0.4 \times 10^{-6}$	0.52 ± 0.10	0.98
Equimolar FtTAoS + PFOS	0.01	$1.8 \pm 0.1 \times 10^{-6}$	0.51 ± 0.06	0.99

[1] PFAAs include PFBA, PFPeA, PFHxA, PFHpA, PFOA, PFBS, PFHxS, and PFOS

For PFOS, decreasing the background NaCl concentration to approximately zero (using deionized water) resulted in a decrease in interfacial sorption, as the decreases in interfacial tension (σ_0-σ) at 0.01 M NaCl were up to 8-times greater than those in deionized water for a given PFOS concentration (based on the data shown in Figure 4, Eq. 3.5, and the regressed parameters shown in Table 14). However, decreasing the NaCl concentration from 0.01 M to 0.001 M resulted in decreases in interfacial tension up to approximately 40% for a given PFOS concentration. In addition, FtTAoS shows greater surface activity than all of the PFAAs examined, which is consistent with the increased carbon chain length (combined fluorinated and non-fluorinated) and molecular weight of FtTAoS relative to the PFAAs examined in this study. These trends are reflected in the regressed Freundlich parameter k (Table 14).

Interfacial Sorption in Single and Mixed Solute Systems

For the equimolar mixture of the eight PFAAs used in this study, the surface adsorption (Γ) was determined by regressing Eq. 3.5 to the PFAA mixture interfacial tension data (using the sum of all the PFAAs for C in Eq. 3.3). Using Eq. 3.4, Γ was then plotted as a function of the total PFAA concentration (Figure 28). Also shown in Figure 28 is the prediction of this Γ based on the single component PFAA data via Eq. 6. Comparison of these two curves show that the Γ for the mixture can accurately (within the 95% confidence interval) be described by the single component Γ data and Eq. 6. Thus, it is reasonable to conclude that for PFAA mixtures of C4 through C8 carboxylates and sulfonates that are dilute (i.e., well below the critical micelle concentration and monolayer surface coverage), interfacial sorption can be reasonably predicted based on single component data, and PFAA interfacial sorption is not impacted by the presence of the other PFAAs in the mixture.

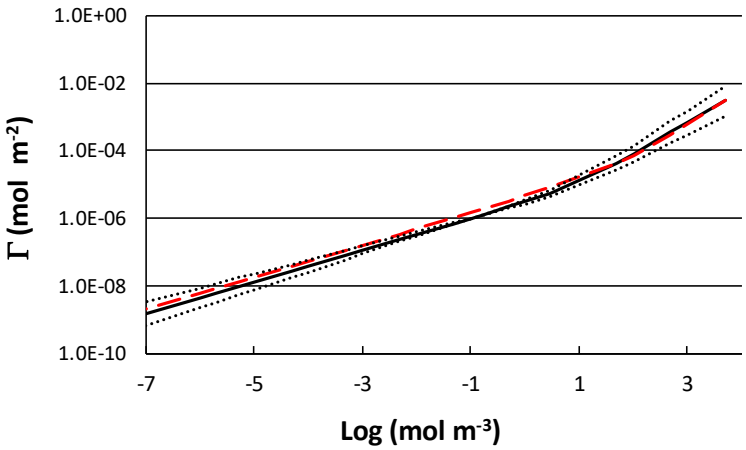

Figure 28: Γ based on the interfacial tension data (Eq. 3.5) from the equimolar PFAA mixture is plotted as the solid line.

The small dots represent the 95% confidence interval of the regressed data (Table 3). The prediction of Γ from the single component PFAA data (Eq. 6) is plotted as the red dashes.

Similar to the data shown in Figure 28, Γ for an equimolar mix of PFOS+ FtTAoS is shown in Figure 29. Comparison of the predicted Γ values (based on the single component data and Eq. 6) to those of mixture (Eqs. 3.2 through 3.5) are consistent with that of the equimolar PFAA mixture shown in Figure 28, showing that the PFOS+ FtTAoS mixture is reasonably described by the single component interfacial tension data. As discussed in the section below, the presence of FtTAoS also did not appear to have a statistically significant impact on PFOS interfacial sorption measured at the lower PFOS and FtTAoS concentrations. Thus, the presence of a polyfluoroalkyl compound with PFOS had little observable impact PFAS sorption, at least at concentrations well below the monolayer coverage and the critical micelle concentration. However, as discussed in the next section, the measured 8:2 FtTAoS interfacial partitioning coefficient was 10x greater than PFOS interfacial partitioning coefficients at low concentration. This suggests interfacial tension data may not capture all of the processes contributing to air-water interfacial partitioning of PFAS at low concentrations.

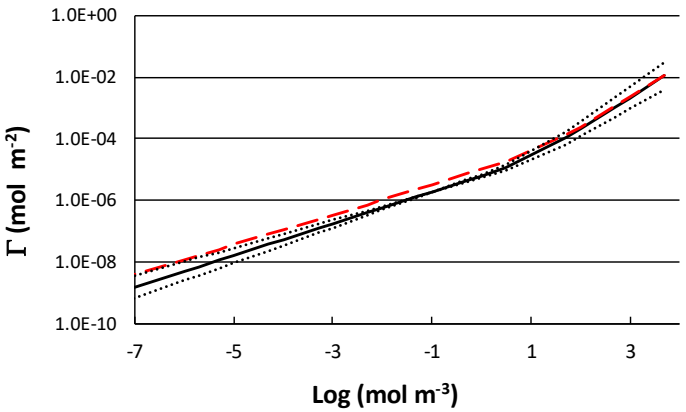

Figure 29: Γ based on the interfacial tension data (Eq. 3.5) from the equimolar PFOS: FtTAoS mixture is plotted as the solid line.

The small dots represent the 95% confidence interval of the regressed data (Table 14). The prediction of Γ from the single component PFOS and FtTAoS data (Eq. 6) is plotted as the red dashes.

Interfacial Sorption at Lower PFAA Concentrations

Results from the film experiments where the interfacial sorption coefficients (k_{aw}) for PFOS in 0.01 M NaCl measured at low (compared to the concentrations used in the interfacial tension experiments, and at concentrations more consistent with those in vadose zone porewaters) PFOS concentrations in both single and multicomponent (equimolar PFAA mixture and equimolar PFOS+ FtTAoS) mixtures are shown in Figure 30. These PFOS concentrations are orders of magnitude below the range where decreases in interfacial tension can be measured (as shown in Figure 25 and Figure 26), so prediction of interfacial uptake is highly dependent upon the sorption model selected. Using the Freundlich parameters (Table 14) regressed from the interfacial tension data (Figure 26), the solid line in Figure 30 represents the model prediction employing the Freundlich model (Eqs. 3.4 and 3.9). For comparison, prediction of k_{aw} at dilute PFOS

concentrations using the Langmuir sorption model (Eqs. 3.7 and 3.8) also is shown as the dashed line.

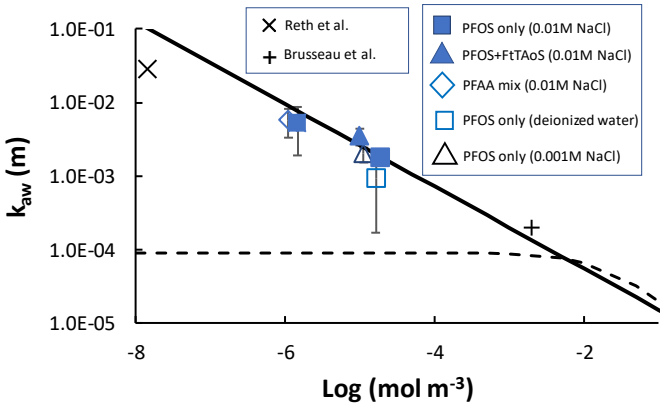

Figure 30: k_{aw} , measured via the film experiments in this study and measured via other techniques in previous studies, as a function of PFOS concentration.

Predicted values of k_{aw} based on interfacial tension data (PFOS in 0.01 M NaCl) using the Freundlich and Langmuir models are shown by the solid and dashed lines, respectively. Freundlich model parameters (Eq. 3.5) regressed to the interfacial tension data were: k = 1.5 ± 0.2 x 10^{-6}, n =0.44 ± 0.08, R^2= 0.98. Langmuir parameters (Eq. 3.8) regressed to the interfacial tension data were: Γ_m = 2.5±0.3 x 10^{-6} mol m^{-2}, α=3.6±1.7 [m^3 mol^{-1}]^2, R^2=0.99. Error bars represent 95% confidence intervals based on at least duplicate samples.

Experimental data from Reth et al.[14] were used to determine k_{aw} for PFOS. Apparent aqueous losses of perfluoroalkyl acids (PFAAs) in the absence of spray removal are attributed by Reth et al. to sorption at the air-water interface (further supported by data presented in their Table 4). Based on data from the second Experiment presented in Table 2 of Reth et al.,[14] PFAAs with perfluorinated carbon chain lengths of C6 through C10 show a clear trend of increasing surface layer concentration and surface enrichment factor with chain length. PFUnA, which has the greatest surface layer concentration within this range, has a surface enrichment factor approximately 10-times greater than that of the potassium salt form of PFOS,[14] and shows approximately a 43% decrease in aqueous concentration due to interfacial adsorption. The approach used to calculate the k_{aw} for PFOS using data from Reth et al. was first based on calculating the k_{aw} for PFUnA as follows:

$$k_{aw}=(C_i - C)\frac{V}{AC} \qquad \text{Eq. 3.10}$$

where C_i is the initial (spiked) PFUnA concentration, C is the PFUnA concentration in the aqueous phase after 24 hours, V is the water volume (88 L of tap water), and A is the air-water surface area (2332 cm^2 based on the vessel radius of 27.25 cm). Based on Eq. 10, the k_{aw} for PFUnA was 0.28 m. Applying the surface enrichment factors calculated by Reth et al. to calculate the k_{aw} for PFOS, the k_{aw} value of 0.028 m shown in Figure 30 was determined (where k_{aw} for PFOS was scaled from the PFUnA value in proportion to their surface enrichment factors).

The use of the Freundlich versus Langmuir sorption models results in very different predictions of k_{aw}, both in magnitude and trend. Consistent with a nearly linear sorption model predicted by the Langmuir model at solute concentrations well below interfacial sorption capacity, values of k_{aw} are constant with respect to PFOS concentration below a PFOS concentration of approximately 0.001 mol m^{-3} (0.5 mg/L). In contrast, the Freundlich model shows that the values of k_{aw} continue to increase as PFOS concentrations become infinitely dilute. In addition, the Freundlich model predicts values of k_{aw} that become orders of magnitude greater than those predicted by the Langmuir model as PFOS concentrations decrease below 10^{-4} mol m^{-3}. Thus, while both the Freundlich and Langmuir models (Eqs. 3.5 and 3.8, respectively) described the PFOS interfacial tension data very well (see Table 14 and Figure 30 ***caption***), the prediction of interfacial sorption and k_{aw} at lower PFOS concentrations differed by orders of magnitude. This difference is important, as PFOS concentrations in porewater measured in SERDP Project ER18-1204 are well below 0.5 mg L^{-1}.

Figure 30 shows that the k_{aw} values measured at low PFOS concentrations are in reasonable (averaging within approximately 25%) agreement with the Freundlich model. Results also show that the PFOS k_{aw} values are the same in both the single solute and mixture experiments, which is consistent with the results shown in Figure **27** and Figure 28 indicating that the dilute PFAS mixtures behave similarly to single solute systems with respect to interfacial adsorption. Furthermore, the measured k_{aw} values from the film experiments indicate that the Freundlich model provides a much better prediction of k_{aw} behavior at field-relevant PFOS concentrations than does the Langmuir model, likely due to the fact that the Freundlich model is based on the surface free energy for partial surface coverage and thus is more appropriate.[6,7]

In addition to the PFOS film experimental results at 0.01M NaCl, experimental k_{aw} results at 0.001 M NaCl and in the absence of salt (deionized water) also are plotted in Figure 30. Results show that the impacts of NaCl concentration within the range examined have a relatively small (less than a factor of 2) impact on the k_{aw} values.

Comparing interfacial tension-based model predictions, Figure 31 shows the predicted k_{aw} values for PFOS based on the Freundlich model (Eqs. 3.4 and 3.9) at multiple NaCl concentrations. Measured PFOS k_{aw} values using the film method for the three NaCl levels (0.01M, 0.001 M, and deionized waters) are also shown in Figure 31. Consistent with the PFOS film experimental results, the difference in the PFOS k_{aw} values at these lower PFOS concentrations is less than a factor of 2 for background NaCl concentrations of 0.001 and 0.01 M. However, the Freundlich model shown in Figure 31 predicts a k_{aw} value approximately 100-times lower in deionized water than when 0.001 or 0.01 M NaCl is present. In contrast, the film data show PFOS k_{aw} values in deionized water are within a factor of 2 to those with 0.01 or 0.001 M NaCl present.

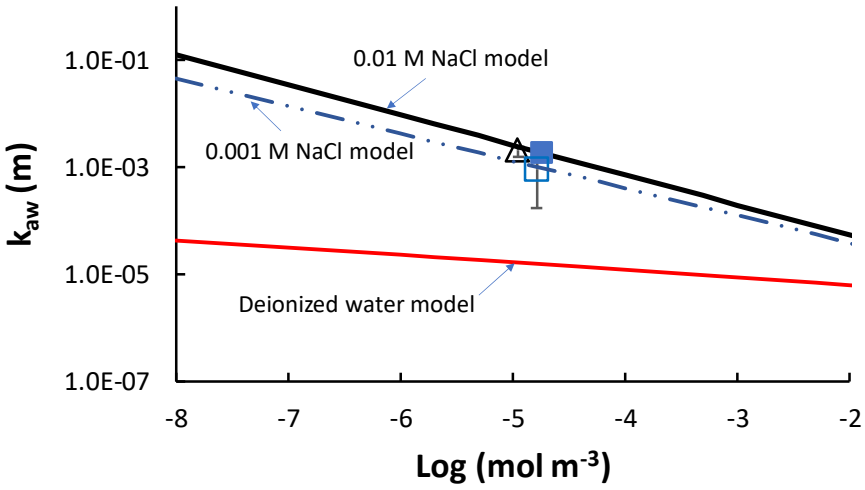

Figure 31: Freundlich-based model predictions of k_{aw} based on the interfacial tension data for PFOS in 0.01 M NaCl, 0.001 M NaCl, and deionized water.

Measure PFOS k_{aw} values via the film method also are shown. Error bars represent 95% confidence intervals. ■ = 0.01 M PFOS NaCl film data, △ = 0.001 M NaCl PFOS film data, □ = deionized water PFOS film data

This apparent discrepancy between the Freundlich model predictions and the film data for the deionized water conditions can be explained by considering both the PFOS and NaCl concentrations present. For the experiments amended with NaCl, the NaCl concentrations were in large molar excess relative to the PFOS concentrations used in the film experiments. The amended NaCl levels also remained in excess at the elevated (> 0.05 mol m^{-3}) PFOS concentrations used in the interfacial tension experiments. Thus, there is consistency when using the Freundlich model to extrapolate PFOS interfacial uptake down to very low PFOS concentrations. However, for the deionized water, this consistency did not exist. At the elevated PFOS concentrations used to measure the interfacial tensions in the deionized water system, the PFOS was in excess relative to any trace NaCl or other salt levels present in the water. Based on a measured conductivity of approximately 1 µS cm^{-1}, approximately 0.02 mol m^{-3} of salts were present in the deionized water, which is 1 to 2 orders of magnitude less than the PFOS levels (Figure 26). At the comparatively low PFOS concentration used in the deionized water film experiments, salt levels of 0.02 mol m^{-3} are in excess relative to the trace PFOS levels. Thus, these results suggest that extrapolation of the Freundlich model using interfacial tension data when the excess electrolyte is not present may result in an underprediction of PFOS interfacial uptake at low (< 0.05 mol m^{-3}) PFOS levels.

Analogous to PFOS in Figure 31, k_{aw} values measured using the film method for PFOA in 0.01 M NaCl are shown in Figure 32; the Freundlich model extrapolated based on the interfacial tension data also is shown in Figure 32. The Freundlich model describes the magnitude and trend of the PFOA k_{aw} values.

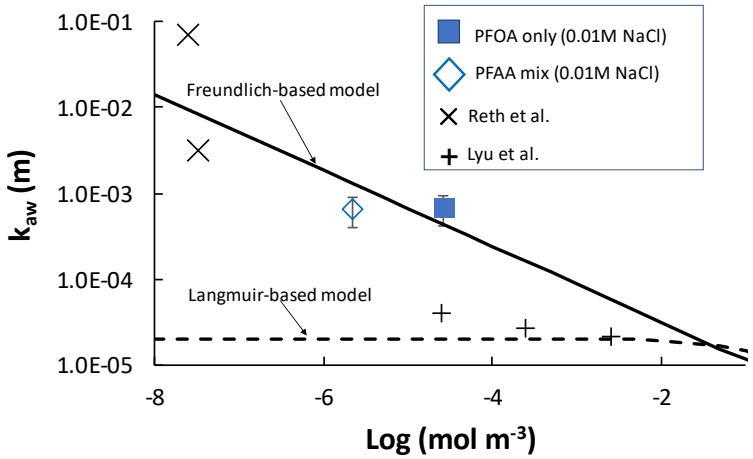

Figure 32: k_{aw}, measured via the film experiments in this study and measured via other techniques in previous studies, as a function of PFOA concentration.
Predicted values of k_{aw} based on interfacial tension data using the Freundlich model (Table 14) are shown by the solid line. Error bars represent 95% confidence intervals based on at least duplicate samples.

The PFOA k_{aw} values obtained by Lyu et al.[10] are approximately 10-times lower than what is predicted by the Freundlich model, as well as the trend displayed by the other data in Figure 32. The reason for this apparent discrepancy is unclear, but may be due to the difficulty in estimating the actual air-water interfacial area that the PFOA was exposed to during the unsaturated flow experiments.[10]

Figure 33 shows the calculated k_{aw} value for 8:2 $FTSO_2PrAd$-DiMeEtS (FtTAoS) in the Wurtsmith groundwater. The k_{aw} for 8:2 $FTSO_2PrAd$-DiMeEtS (FtTAoS) is approximately 10-times greater than for PFOS, despite having the same perfluorinated chain length, and a carbon chain length that differs by only 2 carbons. This difference likely is attributable to the head group, thereby highlighting the potential impact of head group on PFAS interfacial sorption.

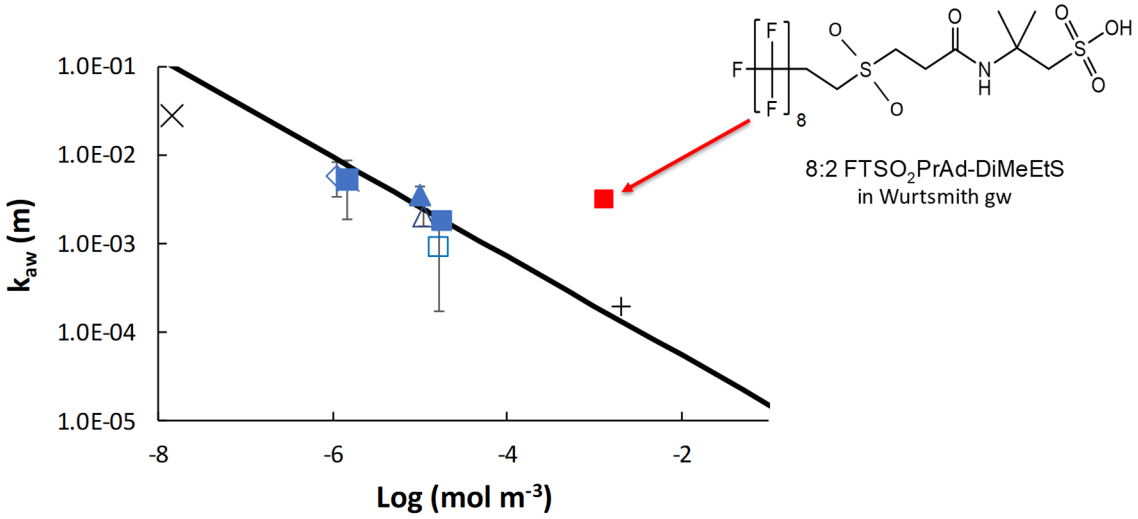

Figure 33: Calculated k_{aw} value for 8:2 FTSO$_2$PrAd-DiMeEtS in the Wurtsmith groundwater compared to the PFOS values in electrolyte (see Figure 30).

It is noted that k_{aw} for PFOS in the Wurtsmith water could not be determined because the elevated PFOS concentration in the Wurtsmith water (1,100 µg/L or 0.0022 mol m^{-3}) results in a k_{aw} that is too small to be accurately measured using the film method described herein; the film method is only effective for determining k_{aw} values that are greater than or equal to approximately 1 x 10^{-3} m.

Interfacial Sorption and PFAA Structure

Figure 34 and Figure 35 show, based on the interfacial tension measurements and application of the Freundlich model, the k_{aw} values for the perfluoroalkyl sulfonates (along with FtTAoS) and the perfluoroalkyl carboxylates, respectively. Values of k_{aw} increase with decreasing PFAS concentrations for all compounds. In addition, within each compound class, k_{aw} increases with increasing perfluorinated chain length. Previous studies[15] have shown that k_{aw} is related to the molar volume of the PFAAs. Figure 36 (top) shows the k_{aw} values determined based on the interfacial tension data and the Freundlich model at a PFAS concentration of 2 x 10^{-6} mol m^{-3}. Consistent with previous work,[15] the PFAA data shown in Figure 36 are reasonably described (R^2=0.88) by an exponential relationship. FtTAoS, with a structure that substantially differs from the PFAAs, does not appear to follow the same trend with molar volume.

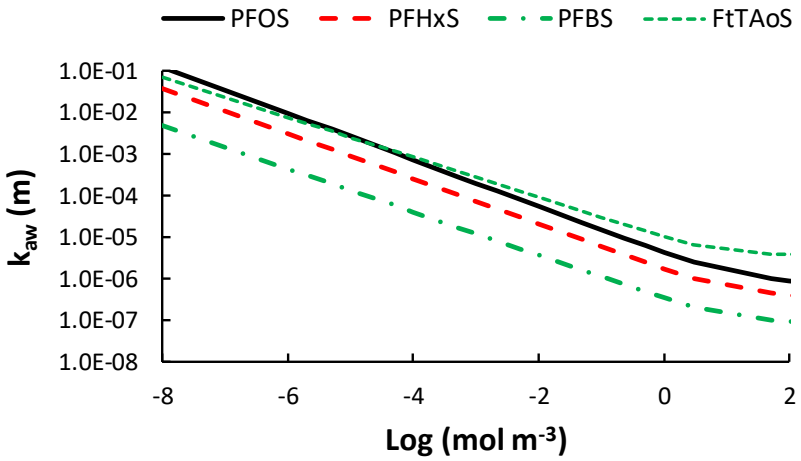

Figure 34: Freundlich-based model predictions of k_{aw} based on the interfacial tension data for the perfluorinated sulfonates and FtTAoS. 0.01 M NaCl was the background salt concentration.

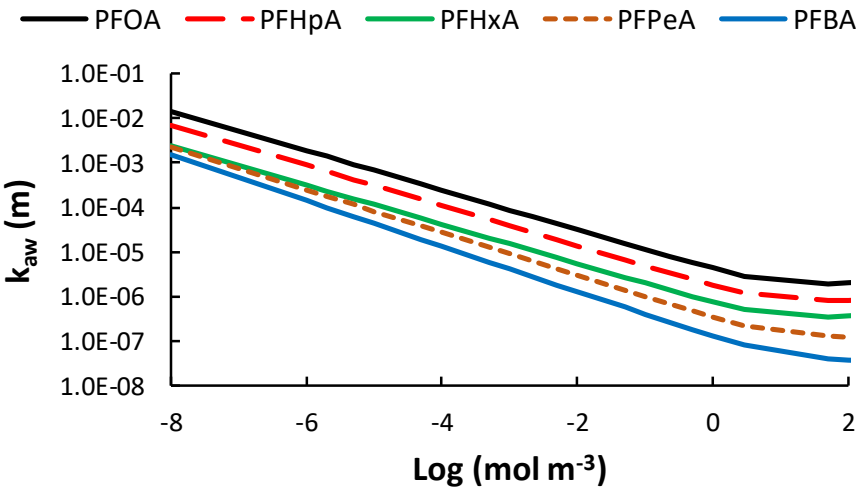

Figure 35: Freundlich-based model predictions of k_{aw} based on the interfacial tension data for the perfluoroalkyl carboxylates. 0.01 M NaCl was the background salt concentration.

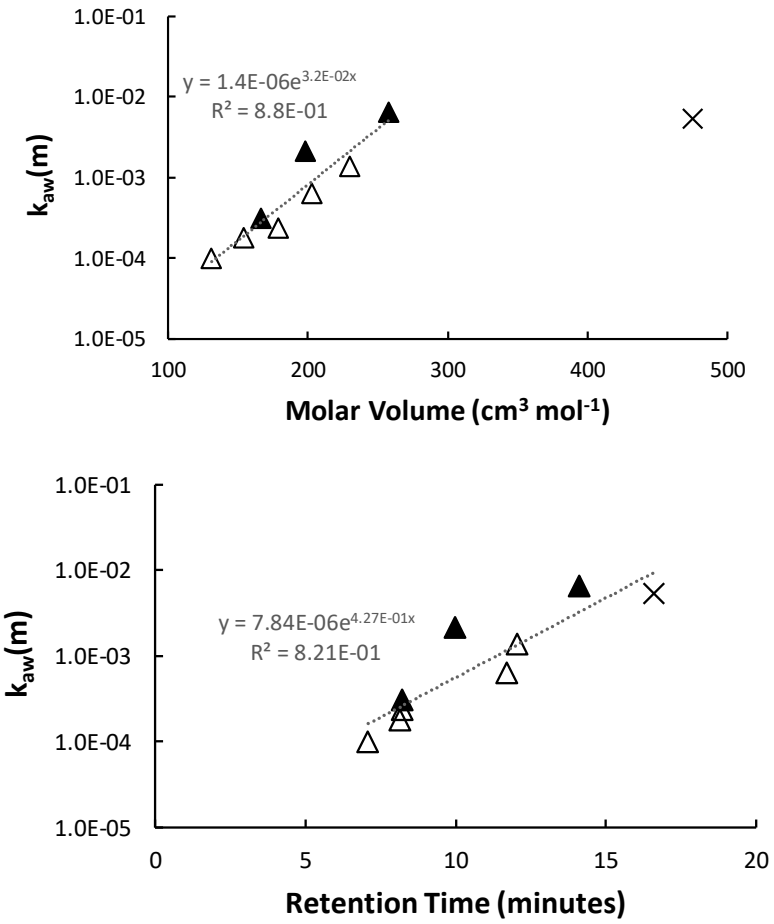

Figure 36: Freundlich model predictions of k_{aw} values as a function of molar volume (top) and chromatographic retention time (bottom) for the perfluorinated sulfonates (filled symbols), perfluorinated carboxylates (open symbols), and FtTAoS (X).
PFAS concentrations of 2 x 10-6 mol m-3 were assumed, and an NaCl concentration of 0.01 M. FtTAoS was not used in the regression shown in the top figure.

Chromatographic retention times are a proxy for relative hydrophobicity of PFAS.[16] Evaluating k_{aw} as a function of retention time using previously described analytical methods,[1,2] the data in Figure 36(bottom) suggest that chromatographic retention time may be related to PFAS uptake at the air-water interface, and may serve as a predictor of k_{aw} for the range of PFAS that are present in many AFFF formulations. Additional study is needed to assess the use of chromatographic retention time as a potential tool for estimating k_{aw} for PFAS.

Task 3.2 PFAS Unsaturated Soil Transport

Development of the Mass Transfer Index Concept

We developed a new Mass Transfer Index (MTI) concept that allows to quantify the impact of pore scale mass transfer mechanisms under equilibrium conditions. This index is important as it allows for the calculation of the impact of pore scale processes of mass transfer affected by the tortuosity of the fluid pathways and immobile water on macroscopic solute breakthrough simulated in column tests. The concept of MTI is introduced through modifying the average linear pore velocity by combining the physical effects of tortuosity and immobile zone on mass transfer and the chemical effects of retardation. In unsaturated flow, the average liner pore velocity is obtained by dividing the specific discharge (or Darcy velocity) by the volumetric water content. Equation 3.15 presents these modifications:

$$v_i = \frac{v_{linear}}{TR_i} = \frac{q}{\theta_w TR_i} \qquad \text{(Eq. 3.15)}$$

where v_i is the velocity for solute i as reflected in the solute breakthrough curve, v_{linear} is the average linear pore velocity, T is the Mass Transfer Index (MTI) introduced as material property of the porous medium, R_i is the retardation factor of solute i, q is the Darcy velocity or specific discharge, and θ_w is the volumetric water content. From Equation 3.11 it is clear the MTI of the porous media at a specific water content adds to the conventional retardation used in reactive transport and will have a major impact on the estimated retardation factor from analyzing a BTC. This concept of tortuosity and immobile water builds on past work which has recently been receiving renewed attention.[28–41]

While several theories of both tortuosity and mobile-immobile water interactions have been reported in literature,[42–46] we believe the MTI presents a simplified and a conceptually correct way of characterizing these processes in homogeneous, low-flow rate systems that are simulated in laboratory column experiments. This is especially important in the context of PFAS, as they are highly soluble chemicals with multi-phase partitioning processes. Properly and explicitly characterizing the physical processes in a system will give us more accurate estimations of retention in future studies.

We conducted 27 low flow rate conservative tracer experiments using a conservative tracer NaCl in three separate columns packed with the same 0.35mm sand where solute conductivity was measured at 15cm, 51 cm, and 83 cm downstream of the inlet using METER 5TE sensors. The power law relationship, typically used to describe changes in dispersion and tortuosity changing effective saturation,[34,47–50] described in Equation 3.16 was used for the fittings of an analytical solution to the advection dispersion presented in Equation 3.17:

$$T = f(S_e) = S_e^n + b \quad \text{(Eq. 3.16)}$$

$$TR_i \frac{dC_i}{dt} = -U \frac{dC_i}{dx} + D \frac{d^2C_i}{dx^2} - T\lambda_i C_i \quad \text{(Eq. 3.17)}$$

Figure 38 shows the variability of the MTI with convolutional variables of concentration and downstream measurement location to demonstrate there is only correlation between the MTI and the degree of saturation. These results demonstrate that a power law fit can accurately predict (average percent error < 10%) the MTI at saturation for a given material with a two-phase system. We also used the data to investigate the MTI variability with saturation in each of the columns. We predicted that irreducible sources of error such as pore scale packing differences, errors in measurement of very lower saturations, and air trapping caused by variable drainage rates can influence the MTI. As can be seen in Figure 37 despite these irreducible sources of error being present in all columns, the fitted parameters of for predicting the MTI as a function of Saturation were statistically similar in all three columns. Furthermore, Pearson Correlation coefficients were greater than 0.8 for all three of the column fittings and the total data fitting, indicating a very high degree of confidence in the associated correlation. Figure 37 and Table 15 show the results of the power law fittings in graphical and tabular formats.

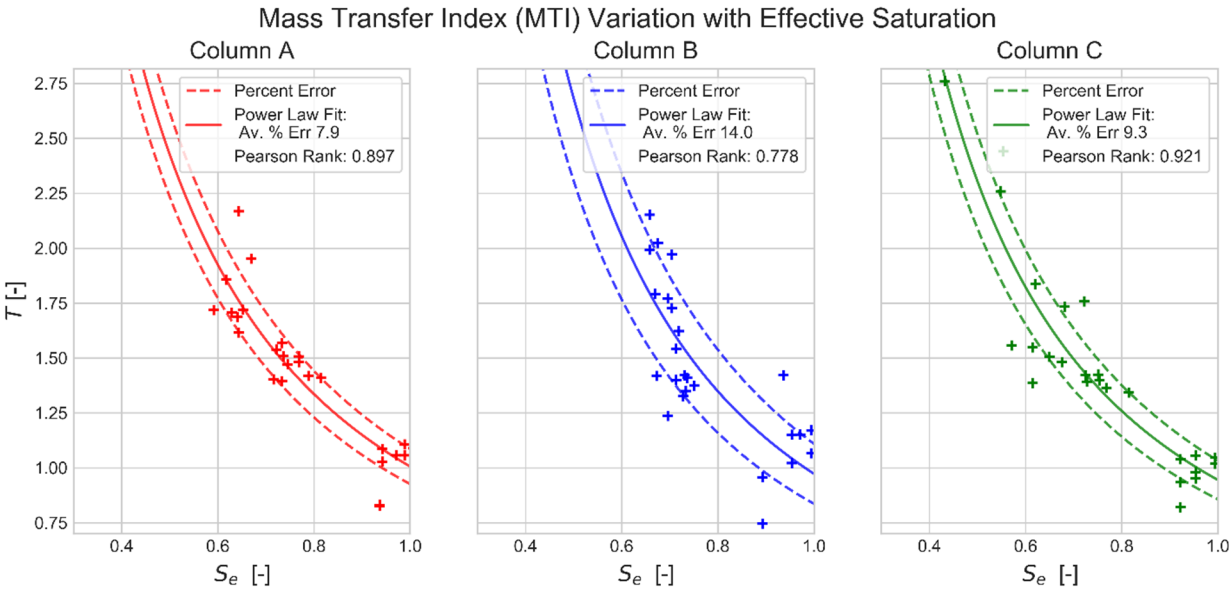

Figure 37: Power law fits for all three columns of the MTI-Saturation function.

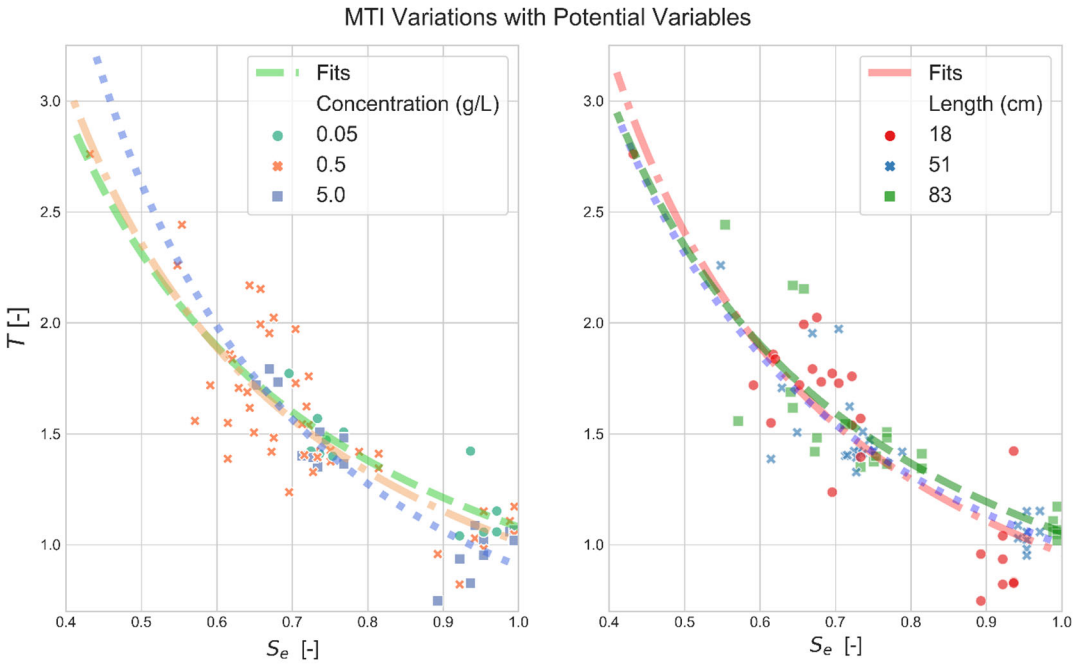

Figure 38: Mass Transfer Index (MTI) vs. Saturation correlation alongside convolutional variables.

Table 15: A table of the fitted power law MTI-Saturation relationship for each individual column and the bulk data for all three columns.

Columns	n	n Std. Error	b	b Std. Error	Avg. Percent Error (%)
A	-1.269	± 0.136	1.006	± 0.049	7.93
B	-1.463	± 0.267	0.973	± 0.086	14.01
C	-1.286	± 0.109	0.945	± 0.051	9.31
Bulk	-1.245	± 0.081	1.002	± 0.081	10.60

Using the MTI to quantify advective tortuosity and mobile-immobile phase effects

While the MTI provides some information on the overall behavior of solutes in a porous media, the absolute value of the MTI alone is not enough to separately assess impacts of tortuosity and mobile/immobile water. Fortunately, there have been some past studies devoted to the study of quantifying the change in diffusive tortuosity of a porous media system as a function of that systems water content. One well-known and widely used formulation for tortuosity was derived by Moldrup et al. 1997[49] for the use in variably saturated soils. This work built on theories derived from the diffusivities of gases in porous media empirically quantified and experimentally validated by Millington and Quirk in 1961.[50] The Moldrup model was specifically created for and validated

using conservative solutes in sieved, uniform porous media, making this model well suited for comparison in this study where similar sands were used. Furthermore, past studies of fully saturated sands and with similar grain size distributions provide results which are well correlated with the Moldrup et al. (1997) model.[49]

A modified version of the mobile-immobile model is presented in the modeling section (3.3) which can be used to directly calculate advective flow path tortuosity in unsaturated sands. We also gain valuable insight by comparing the predicted diffusive tortuosity from Moldrup et al. 1997 (orange) to the regression of the MTI for this sand (blue) in Figure 39 Both the tortuosity and MTI are used to introduce physical retardation correction to the average linear pore velocity (eq. 1 without chemical retardation). A plot comparing the MTI and tortuosity on the saturation allowed us to evaluate the effect of mass transfer to the immobile zone that is not included in the tortuosity derived by Moldrup et al. (1997).[49]

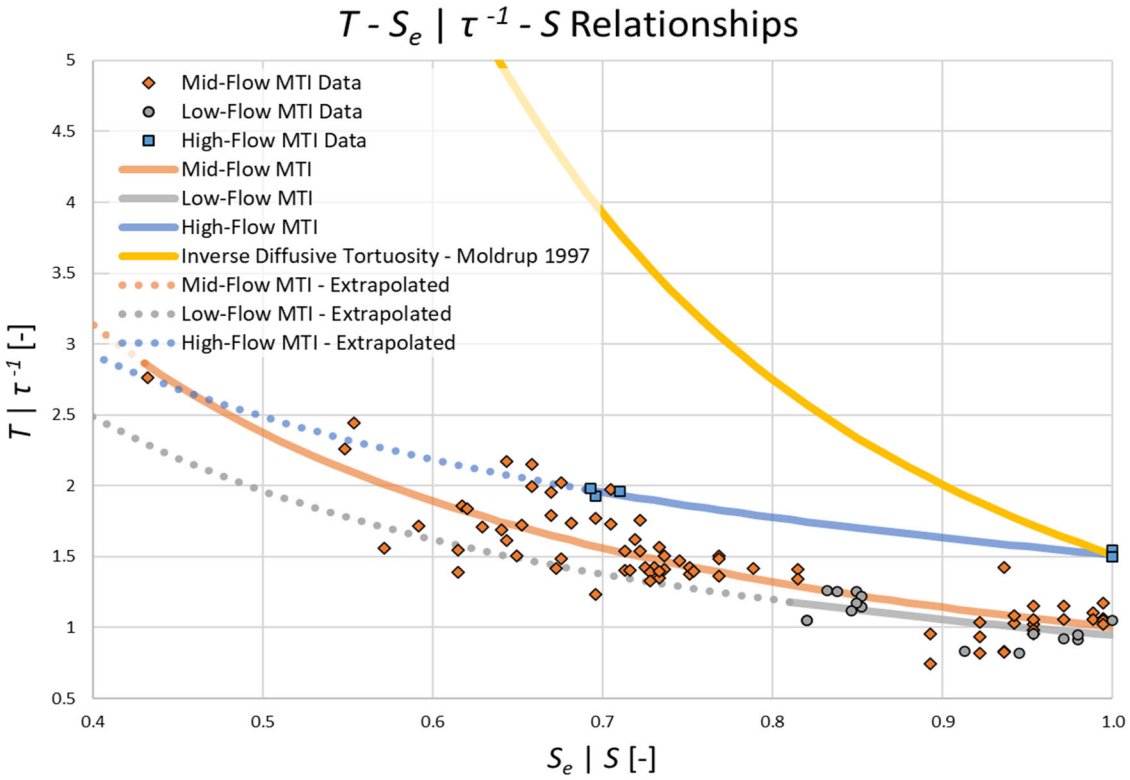

Figure 39: The variability of the MTI and diffusive tortuosity with effective saturation and saturation respectively. For pipe flow, tortuosity increases with decreasing saturation.

Results from the full MTI analysis show there is a consistent power law type relationship across the full range of effective saturation for this idealized media. The MTI tends to increase with decreasing saturation for this media, albeit at a much slower rate than diffusive tortuosity. This finding suggests that while advective flow path tortuosity can delay the expected breakthrough time of conservative tracers, this effect is much less than diffusive tortuosity likely owing to

increased interstitial velocities due to immobilized water, channelization, or "sheet" flow. There also appears to be a clear dependence of the MTI with flow rate, where at lower flow rates the MTI converges to 1. This is consistent with MTI theory, as the system moves to lower velocities, the system becomes more diffusion dominated and the MTI correction becomes less important. This is because the MTI is only applicable for systems where advection is a significant process. The full results of the MTI method are outlined in Stults et al. 2021.[19]

PFOS Column Studies

We conducted five set of experiments with PFOS in triplicate at environmentally relevant concentrations to establish a baseline single phase transport before moving on to complex AFFF mixtures. The five sets of triplicate PFOS studies were conducted in a highly ideal sand described above. All PFOS studies were conducted in very low ionic strength water to minimize the potential for solid phase partitioning, and reduce the overall air-water interfacial sorption for the sake of experimental efficiency.

The five experiments are listed below:

Experiment 1) Fully saturated (S=1.0) at PFOS = 8.0 ug/L.
Experiment 2) Quasi-saturation (S ~ 0.85) at PFOS = 0.8 ug/L
Experiment 3) Quasi-saturation (S ~ 0.85) at PFOS = 53 ug/L
Experiment 4) Low partial saturation (S ~ 0.3) at PFOS = 0.4 ug/L
Experiment 5) Low partial saturation (S ~ 0.3) at PFOS = 45 ug/L

Evaluation of PFOS Transport Under Idealized Conditions

To date, few studies have directly measured the air-water interfacial partitioning coefficient (K_{ia}) values for perfluorooctanoate (PFOA) and, even to a lesser extent, for perfluorooctane sulfonate (PFOS).[10,51–54] Other studies have indirectly used interfacial tension (IFT) measurements to estimate K_{ia} values.[55–58] While many of the results from these studies are consistent, there is disagreement over whether the Langmuir isotherm (which reduces to a linear isotherm with a constant K_{ia} at low concentrations) or Freundlich isotherm (nonlinear throughout the entire concentration range, with Kia increasing with decreasing concentration) model is appropriate for modeling air-water interfacial sorption at low concentrations.[59,60] Selection of a Langmuir versus Freundlich model can result in orders-of-magnitude differences in K_{ia} values at low concentrations, which can lead to large differences in predicted PFAA unsaturated transport. While the Langmuir isotherm is conceptually robust and appropriate at or above a critical reference concentration (CRC),[56,58,61] air-water interfacial isotherm non-linearity for PFOS and PFOA has been demonstrated below the CRC (~1 mg/L for PFOS, ~10 mg/L for PFOA).[10,53] In addition, there are some discrepancies between the K_{ia} values measured for PFOA using equilibrium batch tests[53] and aerosol methods[62,63] as compared to K_{ia} values estimated using the surface microlayer (SML)[63–65]

method and unsaturated column transport experiments, particularly using the constant drainage (CD) method.[10,52,61,66,67]

The aerosol method conducted by McMurdo et al. 2008[62] and Johansson et al. 2019[63] uses the enrichment factor of PFAAs in aerosolized droplets from a sea spray generator to calculate the K_{ia}. This method was used to overcome the flaws associated with the SML method and was considered to be the more reliable measure of air-water interfacial partitioning in the comparative analysis of Johansson et al. 2019.[63] The SML method for estimating K_{ia} values assumes it is possible to sample a 60 micron surface layer by hand using a hydrophobic glass plate and is known to be flawed.[68] This is because the method perturbs the SML, assumes no liquid beyond the SML contacts the glass plate, and introduces and secondary non-wetting phase (the glass plate) with an entirely different hydrophobicity than the air-water interface. The flaws in the SML method are evident in Johansson et al 2019[63] (the SML method dramatically underestimates K_{ia} compared to an aerosol method) and in Le et al. 2021[68] (where the SML method achieved less than 50% removal of a floating powder).

The CD approach generally uses very short (< 0.2 m) columns at somewhat low saturations ($0.6 < S < 0.75$) and relatively high linear pore velocities ($1.0 > v_{lin} > 0.5$ cm/min). Short columns (< 1 m) can exhibit end effects under drainage or imbibition conditions, which results in higher saturation at the outflow, which makes water content non-uniform along the length of the column.[69,70] At lower saturations, larger volume fractions of water become immobilized and greater advective flow path tortuosity develops within the representative elementary volume (REV),[19,36,37] which can cause retention by non-equilibrium partitioning.[19,33,43,46,71] Finally, when non-equilibrium conditions are present, higher linear pore velocities estimated using mobile flow area can potentially cause under-estimation of K_{ia} values.[43,44,46] Though the CD method may be representative of non-Fickian transport that can develop in field conditions, these factors limit the application of CD experimental results in developing a mechanistic understanding of air-water interfacial retention processes. Determination of the appropriate air-water interfacial partitioning isotherm is of critical importance, as even mild non-linearity can significantly alter transport predictions of models.

Experiments 1-3 were conducted under highly ideal conditions (i.e. saturated or quasi-saturated conditions in pure silica media with limited potential for non-Fickian transport). The first PFOS experiments were conducted under saturated conditions to determine the solid phase partitioning of PFOS and establish a transport baseline for comparison to other studies. Experiments 2 & 3 were conducted under quasi-saturated conditions to examine the air-water interfacial partitioning behavior of PFOS absent non-Fickian transport considerations. Experiments were conducted at high and low PFOS concentrations to determine if the air-water interfacial partitioning of PFAS changed significantly with changes in concentration. The Quasi-saturated condition is also referred to as the residual air saturation, and refers to the condition in which positive pressure head exist

on the column but entrapped air-bubbles remain in the system. These conditions are nearly identical to fully saturated conditions and will have negligible non-Fickian transport effects. Linear pore velocities were maintained between 0.3 – 0.6 cm/min in almost all experiments to ensure negligible effects results from non-equilibrium were present between experiments.

Results from Experiment 1 demonstrated PFOS had negligible sorption to the ideal sandy media. This was expected as the media was well cleaned and highly ideal. Experiment 2 demonstrated that PFOS retardation significantly increased when air-water interfacial area was introduced to the system. There was also a clear differentiation in air-water interfacial partitioning between the branched and linear isomers of PFOS. Experiment 3 was conducted at a PFOS concentration nearly 100x higher than Experiment 2, and demonstrated reduced retardation of PFOS. This change in concentration is associated with concentration dependent air-water interfacial partitioning below a critical reference concentration (CRC), and contradicts the frequently used Langmuir isotherm. A summary of the ideal transport experiments are presented in Table 16, and BTC results of Experiments 1-3 are presented in Figure 40.

Table 16: The experimental conditions for all column experiment performed in this study.

The small column studies with SDBS were performed to validate the quasi-saturation method for estimating air-water interfacial partitioning of PFAAs. Conditions in Kim et al. 1997 were recreated for the small column study to ensure consistency with measured K_{ia} values for SDBS. Long column studies were performed with PFOS using the estimated A_{aw} from short column experiments.

Column ID	**Experiment ID**	***S* (-)**	**Chemical Input**	**Background Electrolyte**	**Linear Pore Velocity (*cm/min*)**
Small	Small - Sat	1	SDBS	0.01 M NaCl	0.32
	Small - Unsat1	0.96	SDBS	0.01 M NaCl	0.31
	Small - Unsat2	0.89	SDBS	0.01 M NaCl	0.29
A - Long	1	1	PFOS	$8.0E^{-5}$ M TDS	0.33
	2	0.84	PFOS	$8.0E^{-5}$ M TDS	0.29
	3	0.84	PFOS	$8.0E^{-5}$ M TDS	0.32
B - Long	1	1	PFOS	$8.0E^{-5}$ M TDS	0.44
	2	0.85	PFOS	$8.0E^{-5}$ M TDS	0.43
	3	0.85	PFOS	$8.0E^{-5}$ M TDS	0.46
C - Long	1	1	PFOS	$8.0E^{-5}$ M TDS	0.38
	2	0.82	PFOS	$8.0E^{-5}$ M TDS	0.34
	3	0.82	PFOS	$8.0E^{-5}$ M TDS	0.43
*S is the volume fraction saturation of water porous media.					

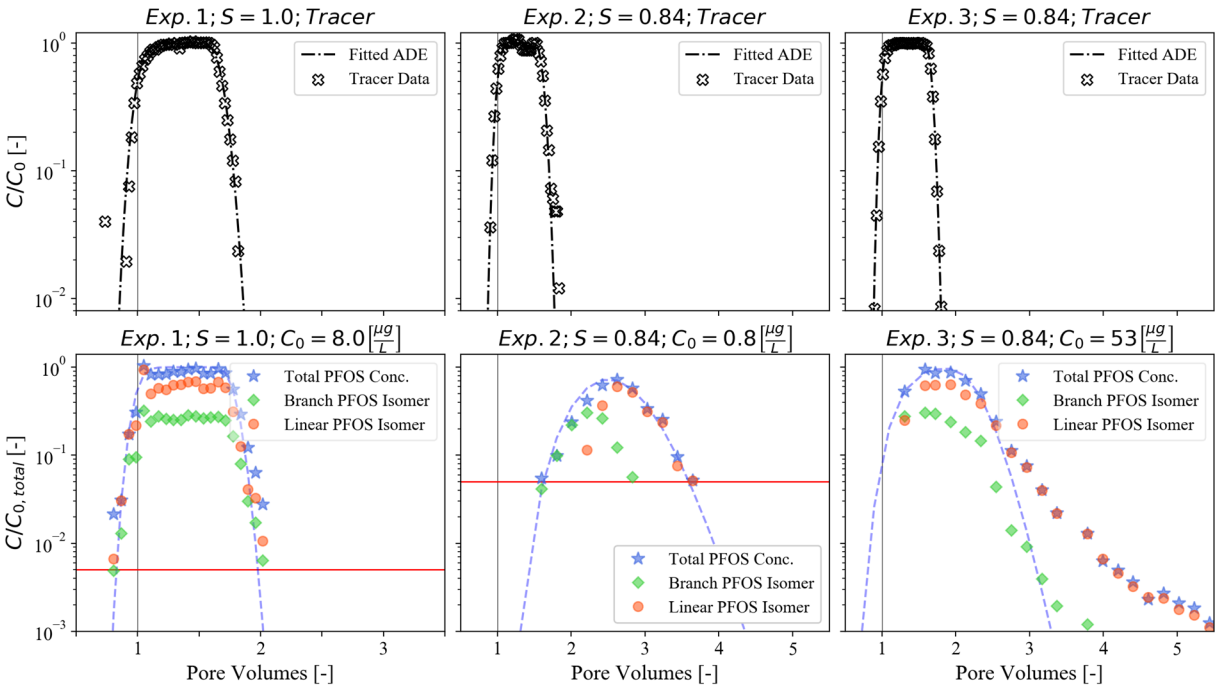

Figure 40: Breakthrough curve results for conservative tracers (0.01 M NaCl) of each experiment (top row), total PFOS concentration, branched isomers concentration, and linear isomer concentration for Exps. 1-3 in Column B.

The red line on the log y-axis plots represents the lower limit of quantitation (LLOQ) of 0.04 µg/L for total PFOS concentration, and the dashed blue line is the equilibrium linear isotherm (or low concentration Langmuir isotherm) fit of the total concentration data.

The fully saturated PFOS BTCs appear ideal, were well fit by the equilibrium ADE, and have similar dispersion to the conservative tracer BTCs under saturated conditions. However, when an air-water interface is introduced to the system, both retardation and dispersion appear to significantly increase. While Experiment 2 appears to be well fit by the ADE, the limit of quantification for this experiment was too close to the maximum concentration to really observe tailing behavior. Experiment 3, conducted at a higher concentration, clearly shows tailing behavior which is consistent with a Freundlich type isotherm. To evaluate the change in K_{ia} with changes in concentration, the empirical correlation presented in Equations 3.18a-b were plotted against the data. The Langmuir isotherm (as derived from IFT data) was obtained from Costanza et al. 2019 along with the error ranges representing uncertainty in ionic strength. The Freundlich data was fit to the data from this study and Schaefer et al. 2019.[53] The full results of this analysis are presented in Figure 41.

$$\textbf{\textit{Freundlich}} \rightarrow K_{ia} = nK_f C_{aq}^{n-1} \qquad \text{(Eq. 3.18a)}$$

$$\textbf{\textit{Langmuir}} \rightarrow K_{ia} = \frac{q_{max}\eta}{(1+\eta C_{aq})^2} \qquad \text{(Eq. 3.18b)}$$

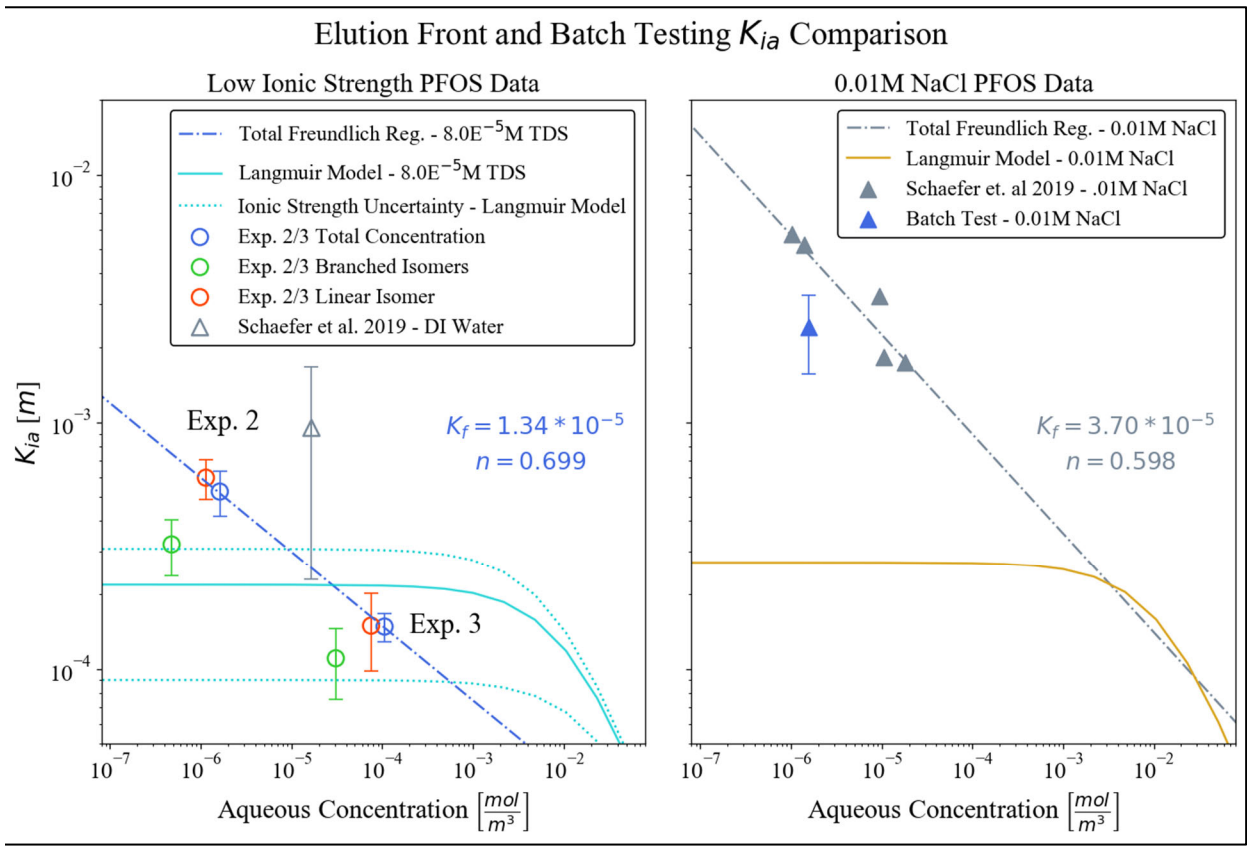

Figure 41: Calculated Kia values from using equilibrium batch (triangles) and quasi-saturation column (circles) methods.

Solid lines represent Langmuir isotherms measured from interfacial tension data in Costanza et al. 2019 (8.0E^{-5} M) and Brusseau et al 2021 (0.01M NaCl) and are plotted for reference only. Dashed lines represent regressed Freundlich isotherms for 0.01M NaCl Schaefer et al. 2019 data (gray) and 8.0E^{-5} M column data from this study. The CRC for PFOS, where the Langmuir isotherm becomes linear, is at approximately 0.001 mol/m^3. The upper and lower bounds of the ionic uncertainty related to ionic strength of solution in the Costanza et al. 2019 model are representative of the highest conductivity measured in the effluent (15µS/cm) and the lowest conductivity of the influent (0.4 µS/cm) respectively.

Results demonstrated clearly demonstrate the K_{ia} of PFOS increases with decreasing concentration in a manner which is well fit by the Freundlich isotherm. Further modeling and analysis is presented to support the application of the Freundlich isotherm and demonstrate the use of the MTI for evaluating systems for non-Fickian transport in unsaturated systems in Stults et al. 2022.[72]

Evaluation of PFOS Transport Under Drainage Conditions

Experiments 4 & 5 were conducted under drainage conditions similar to those in the MTI section to examine the effect of non-Fickian transport. This was done because of a significant body of literature[10,52,55,61,66,67] has been developed which utilizes drainage conditions to estimate the air-water interfacial partitioning of select PFAAs. Contrary to our studies on the subject, analyses conducted with this method typically assert a Langmuir isotherm is appropriate for modeling PFAS air-water interfacial partitioning across the full range of relevant concentrations. However, closer analyses reveal the evidence supporting the use of the Langmuir isotherm for PFOA air-water interfacial partitioning was not as strong as the authors had originally presented.[61,68] Further, in reanalysis of BTCs from these studies using the MTI concept revealed there is likely non-Fickian transport (i.e. significant immobile water volume, "sheet" flow) present in these drainage systems. Figure 42 presents K_{ia} vs concentration data for PFOA at several different ionic strengths fit to the Freundlich isotherm and presented against a Langmuir isotherm derived from IFT data presented in several different studies across multiple research groups.

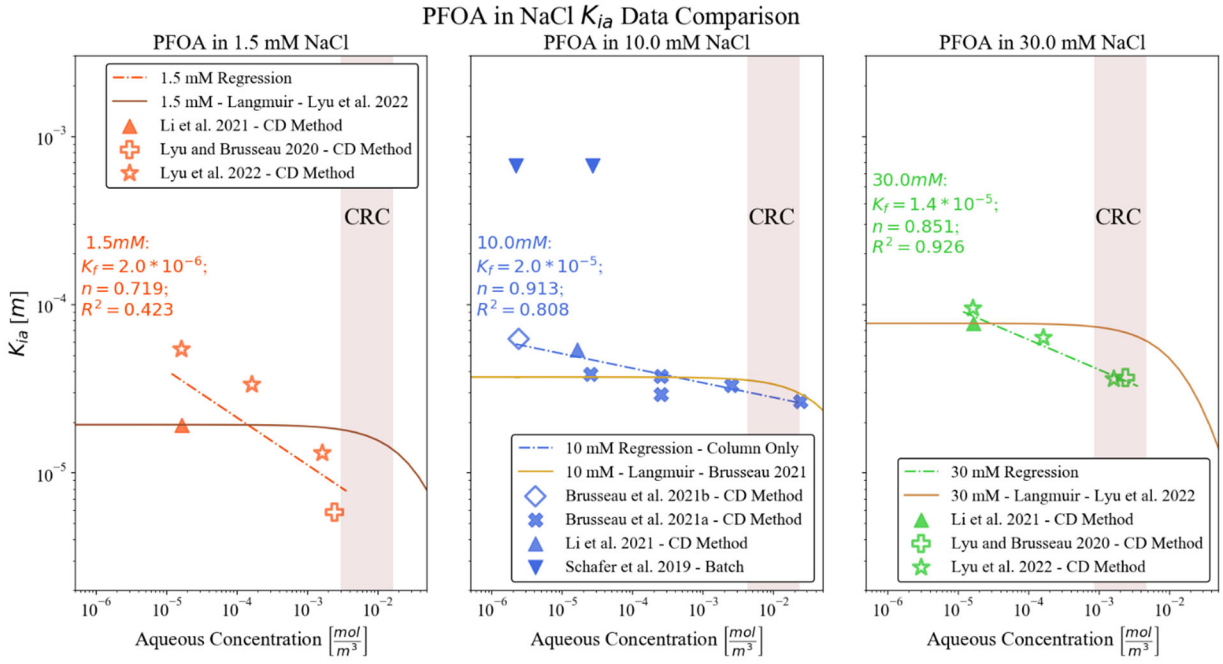

Figure 42: Literature reanalysis of PFOA K_{ia} from drainage method data.
PFOA K_{ia} data in 10 mM NaCl from pan film studies (Schaefer et al. 2019[53] - inverted triangles, middle panel) is presented, but not regressed, to highlight the difference in the K_{ia} measured by the pan film method vs drainage-based methods.

It is clear both from both observation and regression analysis that the K_{ia} calculated clearly increases with decreasing concentration for PFOS well below the CRC for various background electrolyte concentrations. The degree of non-linearity is lower than the degree of non-linearity observed under quasi-saturated conditions, and the results are also less consistent between different

experimental sets. These cursory findings suggest that stochastic variability between experiments is present, which is consistent with the observation of non-Fickian transport elements forming under drainage conditions. To evaluate the impact of non-Fickian conditions on transport of PFOS in our system, Experiments 4 & 5 were conducted at concentration similar to Experiments 2 & 3 respectively but with different saturations, linear pore velocities, and drainage conditions. Table 17summarizes the experimental conditions for the system.

Table 17: Full table of experimental conditions and preliminary results of the Experiments 4 and 5 conducted for the comparative analysis in this study.

Exp. ID	Column ID	C_0 PFOS (ug/L)	S (-)	v (cm/min)	Pe_{PFOS} (-)	Uniform Sat.	MTI (-)	R (-)
4	A	0.42	0.51	1.17	132.0	N	0.93	10.6
	B	0.42	0.34	0.84	0.002	Y	0.72	1244
	C	0.42	0.91	0.51	33.0	Y	1.05	1.3
5	A	45	0.38	0.69	13.4	Y	1.21	6.6
	B	45	0.28	0.61	14.1	Y	1.25	10.7
	C	45	0.33	0.57	29.3	Y	1.06	10.9

Table 17 illustrates the four elements of investigation in this study: 1. Potential use of the MTI concept to predict transport non-idealities in unsaturated systems (all experiments); 2. The effect of water content non-uniformity on conservative and non-conservative solute breakthrough (Experiments 4a and 4c) under standard CD method conditions; 3. the relationship between linear pore velocity and apparent K_{ia} under constant saturation and concentration conditions (Experiments 2, 3, and 5); and 4. The effect of PFOS concentration on rate limited partitioning under highly non-Fickian conditions (Experiments 4b and 5a-c).

Assessing the Potential for Non-Equilibrium Using the MTI

The MTI concept is analogous to the effective porosity concept for saturated systems and is intended to account for the increasingly important impact of immobile water and advective flow path tortuosity in unsaturated systems. Our published studies[19,72] demonstrated that under ideal (pipe-flow) conditions, the MTI should generally increase with decreasing saturation, and should generally follow an inverse power law type relationship. An MTI which is significantly less than 1 ($T < 0.9$) or does not increase with decreasing saturation suggests that significant non-Fickian elements may be present (e.g., relatively large immobile water volume, preferential flow paths, or sheet flow). The potential presence of sheet flow is especially important, as it suggests that the air-water interface is potentially mobilized,[73,74] and therefore sorption to the air-water interface would not delay the emergence of a sorbing solute.

We note that for 4 of the 6 replicates in Experiments 4 and 5, that the MTI is greater than or equal to 1 as determined from conservative NaCl tracers. However, almost all of the calculated MTI values (with the exception of Experiment 4c) are significantly lower than predicted from the power law relationship determined above (in the same sand), suggesting that rate-limited partitioning is likely present in all but one of the experimental replicates. Of particular interest is Experiment 4b (row 2 – Table 1), where the MTI is significantly lower than 0.9 suggesting a significant amount of immobile water is present in the column, which could induce non-equilibrium air-water interfacial partitioning.[72] When the breakthrough curve data for the non-dimensional ADE were fit for PFOS, the resulting Peclet number is much less than 1 (Pe_{4b} = 0.002) and the Retardation factor is unreasonable (R_{4b} = 1244). A Peclet number this low is suggestive of a system where dispersive forces are highly dominant over advective forces, and therefore the underlying assumptions of the Retardation factor approximation no longer apply (i.e. the calculated R value for Experiment 4b cannot be used to approximate a $K_{ia,app}$). Experiment 4b is still useful, however, in demonstrating the significant effect of non-Fickian transport. PFOS had a predicted retardation of 50 using the equilibrium K_{ia} predicted above. However, PFOS clearly begins to emerge around 1 pore volume, suggesting that non-Fickian transport can induce breakthrough of PFOS 50 times earlier than what is predicted by equilibrium models. This is unexpected based on BTC fitting of the conservative tracer alone (absent MTI analysis). Although the conservative tracer for Experiment 4b has slight tailing and Peclet number below 100 ($Pe_{4b,tracer}$ = 38), the system is still well-described by the non-dimensional ADE. Full BTC results for Experiment 4 tracers and PFOS data are presented in Figure 43.

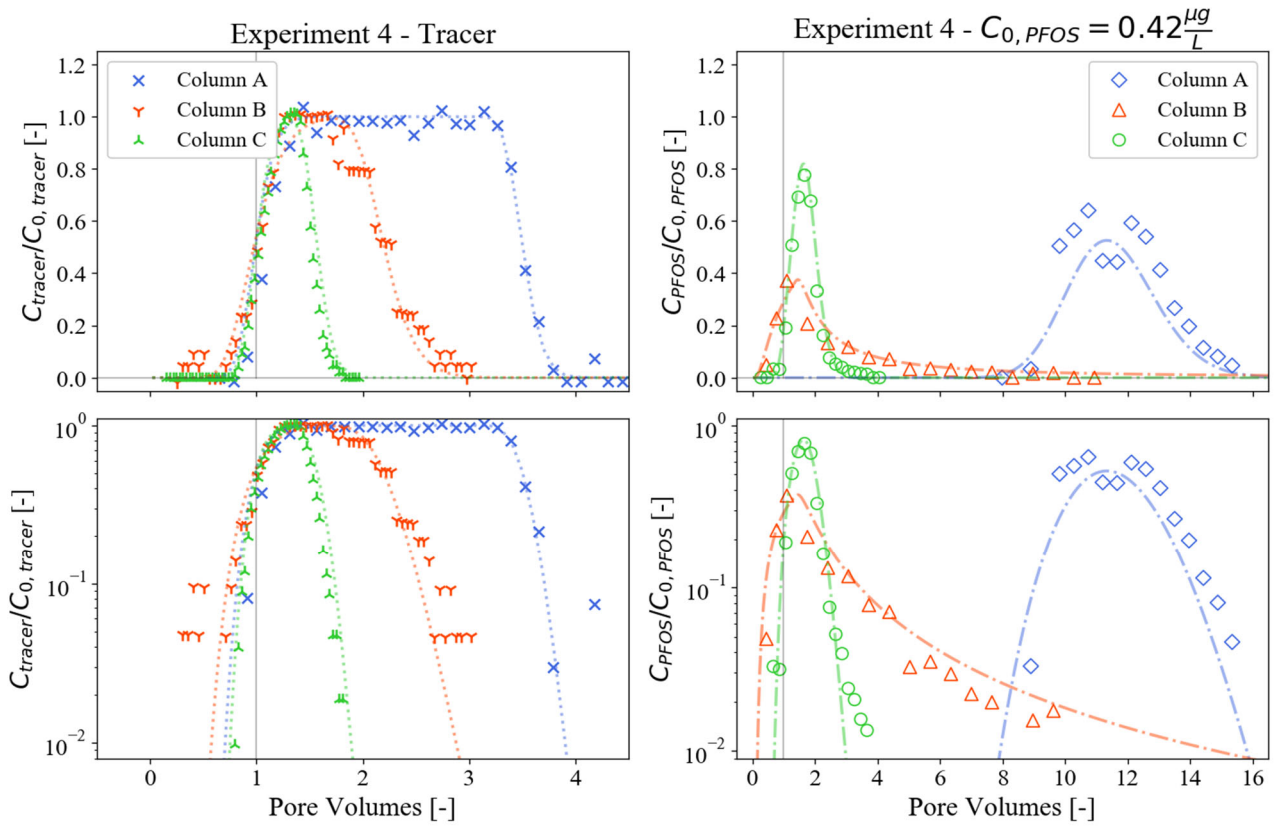

Figure 43: Full BTC results of the 0.01M NaCl conservative tracer (left) and the low concentration PFOS (0.42 µg/L) in MilliQ water (right).

For columns A and B are ideal and well fit by the non-dimensional ADE with a high Peclet number. Column B conservative tracer data is less ideal (more scatter and less goodness of fit to the ADE) with a Peclet number below 50 ($Pe_{tracer\text{-}B} = 38$). PFOS BTC data for column A and C appears ideal and is well fit by the non-dimensional ADE. However, Column B has a highly unusual BTC that is characteristic of non-equilibrium sorption processes. The $K_{ia,app}$ for column B PFOS BTC cannot be calculated, as the Peclet number is less much than 1 ($Pe_{PFOS\text{-}B} = 0.001$) indicating the non-equilibrium or dispersion processes are too great for method of moments assumptions to be applicable.

Effect of Water Content Non-Uniformity on BTCs

Drainage method based studies[10,52,55,61,66,67] suggest that water content is uniform in their gravimetrically monitored systems because of uniform saturations generated during X-ray tomography studies[75,76] and because the conservative tracer BTCs appear to be ideal (i.e. no tailing or appearance of rate limited mass transfer).[10,52,55,61,66,67] However, it is well established that columns of this size often suffer from end effects, or pooling of wetting phase liquid at the base, when unit gradient conditions are not achieved through high suction.[70,77] BTC results from the non-uniform water content experiment (Experiment 4a, Table 17– row 1, Figure 43 – blue x's and diamonds) demonstrate that systems with highly non-uniform water contents can produce breakthrough curves which appear to be ideal. The non-uniformity of the water content in the

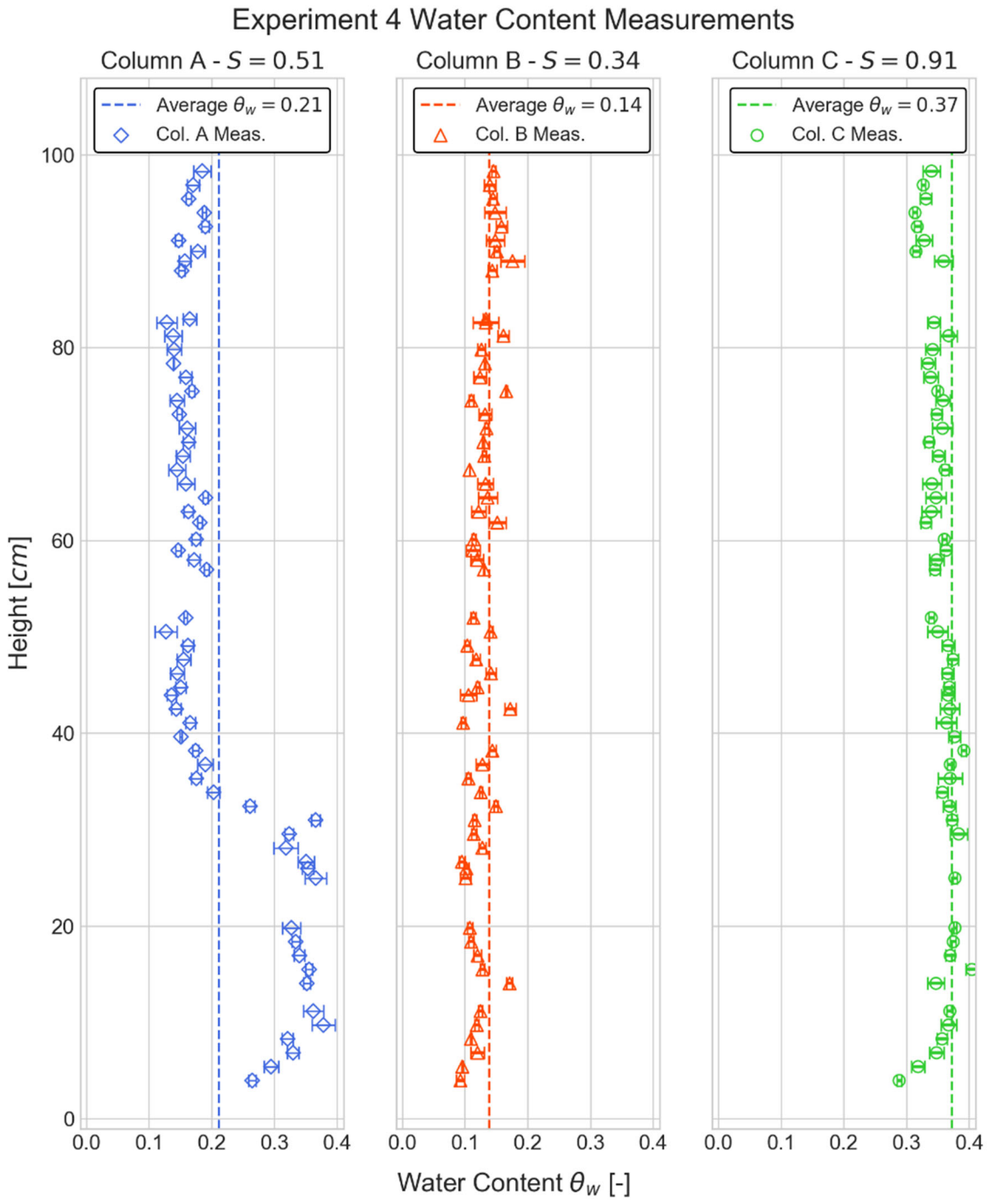

Figure 44: X-ray absorption spectroscopy scans of columns for Experiment 4.

system of Experiment 4a was confirmed using both sensor-based water content measurements and high spatial resolution x-ray absorbance spectroscopy (Figure 44).

Because saturation could be a confounding variable for the system, Experiment 5 replicates were conducted under saturation conditions which were nearly equivalent. Low saturations for experiment were chosen because of the highly non-Fickian transport observed in Experiment 4b at low saturation. Previous pore network modeling studies and experimental modeling studies with high resolution X-ray tomography have demonstrated that lower saturations are associated with increasingly non-Fickian transport.[36,37,78] Linear pore velocity was varied slightly between each experiment to ensure that differences in K_{ia} could potentially emerge. Linear pore velocities were maintained around 0.6 cm/min for this experimental condition to replicate Lyu et al. 2018 linear pore velocities as closely as possible. The BTCs for Experiment 5 are presented in Figure 45, and x-ray spectroscopy scans confirming water content uniformity are presented in the SI.

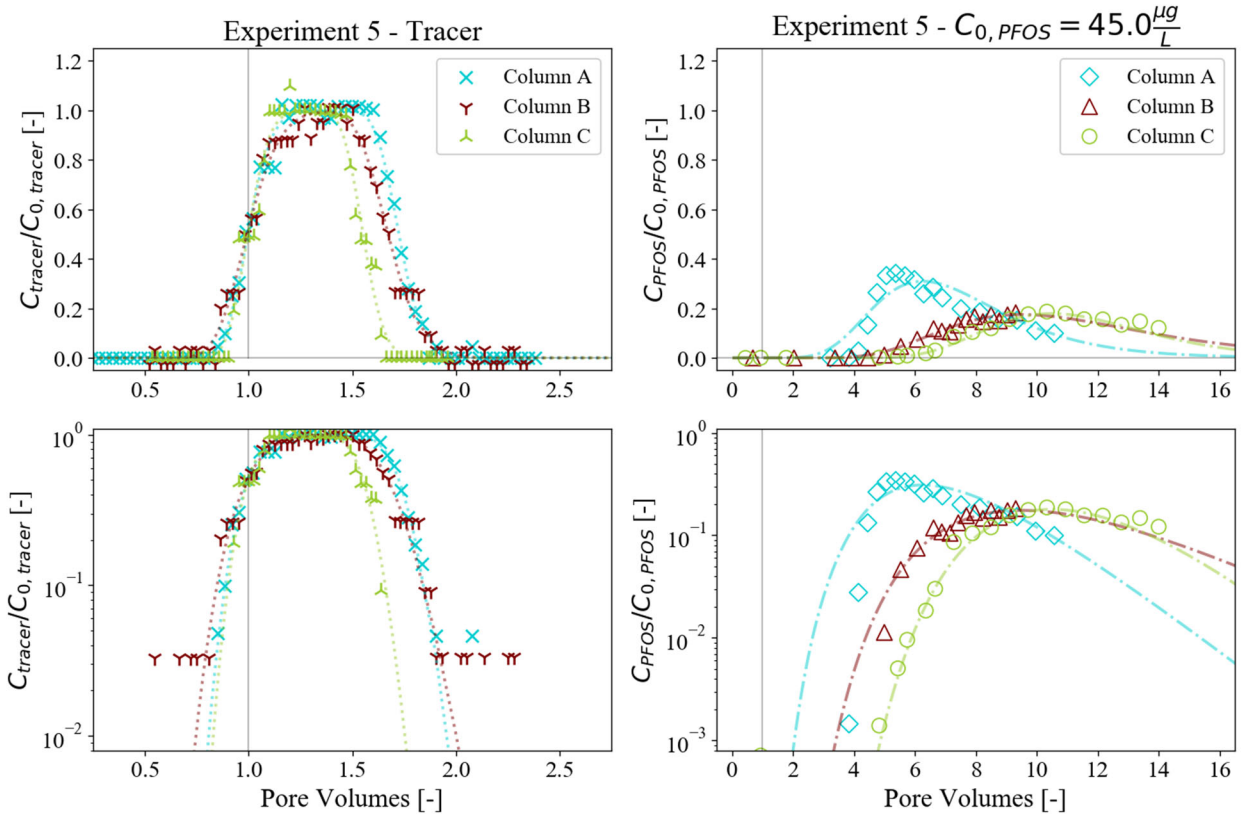

Figure 45: Full BTC results of the 0.01M NaCl conservative tracer (left) and the PFOS in MilliQ water (right).

Conservative tracers appear to be ideal, and are well fit by the non-dimensional ADE with high fitted Peclet number. Noise at the lower end of concentration appears to be an artifact of sensor detection limits. Traits characteristic of isotherm non-linearity are clearly present in Column A of Experiment 5, but are less readily visible in column B and C where Retardation is larger and Peclet number are smaller.

Results of Experiment 5 demonstrate more ideal transport behavior than the low concentration Experiment 4b conducted under similar saturation and velocity conditions. Both the conservative tracers and the PFOS partitioning BTCs were well-fit by the non-dimensional ADE, with Peclet

number significantly greater than 1 (although still less than ideal, Table 17– rows 4 through 6). Sharp elution fronts and BTC asymmetry, which is characteristic of isotherm non-linearity, were apparent. However, some of the BTC asymmetry can potentially be explained by the lower Peclet numbers of the fitted ADE (i.e. dispersive/non-equilibrium forces are significant) as compared to the conservative tracers. MTI values for the Experiment 5 (Table 17– rows 4 through 6) are greater than for Experiment 4b (Table 17– row 2), and the Peclet numbers of fitted ADE for the conservative tracers are much greater as well. These observations are consistent with the more ideal transport behavior of the Experiment 5 replicates. The observation of a very low MTI and extremely early emergence of PFOS suggests Experiment 4b was subject to much greater non-Fickian transport effects (i.e. immobile water, sheet flow) than the Experiment 5. The Peclet numbers of all the fitted PFOS BTCs are also significantly lower than those of the salt tracer (*Pe* > 100), providing further evidence that non-equilibrium is present in this system (see SI 3 of our published study for an in depth discussion of this phenomenon).[72] There appears to be some correlation between the observed retardation factor and linear pore velocity for the replicates in Experiment 5. X-Ray spectroscopy scans of the column during Experiment 5 are presented in Figure 46 to confirm water content uniformity.

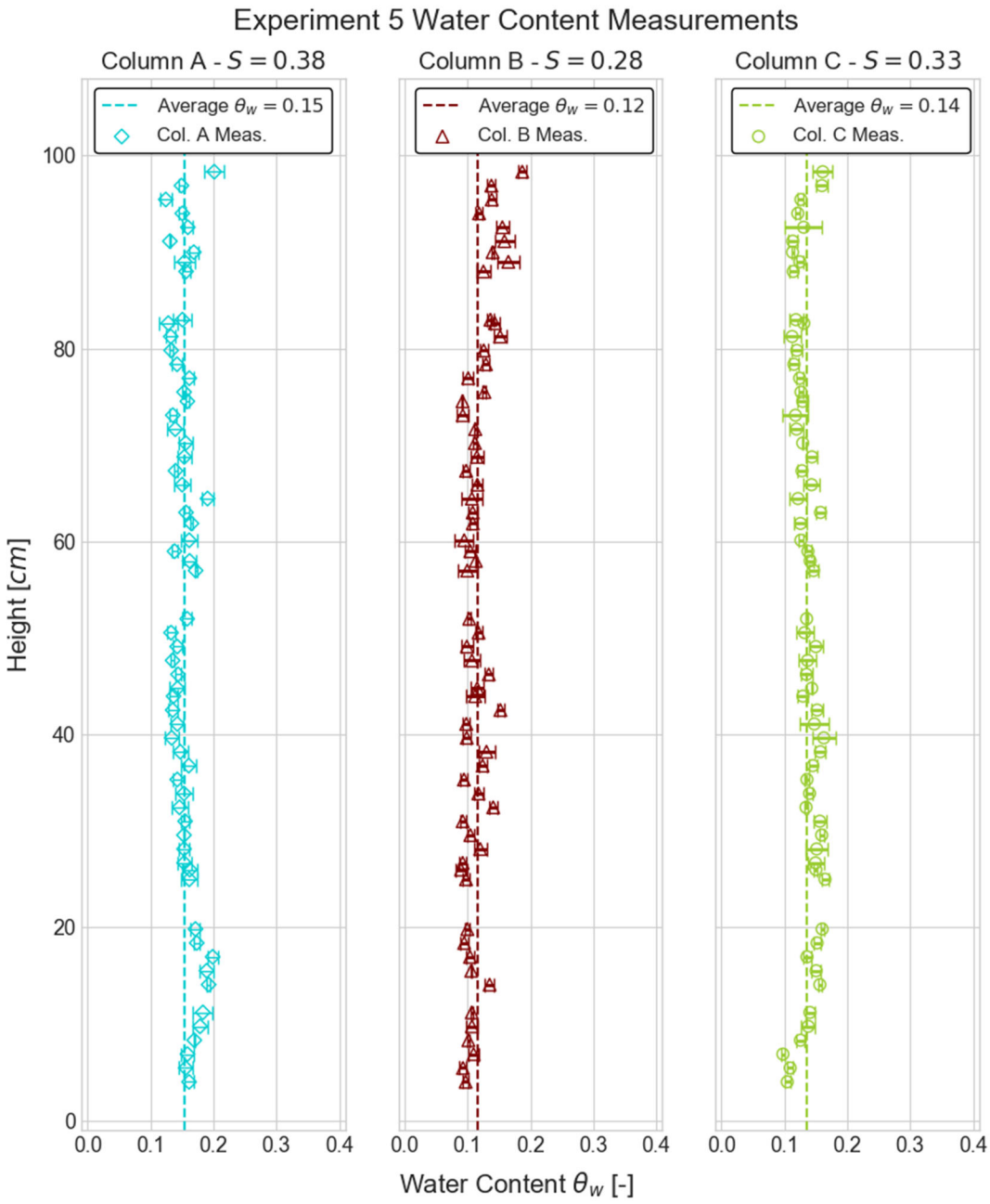

Figure 46: X-ray absorption spectroscopy scans of columns for Experiment set 5.

Transport of PFAAs Mixtures in Realistic Media and Solutions

The final set of experiments involved the transport of PFAAs in a naturally contaminated groundwater mixture. Two groundwaters were mixed together in a 99:1 ratio by volume. The first natural groundwater was from North Carolina and was impacted by PFAES from a local chemical manufacturing facility. The second groundwater was groundwater highly impacted by AFFF. The

two waters were mixed to increase the concentration of PFCAs and PFSAs present in the natural groundwater mixture. The mixed groundwater was well characterized, and synthetic groundwater which mimicked the natural groundwater was prepared to prime the column prior to introduction of PFAS and throughout the end run of the experiment to ensure no differences in back diffusion occurred due to differential electrolyte solutions. Air-water interfacial areas of the quasi-saturated condition for this sand were determined using the SDBS method described in depth in Stults et al. 2022[72] and in the methods section of this report. High and low flow rate experiments were conducted under saturated and unsaturated conditions to observed if PFAS exhibited rate-limited solid or air-water interfacial partitioning under the standard flow rates used for these column experiments. A summary of the experiments run for this study are presented in Table 18, and selected breakthrough curves for saturated and quasi saturated experiments are presented in Figure 47.

Table 18: Experiments and conditions for column studies and batch experiments for the PFAS mixture experimentation.

Column Experiments						
Experiment ID	**Column ID**	**Saturation [-]**	**Linear Pore Velocity [cm/min]**	**MTI [-]**	**Background Electrolyte [M]**	**Contaminant**
Quasi-Sat. SDBS	Small	0.84	0.16	0.98	0.01 NaCl	SDBS
	Small	0.84	0.16	0.99		
Saturated High Flow	D	1	0.6	0.99	0.0036	PFAS Mix
	E	1	0.59	1		
Saturated Low Flow	F	1	0.46	0.95	0.0036	PFAS Mix
Quasi-Sat. High Flow	D	0.93	0.31	0.97	0.0036	PFAS Mix
	E	0.88	0.35	1.03		
Quasi-Sat. Low Flow	F	0.89	0.14	1.01	0.0036	PFAS Mix
Batch Experiments						
Experiment ID	**Methodology**		**Purpose**		**Background Electrolyte [M]**	**Contaminant**
Batch SDBS 1	Standard Batch Sorption Experiments		Solid Phase Sorption of SDBS		0.01 NaCl	SDBS
Batch SDBS 2						
Pan Film 1	Schaefer et al. 2019[53]		Air water interfacial sorption of high K_{ia} PFAS		0.0036	PFAS Mix

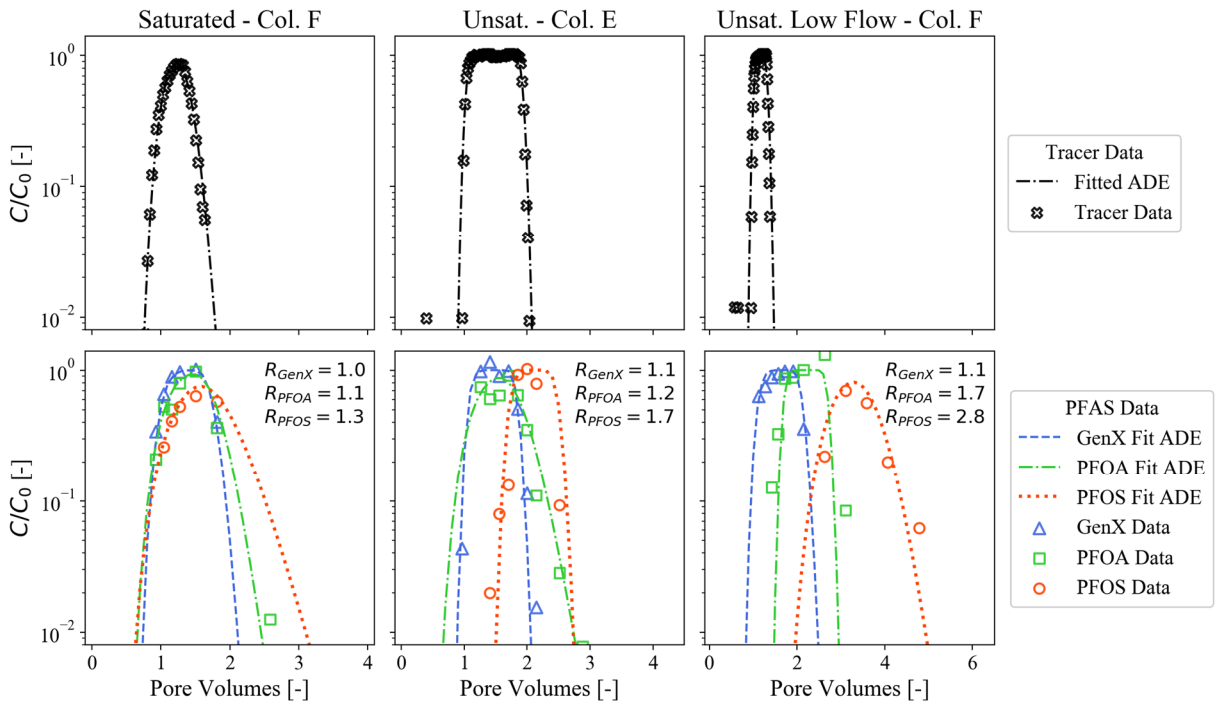

Figure 47: Conservative tracer (0.01 M NaCl) data demonstrates that the porous media is well fit by the non-dimensional ADE with a high Peclet (Pe > 50) number.

Retardation generally increases with decreasing saturation, and some dependance on flow rate is observed for compounds with larger molar masses (i.e. PFOS and PFOA).

Conservative tracers were ideal in this system (Figure 47, top row), indicating any observed rate-limited partitioning was primarily due to chemically driven sorption. BTC results for three PFAS (GenX, PFOA, and PFOS) in Figure 47 clearly demonstrate both an increasing retardation from saturated to quasi-saturated conditions associated with air-water interfacial sorption. The retardation of the three key PFAS significantly increased under quasi-saturated conditions. The retardation of PFOA and PFOS increased with decreasing flow-rate under quasi-saturation as well. To investigate the significance of both the air-water interfacial sorption and rate-limited nature of the sorption, the measured air-water interfacial plus solid phase retardation for the quasi-saturated experiments for each PFAS was derived from the BTC curves (Figure 48). The average retardation and 95% CI of retardation is calculated for all three saturated experiments (Figure 48– blue bars), while the two high flow rate quasi-saturated experiments (Figure 48– red bars) are presented separately from the low-flow rate quasi-saturated experiment (Figure 48– green stars).

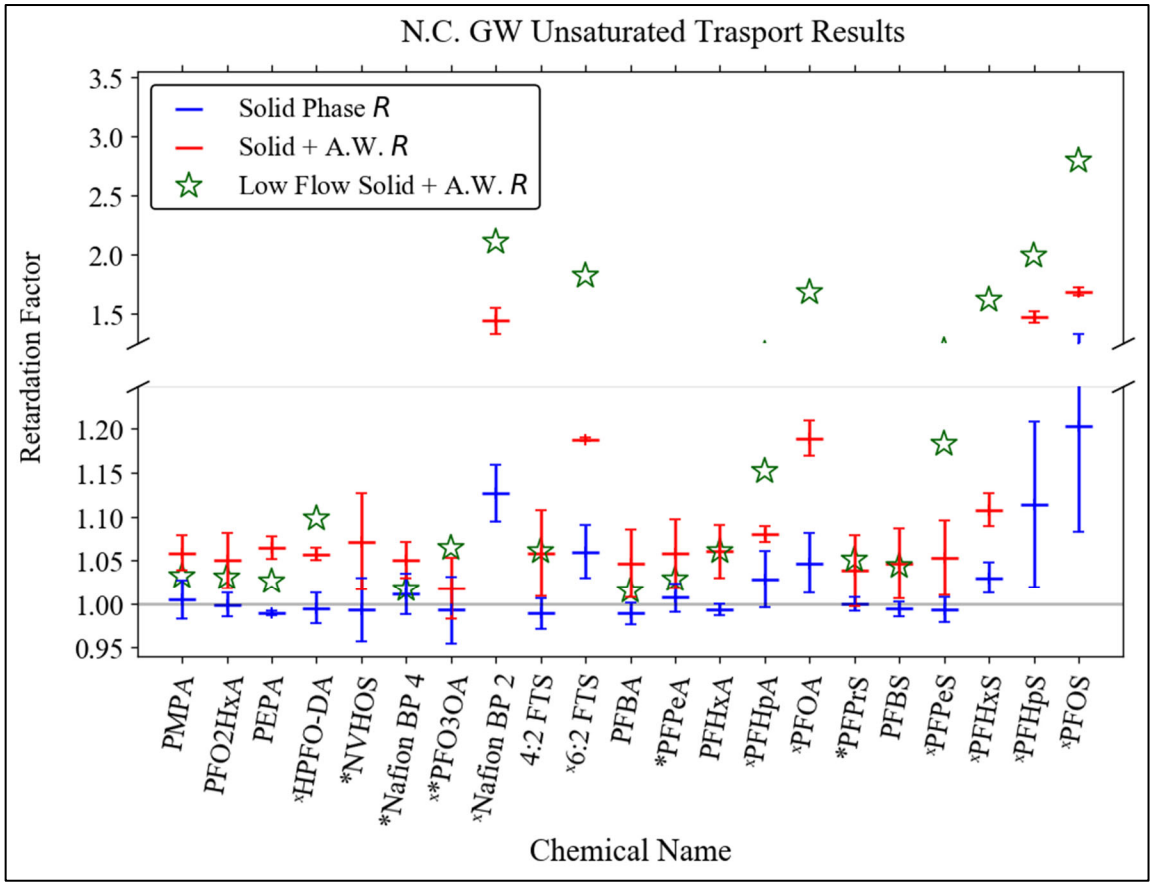

Figure 48: The solid phase retardation factor for quasi-saturated conditions (blue) is calculated using the Kd that was approximated from saturated conditions studies.

Total retardation (red) for the quasi-saturated condition experiments is calculated from the non-dimensional ADE fitting of the BTC data. Error bars for the saturated and total retardation factors are the 95% confidence intervals of measured vales. Low flow rate quasi-saturated experiments (green stars) which have retardation factors greater than the total retardation of the higher flow experiments are considered to have potentially significant rate-limited sorption to the air-water interface.

* *Nonsignificant air-water interfacial partitioning according to column studies*

^{x} *Statistically significant rate-limited air-water interfacial sorption observed*

Results from the retardation factor analysis demonstrate that air-water interfacial sorption in the columns was significant for nearly all of the components in the mixture, with the exception of PFPrS, PFO_3OA, NVHOS, and Nafion ByProduct 4. The effect of rate-limited solid phase sorption was negligible or minimal for all compounds except PFOS. However, many compounds demonstrated significant increases in retardation from the two high flow rate quasi-saturated experiments to the low flow rate quasi-saturated experiment. These results suggest rate-limited sorption to the air-water interface may be significant, even in very low concentration mixtures where competitive sorption due to limited site availability is not present.[55,67] These findings are counter to several past studies using the CD methodology, which assert air-water interfacial sorption can be treated as instantaneous in all cases.[10,51,61] As discussed in our previous

publication,[72] the CD methodology is potentially impacted by non-Fickian transport which can induce rate-limited sorption[28,43] and other transport non-idealities.[19,36,74] Further, this sand was chosen specifically to investigate the potential for rate-limited sorption to develop under more non-ideal quasi-saturated conditions. The sand in this study is fine grained and subangular, meaning that more diffusion-limited immobile water domains are expected to develop in the angular corners of the sand grains, potentially resulting in air-water interfaces in diffusion limited domains. As will be discussed in the results and modeling section, rate-limited partitioning to the air-water interface and solid surface was observed for several of the PFAS with large molar volumes. Equilibrium K_{ia} values for those components were determined using pan film experiments developed in task 3.1 (published in Schaefer et al. 2019).

Task 3.3 PFAS Unsaturated Transport Modeling

Advective Flow Path Tortuosity – Padilla et al. 1999 Reanalysis

Data form Padilla et al. (1999)[33] was processed using Equations 3.19 and 3.21 (y-axis) and plotted against effective saturation (x-axis) in Figure 49. The MTI (T – blue lines/dots) values calculated from Padilla et al. no longer adhere to the empirical relationship with effective saturation when mass transfer limitations are present. However, the advective tortuosity (τ_a – Orange lines/dots) is very well correlated with effective saturation through the power law relationship described in the MTI theory. It should be noted the n-value for Padilla is much smaller than the n-value for the MTI study. This small n-value is why Padilla et al. observed early solute emergence despite increasing tortuosity (i.e. tortuosity effects were overshadowed by increasing velocity as the results of mass balance).

This empirical relationship between the MTI and advective tortuosity is a very important step towards better coupling pore scale mass transfer phenomena with macroscopic observations of fate and transport in unsaturated soils. This supplementary information also demonstrates how the MTI theory can be easily incorporated into more robust macroscopic models.

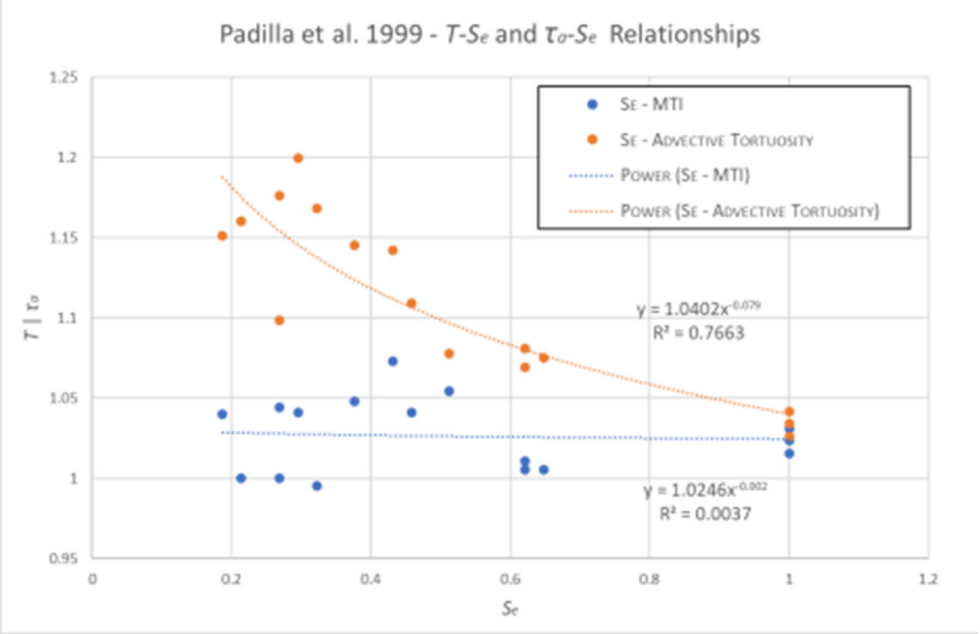

Figure 49: MTI vs. Advective Tortuosity relationships for Padilla et al. 1999 data.

PFOS Isotherm Modeling Using HYDRUS

The linearity of PFAA isotherms below a CRC is a debated topic.[53,59,60] Some have taken a strong stance regarding the appropriateness of the Langmuir isotherm (linear isotherm below a CRC) and estimation of PFAA K_{ia} from IFT data across the full range of relevant PFAA concentrations.[61,68] This topic is of vital importance, as some otherwise comprehensive numerical models currently only consider Langmuir type sorption predicted by IFT data.[81,82] Inspection of the total PFOS BTCs in Figure 40 (particularly the bottom right panel) strongly suggest that an equilibrium-based linear sorption model (equivalent to the equilibrium-based Langmuir model at this concentration) does not adequately describe PFOS retention at the air-water interface, even in this relatively uniform and low-flow system. While a few explanations for these observations are possible, we posit that these data support a non-linear Freundlich isotherm for PFOS retention at the air-water interface below a CRC, or a Freundlich-Langmuir model across the full range of relevant PFAA concentrations. As will be discussed, our assertion of isotherm non-linearity rests on multiple lines of evidence which argue, in our view, against the use of using the Langmuir isotherm assumption and IFT data to predict K_{ia} below a CRC:

1) While some data exist supporting isotherm linearity at low concentrations (i.e., the Langmuir/Linear model), all this evidence has been generated using the potentially problematic CD and SML measurement techniques. The limitations of these techniques are discussed above, with further details provided Stults et al. 2022.[72]

2) The quasi-saturated experimental transport method employed here does not suffer from sampling errors or transport non-idealities which can bias K_{ia} measurements. The ideality of transport is evident in ideal conservative tracer (NaCl) breakthrough curves, a lack of transport non-idealities as verified conceptually and by MTI analysis, consistent air-water interfacial area measurements as verified by SDBS partitioning tracer tests, and ideal/conservative behavior of PFOS in the saturated system. PEST inversion of equilibrium and non-equilibrium HYDRUS models support the Freundlich isotherm, and are in good agreement with data from the K_{ia} vs. Concentration literature analysis.

3) Empirical analysis of K_{ia} vs Concentration for all literature-derived K_{ia} data (excluding the potentially problematic SML and CD datasets) demonstrates that non-linear Freundlich isotherms can be accurately regressed to all of the available data for PFOS. Empirical analysis of compiled CD method data for PFOA reveals there is significant isotherm non-linearity for PFOA as well, albeit less than predicted by the batch method (Figure 41, Figure 42).

The first and third lines of evidence are previously discussed in the results section of Task 3.2, and therefore this section will focus on the second line of evidence. Conservative tracer (NaCl) tests for this system (top row Figure 40) showed no signs of tailing or asymmetry in the BTC for under saturated (Experiment 1) or quasi-saturated (Experiments 2 & 3) conditions. Conservative tracer BTCs could be well fit by the non-dimensional form of the ADE using a Peclet number > 100 for all saturated and quasi-saturated conditions. A high Peclet number and symmetry indicates the volume fraction of immobile zones in this media are negligible, or that transfer into immobile zones can be treated as instantaneous (i.e. no rate-limited sorption).[19,21] There is a high degree of symmetry in the saturated PFOS BTC plots as well as negligible retardation (middle and bottom left panels of Figure 40) for total PFOS (linear and branched isomers). However, in the quasi-saturated condition (Experiments 2 & 3) the branched and linear PFOS isomer begin to demonstrate differential transport BTC asymmetry in the form of tailing, particularly in Experiment 3 where the lower limit of quantification (0.04 µg/L) was much lower than the maximum concentration (53.0 µg/L). This tapered tailing is highly characteristic of concentration dependent sorption.

To evaluate potential explanations for this tapered tailing, PEST inversion of HYDRUS models was performed. Several models (Equilibrium and 2-site non-equilibrium with Freundlich and Linear isotherms) were evaluated, as data do not necessarily rule out transport non-idealities dues to chemically driven rate limitations. Because the retardation and tailing are extremely similar in all of the Experiment 3 BTCs, the linear and branched isomer BTCs from Experiment 3 in column B were chosen as representative modeling data. Inversion of equilbirium and non-equilibrium Freundlich and Linear isotherms demonstrate the Freundlich isotherm is much more highly correlated with the data. The equilibrium and non-equilibrium Freundlich inversion results are essentially idential to one another, suggesting the system is at equilibrium.

Confirmation of equilibrium partitioning from the HYDRUS inversion lends creedence to both the motivation for quasi-saturated column method and the use of the MTI method to analyze systems for rate-limited partitioning. Moreover, the Freundlich *n* values estimated from HYDRUS model inversion range from 0.65-0.7, which is in excellent agreement with the *n* values calculated from K_{ia} vs. concentration analysis (Figure 41). Finally, the BTCs have three primary characteristics which are indicative of isotherm non-linearity: sharp arrival fronts, early and tapered decreases from maximum concentrations, and long tailing. While rate-limited sorption models such as the MIM, dual site nonequilibrium, and MRMT can capture one or two of the previously listed characteristics, only isotherm non-linearity can accurately capture all three features. Full results from the BTC inversions with PEST and HYDRUS are plotted in

Figure 50.

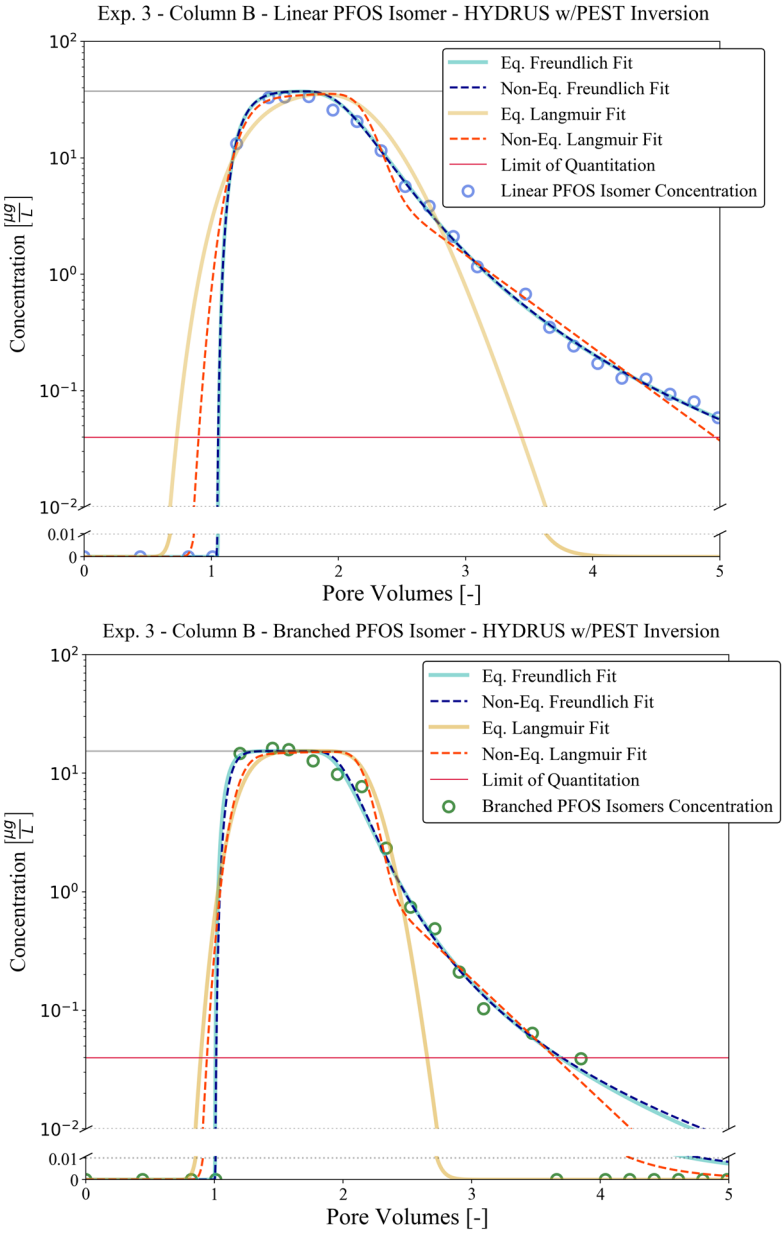

Figure 50: PEST inversion of HYDRUS models for linear and branched isomers of PFOS.

Evaluating non-Equilibrium Air-Water Interfacial Partitioning with $K_{ia,app}$

While the mechanism for rate-limited sorption observed in the mixture experiments cannot be accurately determined, rate-limited sorption for single component experiments is likely due to the presence of non-Fickian transport elements within a system. The single component PFOA from

other literature sources[10,52,55,61,66,67] and Experiment 4/5 PFOS data present an opportunity to develop correlation between the effect of residence time/linear pore velocity on non-equilibrium under drainage conditions.

It is well established that higher linear pore velocities results in a lower residence time for the solute within the representative elementary volume (REV), resulting in non-equilibrium partitioning and retention processes.[22,28] All three replicates in Experiment 5 were purposefully conducted under similar saturation conditions. Only one study involving the CD method thus far (Lyu et al. 2018)[10] has attempted to quantitatively investigate the relationship between the linear pore velocity and the rate-limited air-water interfacial partitioning. Their study determined that linear pore velocity of ~0.6 cm/min in their sand was slow enough to ensure that equilibrium sorption of PFOA to the air-water interface had been reached. However, upon review of Lyu et al. 2018 data in the context of equilibrium data from a pan film study,[53] it appears this conclusion is incorrect. There is a clear correlation of increasing $K_{ia,app}$ with decreasing linear pore velocity down to ~0.2 cm/min. The authors of Lyu et al. 2018[10] believed that equilibrium had been reached because a single $K_{ia,app}$ measured at the 0.6 cm/min linear pore velocity appeared greater than a single K_{ia} measured at a linear pore velocity of 0.2 cm/min. However, the 0.6 cm/min velocity data point was obtained at a significantly higher Saturation than the other experiments. It is clear from reanalysis of the data that K_{ia} is strongly negatively correlated with linear pore velocity, but also may be somewhat positively correlated with Saturation for the CD method. Figure 51 demonstrates the linear pore velocity vs. $K_{ia,app}$ relationship fitted by Equation 3.26, and Figure 52 demonstrates the saturation vs. $K_{ia,app}$ relationship for the 0.6 cm/min study in Lyu et al. 2018.[10]

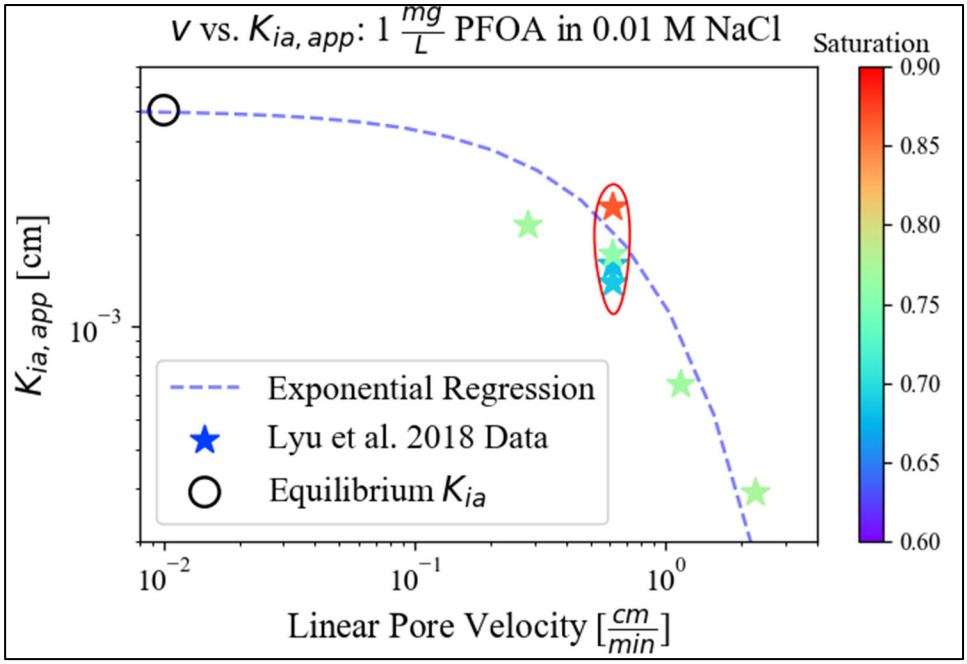

Figure 51: An exponential relationship between linear pore velocity and the $K_{ia,app}$ as demonstrated in Equation 3.26.

A clear trend exists between $K_{ia,app}$ and linear pore velocity for the CD method studies. There appears to be some variability that is also well correlated with saturation, however this may be an artifact of data analysis methods used in Lyu et al. 2018.

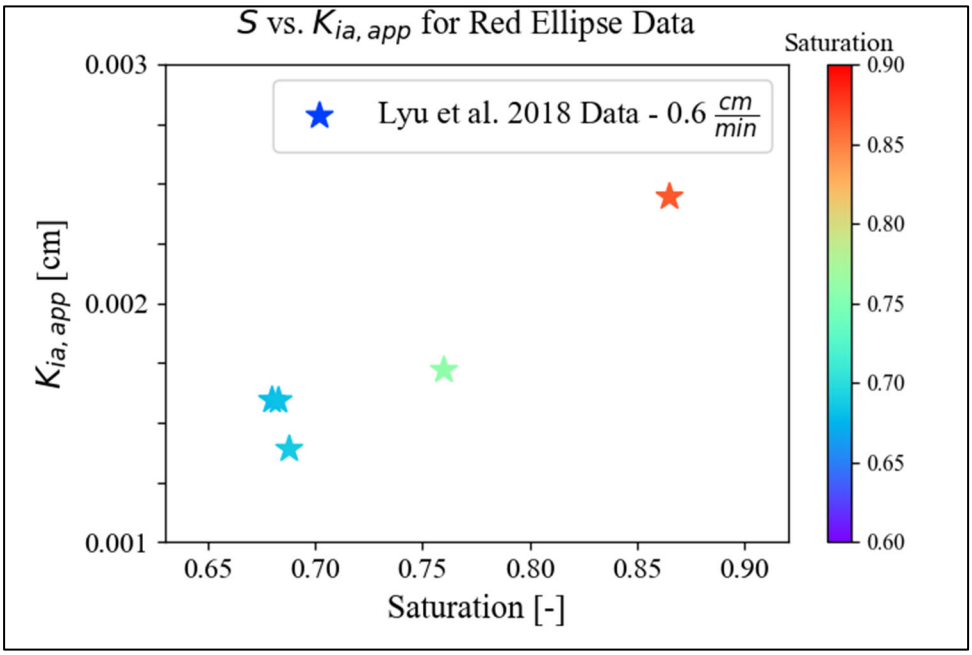

Figure 52: The relationship between Saturation and the apparent *Kia* for Lyu et al. 2018.

The authors of Lyu et al. 2018 assumed their system was measuring equilibrium *Kia* values at 0.6 cm/min based on the single red star measurement. However, closer analysis reveals this is possibly an artifact their data processing methods, as there is an unexplained correlation between S and $K_{ia,app}$.

The exponential regression presented in Equation 3.26 was fit to the $K_{ia,app}$ as a function of linear pore velocity. Equilibrium K_{ia} data was included as the intercept for a linear pore velocity equal to 0, but is shown on the Figure 51 at the linear pore velocity of 0.01 cm/min to fit within the confines of the logarithmic x-axis. $K_{ia,app}$ for PFOA also appears to increase with increasing saturation as well. The reasons for why $K_{ia,app}$ may increase with increasing saturation include data analysis errors (i.e. improper estimation of air-water interfacial areas) or irreducible experimental errors, and are not necessarily mechanistic in nature. Because saturation could be a confounding variable for the system, Experiment 5 replicates were conducted under saturation conditions which are very nearly equivalent to one another. Low saturations for experiment were chosen because of the highly non-Fickian transport observed in Experiment 4b at low saturation. Previous pore network modeling studies and experimental modeling studies with high resolution X-ray tomography have demonstrated that lower saturations are associated with increasingly non-Fickian transport.[36,37,78] Linear pore velocity was varied slightly between each experiment to ensure that differences in K_{ia} could potentially emerge. Linear pore velocities were maintained around 0.6 cm/min for this experimental condition to replicate Lyu et al. 2018 linear pore velocities as closely as possible.

We previously discussed that the results of Experiment 5 demonstrate more ideal transport behavior than the low concentration Experiment 4b conducted under similar conditions. Initial analysis showed inverse correlation between the observed retardation factor and linear pore velocity for the replicates in Experiment 5. When the $K_{ia,app}$ values are calculated for Experiment 5 replicates and fitted to linear pore velocity using the Equation 3.26 empirical regression, the same strong correlation between linear pore velocity and $K_{ia,app}$ emerges as demonstrated in Figure 53.

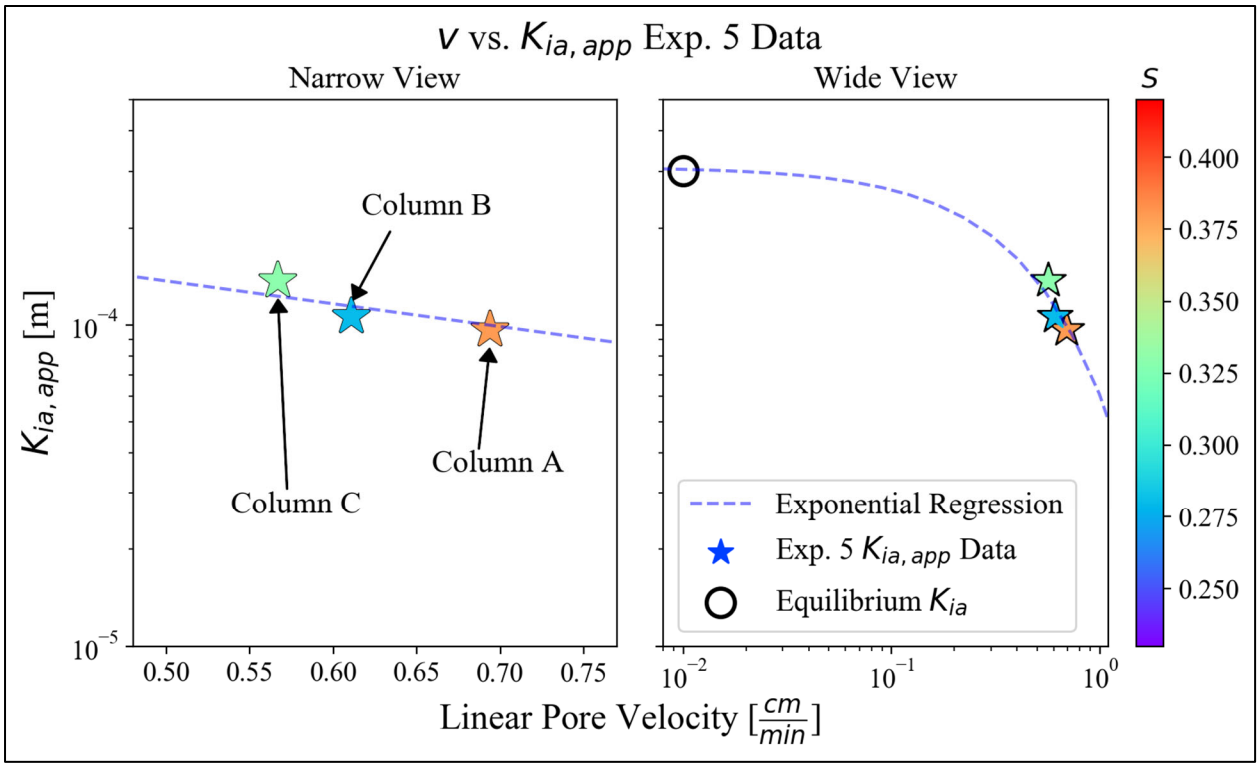

Figure 53: The exponential relationship between linear pore velocity and the apparent K_{ia} developed for Lyu et al. 2018 applied to Experiment 5 data for PFOS at a 45 µg/L concentration.

Results for the $K_{ia,app}$ vs velocity analysis for this study are consistent with analysis and results from Lyu et al. 2018. The predicted *a* fitting values for PFOS and PFOA are 1.63 and 1.46 respectively, suggesting that this correlation is accurate and applicable for other PFAAs in the vadose zone. This finding is especially important, as much of the solute flux in the vadose zone likely occurs during high rainfall events, where linear pore velocities are orders of magnitude greater than average.[83,84] The trend observed between saturation and the $K_{ia,app}$ in Lyu et al. 2018 is likely an artifact of stochastic variability in air-water interfacial area for the CD method,[85] or an error in the estimation of air-water interfacial area used to calculate the $K_{ia,app}$ of Lyu et al. 2018.[85]

ppQSPR Model for Estimating K_{ia} of PFAS

The ppQSPR was constructed using 8 variables which were reflective of hydrophobicity or changing K_{ia} values. A table of the 8 variables and the equilibrium K_{ia} values calculated for each component is presented in Table 19, and equilibrium K_{ia} values vs. concentration are presented in Figure 54.

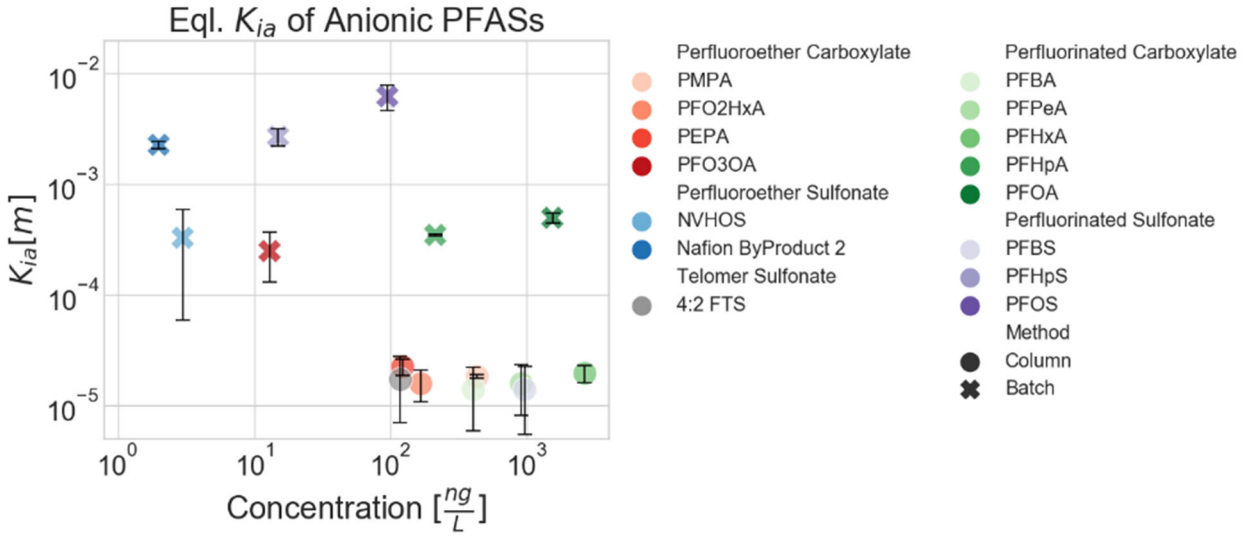

Figure 54: Equilibrium K_{ia} values of anionic PFAS measured from column and batch testing studies.

Detailed descriptions of each of the variables from Table 19 are presented in list format:

1. Total Chain Number: The total number of carbon or oxygen molecules which are not a part of the primary functional group (i.e. the sulfonate or carboxylate head) attached to the molecule.
2. Longest Chain Number: The longest continuous chain of carbon or oxygen molecules attached to the functional group head. (i.e., PFOA has 7 and PFOS has 8 because one of the carbon molecules in PFOA belongs to the carboxylate head group).
3. Longest Fluorinated Chain Number: The longest continuous chain of fluorinated hydrocarbons attached to the head group (i.e., 4:2 FTS has 4 continuous fluorinated hydrocarbons but a total Longest Chain Number of 6).
4. C18 RT: The measured C18 retention time of the molecule using liquid chromatography method.
5. Molar Volume: The measured or estimated molar volume of the molecule in cm^3/mol.
6. $Log_{10}(C)$: The log base 10 value of the PFAS concentration in ng/L.

7. $\underline{\Delta G_0}$: The Gibbs free energy of association to the air-water interface as predicted from IFT data or estimated from molecular property relationships in Le et al. 2021.[80]

8. $\underline{K_{iw,0}}$: The theoretical maximum air-water interfacial partitioning coefficient as predicted from a Langmuir model of IFT data or estimated from molecular property relationships in Le et al. 2021.[80]

Table 19: List of the 8 input variables and the measured K_{ia} values for various PFAS present in the North Carolina groundwater mixture. Compounds with no K_{ia} values measured either had K_{ia} values which were below the limit of quantitation for the pan film or column methods, or exhibited significant non-equilibrium which could not be reconciled. ΔG_0 and $K_{iw,0}$ were obtained form Le et al. 2021.[80]

Compound	**Class**	**Total Chain Number**	**Longest Chain Number**	**Longest Fluorinated Chain Number**	**C18 RT [min]**	**Molar Volume [cm^3/mol]**	**log10(C [ng/L])**	ΔG_0	$K_{iw,0}$	***Kia* (m)**
NVHOS	Ether	5	5	2	5.33	164	0.48	-15.18	-3.67	**3.3E-04**
Nafion ByProduct 2	Ether	9	8	3	6.71	252	0.30	-26.05	-1.92	**2.3E-03**
Nafion ByProduct 4	Ether	7	6	4	4.97	229	1.11	-10.76	-4.89	
HPFO-DA (GenX)	Ether	6	5	3	6.47	189	2.18	-18.67	-5.02	
PEPA	Ether	5	4	2	5.96	161	2.09	-15.1	-5.62	**3.4E-05**
PFO2HxA	Ether	5	5	1	5.65	140	2.22	-9.62	-6.63	**2.4E-05**
PFO3OA	Ether	7	7	1	6.39	174	1.11	-11.28	-6.44	**2.5E-04**
PMPA	Ether	4	3	2	5.29	134	2.64	-11.53	-6.22	**1.6E-05**
4:2 FTS	Telomer Sulfonate	6	6	4	6.26	215	2.07	-21.23	-2.54	**2.6E-05**
6:2 FTS	Telomer Sulfonate	8	8	6	7.13	270	2.83	-28.37	-1.34	
PFBA	PFAA	3	3	3	5.18	127.4	2.61	-15.32	-5.65	**2.1E-05**
PFPeA	PFAA	4	4	4	5.8	154.9	2.96	-17.39	-5.24	**2.4E-05**
PFHxA	PFAA	5	5	5	6.31	182.4	3.43	-20.85	-4.62	**2.9E-05**
PFHpA	PFAA	6	6	6	6.76	209.8	2.33	-22.26	-4.31	**3.5E-04**
PFOA	PFAA	7	7	7	7.14	237.3	3.19	-26.33	-3.64	**5.0E-04**
PFPrS	PFAA	3	3	3	5.3	134.65	2.69	-13.52	-3.86	
PFBS	PFAA	4	4	4	5.83	162.1	2.98	-19.74	-4.68	**2.1E-05**
PFPeS	PFAA	5	5	5	6.33	189.55	2.86	-20.66	-2.66	
PFHxS	PFAA	6	6	6	6.75	217	3.24	-22.01	-4.06	
PFHpS	PFAA	7	7	7	7.09	244.55	1.18	-31.05	-3.02	**2.7E-03**
PFOS	PFAA	8	8	8	7.36	272.1	1.98	-30.61	-2.78	**6.3E-03**

Results from all 246 possible combinations of the eight variables selected for the ppQSPR models demonstrated that Concentration, Molar Volume, Longest Fluorinated Chain Number, and Total Chain Number were the most appropriate variables for quantifying PFAS air-water interfacial partitioning (SI 3). Adjusted R^2 analysis demonstrated that a four parameter QSPR model allowed for the best possible fitting without overparameterization (SI 3). An additional three parameter model which incorporates C18 retention time was included in the analysis as well. This is because a prior study[53] has demonstrated that for surfactants with unusually large head groups or cationic/zwitterionic components, the relationship between molar volume and K_{ia} breaks down. The C18 retention time may be a more applicable surrogate for hydrophobicity in this context. Details on the chromatography used for this system are in SI 5. The most accurate four parameter model variables were the Longest Fluorinated Chain Number, Total Chain Number, Molar Volume [cm^3/mol], and $\log_{10}(C_{aq}$ [ng/L]) (detailed description in SI 3). The C18 retention time model variables were Longest Fluorinated Chain Number, C18 Retention Time [minutes], and $\text{Log}_{10}(C_{aq}$ [ng/L]). The coefficient for the $\text{Log}_{10}(C_{aq}$[ng/L]) parameter is equivalent to the Freundlich model *n* value minus 1. Prior results have demonstrated that the *n* value of the Freundlich model below a CRC is between 0.6-0.7 for PFOS and PFOA. Therefore, a linearized coefficient of -0.35 (i.e. -0.35 = *n* - 1) was assumed for the $\text{Log}_{10}(C_{aq}$[ng/L]) coefficient. The four parameter ("No C18 model") and three parameter ("C18 model") equations are presented in Equations 3.27a-b respectively, the correlation concentration in the QSPR and results of the QSPR analysis are presented in Figure 55a-b for Equations 3.27a-b respectively.

$$\log_{10}\left(K_{ia,LFER}[m]\right) = [(0.41 \pm 0.14) * \text{LongestFChain}] + [(0.74 \pm 0.22) * \text{TotalChain}] - [(0.023 \pm 0.012) * \text{MolarVolume}] - [(0.35 \pm 0.15) * \log_{10}\left(C_{aq}\left[\frac{ng}{L}\right]\right)] + (-4.6 \pm 0.9) \quad \textbf{(Eq. 3.27a)}$$

$$\log_{10}\left(K_{ia,LFER}[m]\right) = [(0.078 \pm 0.10) * \text{LongestFChain}] + [(0.80 \pm 0.31) * \text{C18\_RT}] + [(-0.35 \pm 0.15) * \log_{10}\left(C_{aq}\left[\frac{ng}{L}\right]\right)] + (-8.5 \pm 1.5) \quad \textbf{(Eq. 3.27b)}$$

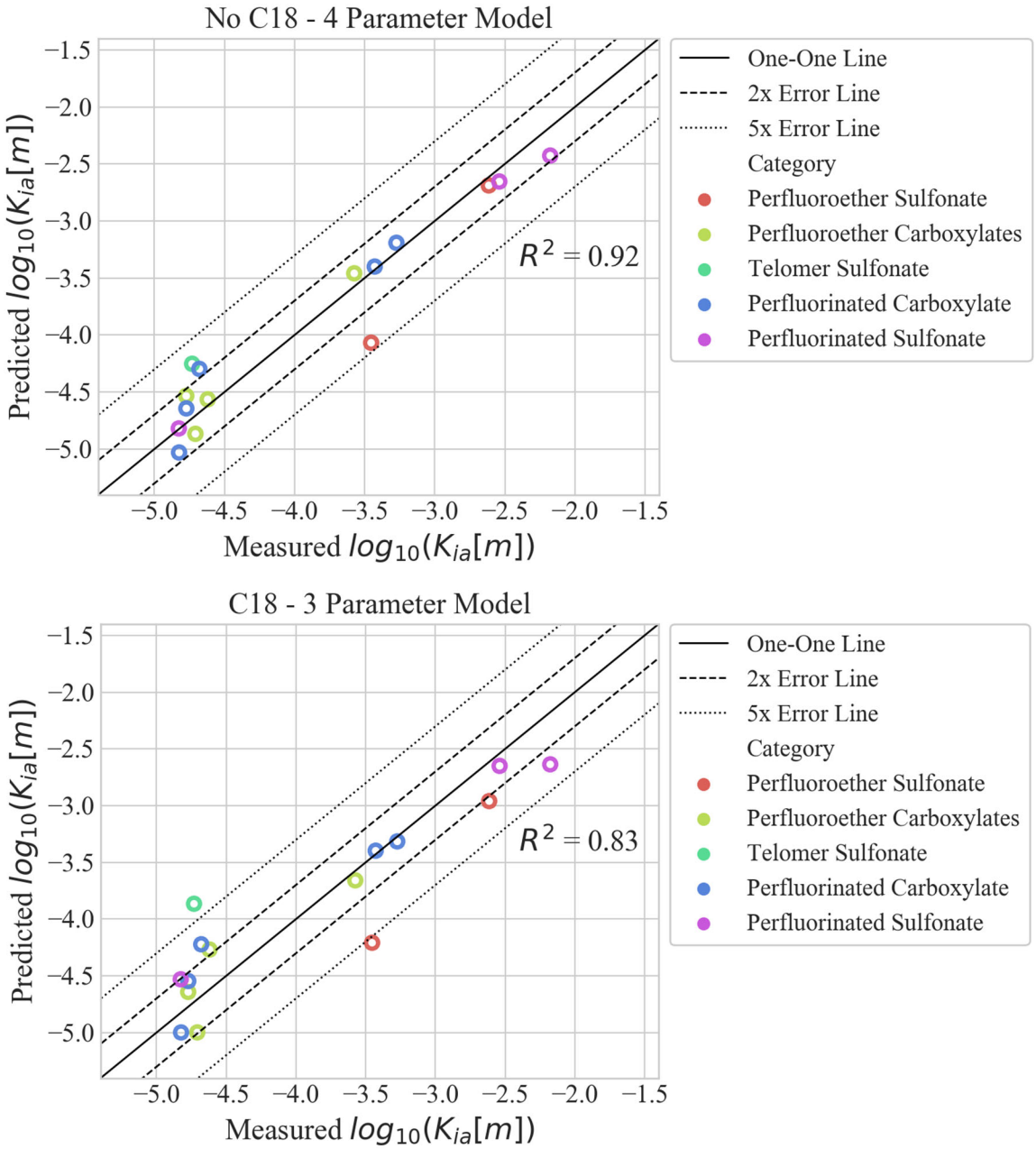

Figure 55: (a) Results of the predicted K_{ia} vs. measured K_{ia} for the QSPR model which does not include C18 retention time as a parameter (Equation 3.27a); (b) Results of the predicted K_{ia} vs. measured K_{ia} for the QSPR model which does C18 retention time as a parameter (Equation 3.27b).

Equilibrium K_{ia} values obtained from either column or pan film testing were used for fitting the multi-parameter regression models. No duplicate values of K_{ia} were used for any compound. Results indicate that both the model which includes C18 retention time (Equation 3.27b) and the model which does not include C18 retention time (Equation 3.27a) provide very good

approximations of equilibrium K_{ia} values for a variety of anionic PFAS (R^2 of 0.92 and 0.83 respectively). While the four parameter QSPR model which does not include C18 retention time has a better goodness of fit to the data, the three parameter C18 retention time model may still be preferred. This is because Schaefer et al. 2019[53] demonstrated that for 6:2 Fluorotelomer Thioether Amido Sulfonate (6:2 FtTAoS), the C18 retention time provided a much better approximation of the equilibrium air-water interfacial partition approximation than molar volume or traditional parameters used in QSPRs.

While the log-log calibration data in Figure 55a-b provide strong evidence for the ability of the concentration dependent QSPRs to predict K_{ia} values of PFAS, it does not demonstrate how the QSPRs perform across relevant concentration ranges. To evaluate the performance of both QSPRs across relevant ranges of PFAS concentrations, the ppQSPR prediction was plotted against the available 0.01 M NaCl electrolyte data from Schaefer et al. 2019.[53] This data set was chosen because it used the same equilibrium pan film method employed for PFAS in this study for calculating K_{ia} . Further, IFT modeling results from Costanza et al. 2019[58] and Brusseau et al. 2021[55] demonstrate that PFOS and PFOA should have similar (i.e. within one order of magnitude) K_{ia} values in 0.0036 M and 0.01 M NaCl. This equivalency is approximate, as prior studies have demonstrated that counterion type (i.e Na^+ or Ca^{2+}) can significantly affect the equilibrium air-water interfacial partitioning of surfactants, particularly below 0.01M ionic strength.[66,67,86] Unfortunately, most available K_{ia} data was acquired using the SML or CD methods, which likely suffer from critical limitations, as discussed in our previous study.[72] While GenX demonstrated statistically significant non-equilibrium within a 95% confidence interval, the non-equilibrium observed was extremely small (< 10% statistically significant increase in K_{ia} between high and low flow rate experiments). Because GenX data points are likely near equilibrium, but were not used in the regression to develop the ppQSPRs, the column based K_{ia} values can serve as a way of validating the estimates produced by the ppQSPRs. The no C18 and C18 ppQSPR predictions across a full range of relevant PFAS concentrations for PFOS, PFOA, and GenX are presented in Figure 56, along with all available equilibrium K_{ia} data in 0.01 M NaCl,[53,87] 0.003M NaCl,[88] and the Langmuir isotherm for each component in 0.01M NaCl.[55]

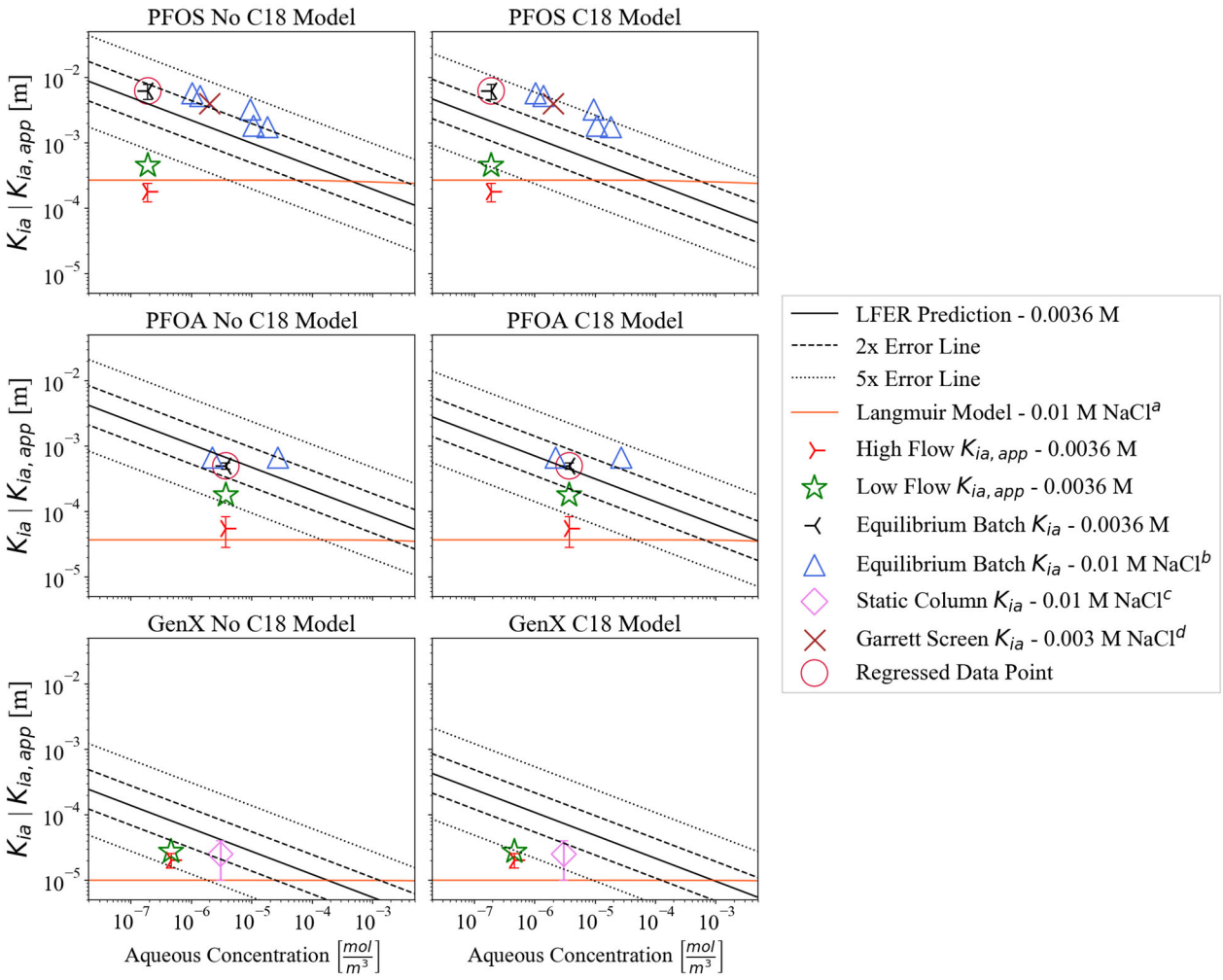

Figure 56: The QSPR prediction (black line) for the full concentration range for 3 representative PFAS (GenX, PFOA, and PFOS).

Under rate limited transport conditions, as present in the high flow column studies, calculated K_{ia} values are in good agreement with the Langmuir model. This suggests many of the drainage method studies suffer from rate-limited transport phenomena.

[a] Brusseau et al. 2021[55]; [b] Schaefer et al. 2019[53]; [c] Schaefer et al. 2022 (1)[87]; [d] Schaefer et al. 2022 (2)[88]

Results from plotting the ppQSPR as a function of concentration demonstrates excellent agreement with equilibrium K_{ia} values (but not necessarily non-equilibrium $K_{ia,app}$ data) not only with the data from this study, but also with 0.01M NaCl PFOS and PFOA data from previous studies.[53,55,87,88] In general, the "no C18" model seems to perform better than the C18 model, especially for the case of GenX. However, while we suspect the equilibrium K_{ia} of GenX will be similar to the low flow rate K_{ia} calculated from the quasi-saturated Experiment based on the very small increase between high and low flow experiments, it may be significantly higher. In this case, the C18 QSPR model may be more accurate. Another key point demonstrated by Figure 56 is the effect of non-equilibrium on prediction of K_{ia} values from column studies. For the case of PFOS, the

non-equilibrium K_{ia} predicted from the quasi-saturated column study was 10-30x lower than the equilibrium value. For PFOA, the non-equilibrium values were 2-10x lower as well. If we had simply assumed the high flow rate K_{ia} values were equilibrium K_{ia} values for PFOS and PFOA, we would have concurred with CD method studies regarding the applicability of the Langmuir isotherm for PFAS.[55,61] However, these data suggest that rate-limited air-water interfacial partitioning is possible in column studies, even under highly ideal quasi-saturated conditions. There seems to be a correlation with decreasing concentration, increasing K_{ia}, and increasing rate-limited air-water interfacial partitioning. Unfortunately, because this study was conducted in a mixture of PFAS rather than with single components, it is not possible to determine the underlying mechanism. These findings call into further question the appropriateness of the assumption that the air-water interfacial partitioning is at rapid equilibrium.

Conclusions and Implications for Future Research and Implementation

Using a soil known to support PFAS source zones, a commercial AFFF with multiple anionic and zwitterionic PFAS species, and one-dimensional saturated column experiments, we observed significant PFAS mass retention which was best described by a multi-parameters quantitative-structure property relationship. Retention of anionic PFAS was generally low until the fluorinated chain comprised at least eight (8) fluorinated C atoms. Even more important for site managers and policy makers was the observation that for anionic PFAS, soil and sediment properties in systems with negligible organic carbon content have little relevance for their retention behavior. Instead, the overriding control towards environmental matrices was the size of the fluorocarbon chain and the associated thermodynamic impetus to be expelled from the aqueous phase. The retention of zwitterionic PFAS was related to the PFAS molar mass and the # of N atoms incorporated in the molecule. Zwitterionic PFAS also showed significant tendencies to actually bind with environmental matrices through electrostatic mechanisms. Given the fact that the soil chosen for this investigation was a sandy matrix almost devoid of clay and with miniscule surface reactivity, we posit that we have investigated the equivalent of a best case scenario for soil contamination with PFAS – almost any other soil matrix will retain both anionic and zwitterionic PFAS to a significantly larger extent. Finally, our research showed that the fraction of soil organic carbon present (f_{OC}) does not represent a single value predictor for retention of all PFAS in source zones and that there are other influencing variables such as the mineral phase or the quality of the organic carbon, which should also be considered. Future research is aimed at determining if PFAS and NAPL associate as microemulsions or as non-microemulsion mixtures at fire-fighter training sites, which is the first step toward understanding if residual NAPL acts as a sink for PFAS and thus, a potential long-term source of PFAS to groundwater.

OUTREACH/EDUCATION

In an effort to communicate the scientific findings from Task 1, a series of publicly available, practitioner-oriented educational modules was assembled. The overall goal of these modules was to support the management of PFAS source zones through three major educational avenues:

1. Know how different types of PFAS interact with different constituents of the soil source zone matrix
2. Use mechanistic insight to estimate odds for PFAS retention, release, and transport at site with available characterization information
3. Know where to find publicly available data that support the above objectives

Module One provides introductory background information on the origin of different soil matrix properties. Module Two provides a theoretical framework of PFAS physiochemical properties. Module Three includes information on how soil matrix properties and PFAS physiochemical properties can interact and relate to PFAS retention or release. Module Four gives an overview of the types of soil matrix data available in public databases for a site of interest to the stakeholder/user of the Technology Transfer Modules, use as well as practical applications of the information in Modules One through Three. To summarize, the four modules go over key mechanisms related to the retention and release of PFAS from source zones as a result of the interplay between PFAS molecular chemistry, environmental matrix (soil) properties, and the solvent (aqueous) phase.

This research has provided a comprehensive framework for evaluating the air-water interfacial partitioning & non-Fickian transport properties of PFASs at a laboratory scale. The improved understanding air-water interfacial partitioning & non-Fickian transport can be scaled up to numerical models and conceptual models used to evaluate the fate and transport of PFASs at field sites. Key findings of the work include: the development of a simple empirical model to evaluate the potential for non-Fickian transport to develop unsaturated porous media; non-Fickian transport can reduce the observed retention of PFASs in to the air-water interface by over 10 fold as compared to equilibrium models; the development of a quasi-saturated column method to minimize the impact of non-Fickian transport in multi-phase partitioning column studies; development of a multiparametric QSPR models to approximate the K_{ia} of PFAS under relevant environmental conditions. Future studies can build on the work presented here by studying PFAS transport under more realistic (e.g., drainage and imbibition from rainfall) conditions using the simplified empirical models for estimating non-Fickian transport and the K_{ia} of PFASs. Further work is also needed on the effects of organic carbon, competitive sorption, and multi-component solution effects on PFAS transport in the vadose zone. Validating the numerical models developed herein for field conditions can be done through controlled/well monitored lysimeter studies as well.

KEY POINTS

(By Task)

Key points from Task 1

- The soil being used in the column flow-through studies for this task (and for Task 2) is relatively unreactive and contains mainly hydrophobic retention mechanisms.
- The Grayling soil collected from Wurtsmith Air Force Base is found at many US military sites so that results from the study will be relevant for a number of military sites.

Key Points from Task 2

- When adequate mixing energy is used, combining AFFF and Jet Fuel results in a viscous microemulsion. The microemulsion was evidenced for application strength AFFF (3 wt.%) as well as diluted AFFF (0.375 wt.%).
- The microemulsion formed by AFFF and Jet Fuel is a Winsor Type II, thus, PFAS and other surfactants leave the aqueous phase and reside within the jet fuel to form the microemulsion.
- The flow of AFFF in porous media, at flow rates that resemble those measured in the field, generates adequate mixing energy to form a microemulsion with resident jet fuel *in-situ*.
- When formed in-situ, the viscous Winsor Type II microemulsion is difficult to displace, and likely contains the bulk of PFAS compounds (based on preliminary screening of effluent samples).
- A scenario where jet fuel was allowed to infiltrate the subsurface prior to AFFF application would like result in Type II microemulsion forming *in-situ* and acting as a PFAS source.
- PFAS was retained by relatively inert, clean sand (OK-75) under dynamic (flow) conditions indicating adsorption phenomena where surface charge is lacking.
- PFAS retention and retardation by clean sand (OK-75) under dynamic (flow) conditions appears related to both carbon-fluorine chain length and functional group.
- The PFAS retention appears to reach a saturation limit for the inert (OK-75) sand after 4 applications of AFFF-1, each approximately 0.5 pore volumes.
- Similar results were observed with respect to PFAS retention and retardation by the C2 horizon soil, a field-obtained sand containing low organic carbon and low clay content, under dynamic (flow) conditions: a) retention and retardation appear to be related to both carbon-fluorine chain length and functional group, and b) adsorption was observed onto media where the degree of surface charge is lacking.
- Repeated applications of AFFF resulted in behavior indicative of surfactant-surfactant adsorption, where sorbed species from the first application serve as sorption sites for species

during subsequent AFFF applications. This is a very subtle yet highly important observation with regard to the use of single component or even multi-component solutions to conduct research studies*: the interactions between the AFFF components will not captured in most studies unless actual AFFF solutions are used* and thus results may not accurately reflect field observations.

Practical Implications

- AFFF interacts with LNAPL present in the subsurface and forms LPME. This stable phase will retain a high percentage of the PFAS components in AFFF (PFAS sink) and can act as a future source of PFAS to groundwater.
- The LPME phase will not be easily transported within the subsurface environment due to the high viscosity at (low) shear rates that reflect flow rates achievable in the field.
- LPME formed *in-situ* can act to block pores and affect the flow of other phases, such as groundwater or remediation amendments being delivered to the subsurface.
- Attempts to model PFAS transport using adsorption measurements conducted with single component solutions will not capture the interactions between the PFAS components in AFFF, leading to poor correlation with field observations. A model that can capture the behavior, or adsorption data using PFAS solutions based on composition of actual AFFF, are strongly suggested.

Key Points from Task 3

- Sorption of PFAS at environmentally relevant concentrations (ng/L – µg/L) at the air-water interface is best modeled by Freundlich models. If the Langmuir model is used, the mass of PFAS at the interface is underpredicted.
- Correlations between air-water partition coefficient (K_i) and chromatographic retention time indicate that for new precursors, K_is can be predicted from retention times.
- A new conceptual model was developed to help explicitly account for previously underexamined mass transfer processes in unsaturated soils
  - This new model is undergoing the final stages of experimental validation and analysis
  - Can help account for potential discrepancies in retardation factor analysis typically done using the moment method of analysis.
  - This model can eventually be upscaled for use on field sites to reduce the complexity and potential sources of error in large scale models.
- Experimental validation of the MTI found a semi-empirical relationship between the saturation and breakthrough curve observation points.

  - This semi-empirical relationship does not vary with solute concentration nor longitudinal observation point, reinforcing the conceptual foundations of the model.

- Experimental studies on PFOS breakthrough in unsaturated sands have begun and are mostly complete. Experimental studies on breakthrough of AFFF mixtures will take place once PFOS experiments are completed and fully analyzed.
- Python based breakthrough curve and isotherm fitting tools which attempt to reconcile problems with typical methods of these analyses.
  - The BTC analyzer incorporates the mass transfer index model, and is the first step towards upscaling PFAS sorption models.
  - The isotherm fitting model is useful for those who wish to create more accurate and diverse isotherms of PFAS sorption.

Practical Implications

Results of this project clearly highlight the importance of PFAS adsorption at the air-water interface as a potentially important retention mechanism at AFFF-impacted sites. Specifically, PFAS retention at air-water interfaces, especially at low PFAS aqueous concentrations, may be substantially greater than what many conventional experimental and modeling approaches suggest. Such retention may explain PFAS persistence in relatively shallow soils at many of the DoD's historic AFFF-impacted sites. While this greater PFAS interfacial retention may result in extended PFAS persistence in soils moving forward, the enhanced retention may also be playing an important role with respect to mitigating PFAS mass discharge to groundwater, and thereby serving as an important attenuation mechanism that should be incorporated in conceptual site models. Field characterization efforts should focus on quantifying this PFAS retention under site-specific conditions, and site evaluation efforts should include more appropriate interfacial adsorption models (e.g., Freundlich) in the larger-scale leaching models that are currently being developed and validated as part of multiple DoD-funded research efforts.

Literature Cited (organized by subsection or task as noted)

Executive Summary and Background

1. Place, B. J.; Field, J. A., Identification of novel fluorochemicals in aqueous film-forming foams used by the US military. *Environ. Sci. Technol.* **2012,** *46*, (13), 7120-7127.
2. Backe, W. J.; Day, T. C.; Field, J. A., Zwitterionic, cationic, and anionic fluorinated chemicals in aqueous film forming foam formulations and groundwater from us military bases by nonaqueous large-volume injection HPLC-MS/MS. *Environ. Sci. Technol.* **2013,** *47*, (10), 5226-5234.
3. Garcia, R. A.; Chiaia-Hernandez, A. C.; Lara-Martin, P. A.; Loos, M.; Hollender, J.; Oetjen, K.; Higgins, C. P.; Field, J. A., Suspect Screening of Hydrocarbon Surfactants in AFFFs and AFFF-Contaminated Groundwater by High-Resolution Mass Spectrometry. *Environ. Sci. Technol.* **2019,** *53*, (14), 8068-8077.
4. Pabon, M., Personal Communication. In Field, J., Ed. ATOFINA Levalloix-Perret, France, 2002.
5. Moody, C. A.; Field, J. A., Perfluorinated surfactants and the environmental implications of their use in fire-fighting foams. *Environ. Sci. Technol.* **2000,** *34*, 3864-3869.
6. Martin, T., Fire-Fighting Foam Technology. In *Foam Engineering: Fundamentals and Application*, Stevenson, P., Ed. JOhn Wiley & Sons Ltd: Pondicherry, India, 2012; p 527.
7. Anderson, R.; Long, G.; Porter, R.; Anderson, J., Occurrence of select perfluoroalkyl substances at US Air Force aqueous film-forming foam release sites other than fire-training areas: Field-validation of critical fate and transport properties. *Chemosphere* **2016,** *150* 678-685.
8. McGuire, M. E.; Schaefer, C.; Richards, T.; Backe, W. J.; Field, J. A.; Houtz, E.; Sedlak, D. L.; Guelfo, J. L.; Wunsch, A.; Higgins, C. P., Evidence of remediation-induced alteration of subsurface poly- and perfluoroalkyl substance distribution at a former firefighter training area. *Environ. Sci. Technol.* **2014,** *48*, (12), 6644-6652.
9. Schultz, M. M.; Barofsky, D.; Field, J., Quantitative determination of fluorinated alkyl substances by large-volume-injection liquid chromatography tandem mass spectrometry-characterization of municipal wastewaters. *Environ. Sci. Technol.* **2006,** *40*, (1), 289-295.
10. U.S. EPA Office of Water *Provisonal Health Advisories for Perfluooctanoic Acid (PFOA) and Perfluorooctane Sulfonate (PFOS)*; January 8, 2009.
11. US EPA, **2022** https://www.epa.gov/sdwa/questions-and-answers-drinking-water-health-advisories-pfoa-pfos-genx-chemicals-and-pfbs.

12. Barzen-Hanson, K. A.; Davis, S. E.; Kleber, M.; Field, J. A., Sorption of Fluorotelomer Sulfonates, Fluorotelomer Sulfonamido Betaines, and a Fluorotelomer Sulfonamido Amine in National Foam Aqueous Film-Forming Foam to Soil. *Environ. Sci. Technol.* **2017,** *51*, (21), 12394-12404.

13. Xiao, F.; Jin, B. S.; Golovko, S. A.; Golovko, M. Y.; Xing, B. S., Sorption and Desorption Mechanisms of Cationic and Zwitterionic Per- and Polyfluoroalkyl Substances in Natural Soils: Thermodynamics and Hysteresis. *Environ. Sci. Technol.* **2019,** *53*, (20), 11818-11827.

14. Nickerson, A.; Maizel, A. C.; Kulkarni, P. R.; Adamson, D. T.; Kornuc, J. J.; Higgins, C. P., Enhanced Extraction of AFFF-Associated PFASs from Source Zone Soils. *Environ. Sci. Technol.* **2020,** *54*, (8), 4952-4962.

15. Nickerson, A.; Rodowa, A. E.; Adamson, D. T.; Field, J. A.; Kulkarni, P. R.; Kornuc, J. J.; Higgins, C. P., Spatial Trends of Anionic, Zwitterionic, and Cationic PFASs at an AFFF-Impacted Site. *Environ. Sci. Technol.* **2021,** *55*, (1), 313-323.

16. Adamson, D. T.; Nickerson, A.; Kulkarni, P. R.; Higgins, C. P.; Popovic, J.; Field, J.; Rodowa, A.; Newell, C.; DeBlanc, P.; Kornuc, J. J., Mass-Based, Field-Scale Demonstration of PFAS Retention within AFFF-Associated Source Areas. *Environ. Sci. Technol.* **2020,** *54*, (24), 15768-15777.

17. Adamsona, D.; Kulkarnia, P.; Nickerson, A.; Higgins, C.; Field, J.; Schwichtenberg, T.; Newell, C.; Kornuc, J., Characterization of relevant site-specific PFAS fate and transport processes at multiple AFFF sites. *Environ Adv* **2022,** *7, doi.org/10.1016/j.envadv.2022.100167*.

18. Higgins, C. P.; Luthy, R. G., Sorption of perfluorinated surfactants on sediments. *Environ. Sci. Technol.* **2006,** *40*, (23), 7251-7256.

19. Higgins, C. P.; Luthy, R. G., Modeling sorption of anionic surfactants onto sediment materials: An a priori approach for perfluoroalkyl surfactants and linear alkylbenzene sulfonates. *Environ. Sci. Technol.* **2007,** *41*, (9), 3254-3261.

20. Pan, G.; You, C., Sediment-water distribution of perfluorooctane sulfonate (PFOS) in Yangtze River Estuary. *Environ. Pollut.* **2010,** *158*, (5), 1363-1367.

21. Li, Y. S.; Oliver, D. P.; Kookana, R. S., A critical analysis of published data to discern the role of soil and sediment properties in determining sorption of per and polyfluoroalkyl substances (PFASs). *Sci. Total Environ.* **2018,** *628-629*, 110-120.

22. Figueroa-Diva, R. A.; Vasudevan, D.; MacKay, A. A., Trends in soil sorption coefficients within common antimicrobial families. *Chemosphere* **2010,** *79*, (8), 786-793.

23. Jones, A. D.; Bruland, G. L.; Agrawal, S.; Vasudevan, D., Factors influencing the sorption of oxytetracycline to soils. *Abstracts of Papers of the American Chemical Society* **2004,** *228*, U641-U641.

24. Vasudevan, D.; Bruland, G. L.; Torrance, B. S.; Upchurch, V. G.; MacKay, A. A., pH-dependent ciprofloxacin sorption to soils: Interaction mechanisms and soil factors influencing sorption. *Geoderma* **2009,** *151*, (3-4), 68-76.

25. Knag, M.; Tammelin, T.; Bilkova, K.; Johansson, L. S.; Gulbrandsen, E.; Sjoblom, J., Adsorption of polycation and anionic surfactant onto iron surfaces and the inhibition of carbon dioxide corrosion. *Journal of Dispersion Science and Technology* **2006,** *27*, (2), 277-292.

26. Sheng, J., Modern Chemical Enhanced Oil Recovery: Theory and Practice. Gulf Publishing Company: Houston, TXx. **2011**.

27. Lake, L. J., R.; Rossen, W.; Pope, G. Fundamentals of Enhanced Oil Recovery. Society of Petroleum Engineers: Richardson, TX, 2014.

28. Schaefer, C. E.; Culina, V.; Nguyen, D.; Field, J., Uptake of Poly- and Perfluoroalkyl Substances at the Air Water Interface. *Environ. Sci. Technol.* **2019,** *53*, (21), 12442-12448.

29. Brusseau, M. L., Assessing the potential contributions of additional retention processes to PFAS retardation in the subsurface. *Sci. Total Environ.* **2018,** *613*, 176-185.

30. Lyu, Y.; Brusseau, M. L., The influence of solution chemistry on air-water interfacial adsorption and transport of PFOA in unsaturated porous media. *Sci. Tot. Environ.* **2020,** *713*, Article no. 136744.

31. Lyu, Y.; Brusseau, M. L.; Chen, W.; Yan, N.; Fu, X. R.; Lin, X. Y., Adsorption of PFOA at the air-water interface during transport in unsaturated porous media. *Environ. Sci. Technol.* **2018,** *52*, (14), 7745-7753.

32. Hao, S. L.; Choi, Y. J.; Wu, B. R.; Higgins, C. P.; Deeb, R.; Strathmann, T. J., Hydrothermal alkaline treatment for destruction of per- and polyfluoroalkyl substances in aqueous film-forming foam. *Environ. Sci. Technol.* **2021,** *55*, (5), 3283-3295.

33. Goss, K. U.; Bronner, G., What is so special about the sorption behavior of highly fluorinated compounds? *Journal of Physical Chemistry A* **2006,** *110*, (30), 9518-9522.

34. Cowan, C. T.; White, D., The Mechanism of Exchange Reactions Occuring Between Sodium Montmorillonite and Various n-Primary Aliphatic Amine Salts *Transactions of the Faraday Society* **1958,** *54*, 691-697.

35. Martz, M. H., J.; Marschner, B.; Stumpe, B., , Effects of soil organic carbon (SOC) content and accessibility in subsoils on the sorption processes of the model pollutants nonylphenol (4-n-NP) and perfluorooctanoic acid (PFOA). *Sci Total Environ* **2019,** *672*, 162-173.

36. Nguyen, T. M. H. B., J.; Thompson, K.; Thompson, J.; Kabiri, S.; Navarro, D. A.; Kookana, R. S.; Grimison, C.; Barnes, C. M.; Higgins, C. P.; McLaughlin, M. J.; Mueller, J. F., , Influences of Chemical Properties, Soil Properties, and Solution pH on Soil-Water Partitioning Coefficients of Per- and Polyfluoroalkyl Substances (PFASs). *Environ Sci Technol* **2020,** *54*, (24), 15883-15892.

37. Schaefer, C. E.; Nguyen, D.; Christie, E.; Shea, S.; Higgins, C. P.; Field, J. A., Desorption of Poly- and Perfluoroalkyl Substances from Soil Historically Impacted with Aqueous Film-Forming Foam. *J Environ Eng* **2021,** *147*, (2).

Methods and Materials, Results and Discussion Sections (organized by task)

Task 1

1. Dwarakanath, V.; Kostarelos, K.; Pope, G. A.; Shotts, D.; Wade, W. H., Anionic surfactant remediation of soil columns contaminated by nonaqueous phase liquids. *Journal of Contaminant Hydrology* **1999,** *38*, (4), 465-488.

2. Kostarelos, K.; Pope, G. A.; Rouse, B. A.; Shook, G. M., A new concept: the use of neutrally-buoyant microemulsions for DNAPL remediation. *Journal of Contaminant Hydrology* **1998,** *34*, (4), 383-397.

3. Kostarelos, K.; Sharma, P.; Christie, E.; Wanzek, T.; Field, J., Viscous Microemulsions of Aqueous Film-Forming Foam (AFFF) and Jet Fuel A Inhibit Infiltration and Subsurface Transport. *Environmental Science & Technology Letters* **2021,** *8*, (2), 142-147.

4. Brusseau, M. L.; Yan, N.; Van Glubt, S.; Wang, Y.; Chen, W.; Lyu, Y.; Dungan, B.; Carroll, K. C.; Holguin, F. O., Comprehensive retention model for PFAS transport in subsurface systems. *Water Res* **2019,** *148*, 41-50.

5. Guelfo, J. L.; Wunsch, A.; McCray, J.; Stults, J. F.; Higgins, C. P., Subsurface transport potential of perfluoroalkyl acids (PFAAs): Column experiments and modeling. *J Contam Hydrol* **2020,** *233*, 103661.

6. Stark, J. R.; Cummings, T. R.; Twenter, F. R. *Ground-water contamination at Wurtsmith Air Force Base, Michigan*; 83-4002; Lansing, MI, 1983.

7. Backe, W. J.; Day, T. C.; Field, J. A., Zwitterionic, cationic, and anionic fluorinated chemicals in aqueous film forming foam formulations and groundwater from U.S. military bases by nonaqueous large-volume injection HPLC-MS/MS. *Environ Sci Technol* **2013,** *47*, (10), 5226-34.

8. Hao, S.; Choi, Y. J.; Wu, B.; Higgins, C. P.; Deeb, R.; Strathmann, T. J., Hydrothermal Alkaline Treatment for Destruction of Per- and Polyfluoroalkyl Substances in Aqueous Film-Forming Foam. *Environ Sci Technol* **2021,** *55*, (5), 3283-3295.

9. Nickerson, A.; Maizel, A. C.; Kulkarni, P. R.; Adamson, D. T.; Kornuc, J. J.; Higgins, C. P., Enhanced Extraction of AFFF-Associated PFAS from Source Zone Soils. *Environ Sci Technol* **2020,** *54*, (8), 4952-4962.

10. Chai, T.; Draxler, R. R., Root mean square error (RMSE) or mean absolute error (MAE)? – Arguments against avoiding RMSE in the literature. *Geoscientific Model Development* **2014,** *7*, (3), 1247-1250.

11. Runkel, R. L., Solution of the advection-dispersion equation: Continuous load of finite duration. *J Environ Eng-Asce* **1996,** *122*, (9), 830-832.

12. Brusseau, M. L.; Rao, P. S. C., Sorption Nonideality during Organic Contaminant Transport in Porous-Media. *Crit Rev Env Contr* **1989,** *19*, (1), 33-99.

13. Shackelford, C. D.; Malusis, M. A.; Majeski, M. J.; Stern, R. T., Electrical Conductivity Breakthrough Curves. *Journal of Geotechnical and Geoenvironmental Engineering* **1999,** *125*, (4), 260-270.

14. Drummond, J. D.; Covino, T. P.; Aubeneau, A. F.; Leong, D.; Patil, S.; Schumer, R.; Packman, A. I., Effects of solute breakthrough curve tail truncation on residence time estimates: A synthesis of solute tracer injection studies. *J Geophys Res-Biogeo* **2012,** *117*.

15. Nguyen, T. M. H.; Braunig, J.; Kookana, R. S.; Kaserzon, S. L.; Knight, E. R.; Vo, H. N. P.; Kabiri, S.; Navarro, D. A.; Grimison, C.; Riddell, N.; Higgins, C. P.; McLaughlin, M. J.; Mueller, J. F., Assessment of Mobilization Potential of Per- and Polyfluoroalkyl Substances for Soil Remediation. *Environ Sci Technol* **2022,** *56*, (14), 10030-10041.

16. Xiao, F.; Jin, B.; Golovko, S. A.; Golovko, M. Y.; Xing, B., Sorption and Desorption Mechanisms of Cationic and Zwitterionic Per- and Polyfluoroalkyl Substances in Natural Soils: Thermodynamics and Hysteresis. *Environ Sci Technol* **2019,** *53*, (20), 11818-11827.

- 17. Stults, J. F.; Choi, Y. J.; Schaefer, C. E.; Illangasekare, T. H.; Higgins, C. P., 2022 Estimation of Transport Parameters of Perfluoroalkyl Acids (PFAAs) in Unsaturated Porous Media: Critical Experimental and Modeling Improvements. *Environmental Science & Technology*. . https: //doi.org/10.1021/acs.est.2c00819.

18. Li, Z. Y.; Lyu, X. Y.; Gao, B.; Xu, H. X.; Wu, J. C.; Sun, Y. Y., Effects of ionic strength and cation type on the transport of perfluorooctanoic acid (PFOA) in unsaturated sand porous media. *Journal of Hazardous Materials* **2021,** *403*.

19. Kirby, B. J., *Micro- and Nanoscale Fluidics: Transport in Microfluidic Devices*. Cambridge University Press: 2010.

20. Brusseau, M. L., The influence of molecular structure on the adsorption of PFAS to fluid-fluid interfaces: Using QSPR to predict interfacial adsorption coefficients. *Water Res* **2019,** *152*, 148-158.

21. Nickerson, A.; Rodowa, A. E.; Adamson, D. T.; Field, J. A.; Kulkarni, P. R.; Kornuc, J. J.; Higgins, C. P., Spatial Trends of Anionic, Zwitterionic, and Cationic PFAS at an AFFF-Impacted Site. *Environ Sci Technol* **2021,** *55*, (1), 313-323.

22. Adamson, D. T.; Nickerson, A.; Kulkarni, P. R.; Higgins, C. P.; Popovic, J.; Field, J.; Rodowa, A.; Newell, C.; DeBlanc, P.; Kornuc, J. J., Mass-Based, Field-Scale Demonstration of PFAS Retention within AFFF-Associated Source Areas. *Environ Sci Technol* **2020,** *54*, (24), 15768-15777.

23. Goss, K.; Bronner, G., What Is So Special about the Sorption Behavior of Highly Fluorinated Compounds? *Journal of Physical Chemistry* **2006**.

24. Cowan, C. T.; White, D., The Mechanism of Exchange Reactions Occuring Between Sodium Montmorillonite and Various n-Primary Aliphatic Amine Salts. *Transactions of the Faraday Society* **1958,** *54*, 691-697.

25. Mejia-Avendano, S.; Zhi, Y.; Yan, B.; Liu, J., Sorption of Polyfluoroalkyl Surfactants on Surface Soils: Effect of Molecular Structures, Soil Properties, and Solution Chemistry. *Environ Sci Technol* **2020,** *54*, (3), 1513-1521.

26. Barzen-Hanson, K. A.; Davis, S. E.; Kleber, M.; Field, J. A., Sorption of Fluorotelomer Sulfonates, Fluorotelomer Sulfonamido Betaines, and a Fluorotelomer Sulfonamido Amine in National Foam Aqueous Film-Forming Foam to Soil. *Environ Sci Technol* **2017,** *51*, (21), 12394-12404.

27. Nguyen, T. M. H.; Braunig, J.; Thompson, K.; Thompson, J.; Kabiri, S.; Navarro, D. A.; Kookana, R. S.; Grimison, C.; Barnes, C. M.; Higgins, C. P.; McLaughlin, M. J.; Mueller, J. F., Influences of Chemical Properties, Soil Properties, and Solution pH on Soil-Water Partitioning Coefficients of Per- and Polyfluoroalkyl Substances (PFAS). *Environ Sci Technol* **2020,** *54*, (24), 15883-15892.

28. Shafique, U.; Dorn, V.; Paschke, A.; Schuurmann, G., Adsorption of perfluorocarboxylic acids at the silica surface. *Chem Commun (Camb)* **2017,** *53*, (3), 589-592.

29. Chen, H.; Reinhard, M.; Nguyen, V. T.; Gin, K. Y., Reversible and irreversible sorption of perfluorinated compounds (PFCs) by sediments of an urban reservoir. *Chemosphere* **2016,** *144*, 1747-53.

30. Brusseau, M. L., Simulating PFAS transport influenced by rate-limited multi-process retention. *Water Res* **2020,** *168*, 115179.

31. Martz, M.; Heil, J.; Marschner, B.; Stumpe, B., Effects of soil organic carbon (SOC) content and accessibility in subsoils on the sorption processes of the model pollutants nonylphenol (4-n-NP) and perfluorooctanoic acid (PFOA). *Sci Total Environ* **2019,** *672*, 162-173.

32. Schaefer, C. E.; Nguyen, D.; Christie, E.; Shea, S.; Higgins, C. P.; Field, J. A., Desorption of Poly- and Perfluoroalkyl Substances from Soil Historically Impacted with Aqueous Film-Forming Foam. *J Environ Eng* **2021,** *147*, (2).

33. Fabregat-Palau, J.; Vidal, M.; Rigol, A., Modelling the sorption behaviour of perfluoroalkyl carboxylates and perfluoroalkane sulfonates in soils. *Sci Total Environ* **2021,** *801*, 149343.

34. Johnson, R. L.; Anschutz, A. J.; Smolen, J. M.; Simcik, M. F.; Penn, R. L., The adsorption of perfluorooctane sulfonate onto sand, clay, and iron oxide surfaces. *J Chem Eng Data* **2007,** *52*, (4), 1165-1170.

35. Li, F.; Fang, X.; Zhou, Z.; Liao, X.; Zou, J.; Yuan, B.; Sun, W., Adsorption of perfluorinated acids onto soils: Kinetics, isotherms, and influences of soil properties. *Sci Total Environ* **2019,** *649*, 504-514.

36. Yan, W.; Qian, T.; Zhang, L.; Wang, L.; Zhou, Y., Interaction of perfluorooctanoic acid with extracellular polymeric substances - Role of protein. *J Hazard Mater* **2021,** *401*, 123381.

Task 2

1 Sheng, J. Modern Chemical Enhanced Oil Recovery: Theory and Practice. Gulf Publishing Company: Houston, TX, **2011**.

2 Lake, L.; Johns, R.; Rossen, W.; Pope, G. Fundamentals of Enhanced Oil Recovery. Society of Petroleum Engineers: Richardson, TX, **2014**.

3 Place, B. J.; Field, J. A., Identification of novel fluorochemicals in aqueous film-forming foams used by the US military. Environ. Sci. Technol. **2012**, 46, (13), 7120-7127, OCA.0025.0002.0245 at 0245 and 0249.

4 Schultz, M. M.; Barofsky, D.; Field, J. A., Quantitative determination of fluorotelomer sulfonates in groundwater by LC MS/MS. *Environ. Sci. Technol.* **2004**, *38*, (6), 1828-1835.

5 Preparation of Synthetic Tap Water for the JSAWM Program, downloaded Feb **2019**.

https://studylib.net/doc/7577859/preparation-of-synthetic-tapwater-for-the-jsawm-program1

6 Debye, P., Light scattering in solutions *J Appl Physics* **1944**, *15*, 338-342.

7 Debye, P., Light scattering in soap solutions. *Ann. N.Y. Acad. Sci* **1949**, *51*, 575-563. 33: Mysels, K.; Princen, L., Light scattering by some lauryl sulfate solutions. *J. Phys. Chem* **1959**, *63*, 1696-1700.

8 Mysels, K.; Princen, L., Light scattering by some lauryl sulfate solutions. J. Phys. Chem **1959**, 63, 1696-1700.

9 Singh, R. Multifunctional Foams and Emulsions for Subsurface Applications. University of Texas at Austin., **2017**.

10 TA Instruments https://www.tainstruments.com/products/rheology/discovery-hybrid-rheometers/ (Accessed 28 June 2020).

11 Paar Instruments. https://www.anton-paar.com/?eID=documents Download&document=18378&L=0

12 Stark, J. R.; Cummings, T. R.; Twenter, F. R. "Ground-water contamination at Wurtsmith Air Force Base, Michigan." 83-4002; Lansing, MI, **1983**.

13 Barton, Gary J., "Contributing areas of water-supply wells in Elkton and Pigeon, Huron County, M ichigan," *USGS Water-Resources Investigations Report* 94-4089, **1995**. https://doi.org/10.3133/wri944089

14 Ramsburg, C. A.; Pennell, K. D.; Kibbey, T. C. G.; Hayes, K. F., Use of a surfactant-stabilized emulsion to deliver 1-butanol for density-modified displacement of trichloroethene. *Environ. Sci. Technol.* **2003**, *37*, (18), 4246-4253.

15 Zhou, M. F.; Rhue, R. D., Screening commercial surfactants suitable for remediating DNAPL source zones by solubilization. *Environ. Sci. Technol.* **2000**, *34*, (10), 1985-1990.

16 Meng, P. P.; Deng, S. B.; Du, Z. W.; Wang, B.; Huang, J.; Wang, Y. J.; Yu, G.; Xing, B. S., Effect of hydro-oleophobic perfluorocarbon chain on interfacial behavior and mechanism of perfluorooctane sulfonate in oil-water mixture. Scientific Reports 2017, 7.

17 Kissa, E., *Fluorinated surfactants: Synthesis, Properties, and Applications*. Marcel Dekker: New York, **1994**; Vol. 50.

18 Martin, T., Fire-Fighting Foam Technology. In *Foam Engineering: Fundamentals and Application*, Stevenson, P., Ed. JOhn Wiley & Sons Ltd: Pondicherry, India, **2012**; p 527.

19 Bergeron, V.; Fagen, M.; Radke, C., Generalized entering coefficient: A criterion for foam stability against oil in porous media. *Langmuir* **1993**, *9*, (7), 1704-1713.

Task 3

1 Harding-Marjanovic, K. C.; Houtz, E. F.; Yi, S.; Field, J. A.; Sedlak, D. L.; Alvarez-Cohen, L. Aerobic Biotransformation of Fluorotelomer Thioether Amido Sulfonate (Lodyne) in AFFF-Amended Microcosms. *Environ. Sci. Technol.* **2015**, *49* (13), 7666–7674. https: //doi.org/10.1021/acs.est.5b01219.

2 Backe, W. J.; Day, T. C.; Field, J. A. Zwitterionic, Cationic, and Anionic Fluorinated Chemicals in Aqueous Film Forming Foam Formulations and Groundwater from U.S. Military Bases by Nonaqueous Large-Volume Injection HPLC-MS/MS. *Environ. Sci. Technol.* **2013**, *47* (10), 5226–5234. https: //doi.org/10.1021/es3034999.

3 Anastasiadis, S. H.; Chen, J. K.; Koberstein, J. T.; Siegel, A. F.; Sohn, J. E.; Emerson, J. A. The Determination of Interfacial Tension by Video Image Processing of Pendant Fluid Drops. *J. Colloid Interface Sci.* **1987**, *119* (1), 55–66. https: //doi.org/10.1016/0021-9797(87)90244-X.

4 Adamson, A.; Gast, A. *Physical Chemistry of Surfaces*; John Wiley & Sons, Ltd: New York, 1997.

5 Gurkov, T. D.; Dimitrova, D. T.; Marinova, K. G.; Bilke-Crause, C.; Gerber, C.; Ivanov, I. B. Ionic Surfactants on Fluid Interfaces: Determination of the Adsorption; Role of the Salt and the Type of the Hydrophobic Phase. *Colloids Surfaces A Physicochem. Eng. Asp.* **2005**, *261* (1–3), 29–38. https: //doi.org/10.1016/j.colsurfa.2004.11.040.

6 Weber, W. J.; Voice, T. C.; Pirbazari, M.; Hunt, G. E.; Ulanoff, D. M. Sorption of Hydrophobic Compounds by Sediments, Soils and Suspended Solids-II. Sorbent Evaluation Studies. *Water Res.* **1983**, *17* (10), 1443–1452. https: //doi.org/10.1016/0043-1354(83)90276-2.

7 Henry, D. C. LX. A Kinetic Theory of Adsorption . *London, Edinburgh, Dublin Philos. Mag. J. Sci.* **1922**, *44* (262), 689–705. https: //doi.org/10.1080/14786441108634035.

8 Baig, K. S.; Doan, H. D.; Wu, J. Multicomponent Isotherms for Biosorption of Ni2+ and Zn2+. *Desalination* **2009**, *249* (1), 429–439. https: //doi.org/10.1016/j.desal.2009.06.052.

9 Vecitis, C. D.; Park, H.; Cheng, J.; Mader, B. T.; Hoffmann, M. R. Enhancement of Perfluorooctanoate and Perfluorooctanesulfonate Activity at Acoustic Cavitation Bubble Interfaces. *J. Phys. Chem. C* **2008**, *112* (43), 16850–16857. https: //doi.org/10.1021/jp804050p.

10 Lyu, Y.; Brusseau, M. L.; Chen, W.; Yan, N.; Fu, X.; Lin, X. Adsorption of PFOA at the Air-Water Interface during Transport in Unsaturated Porous Media. *Environ. Sci. Technol.* **2018**, *52* (14), 7745–7753. https: //doi.org/10.1021/acs.est.8b02348.

11 Silva, J. A. K.; Martin, W. A.; Johnson, J. L.; McCray, J. E. Evaluating Air-Water and NAPL-Water Interfacial Adsorption and Retention of Perfluorocarboxylic Acids within the Vadose Zone. *J. Contam. Hydrol.* **2019**, *223* (November 2018). https: //doi.org/10.1016/j.jconhyd.2019.03.004.

12 Brusseau, M. L. Assessing the Potential Contributions of Additional Retention Processes to PFAS Retardation in the Subsurface. *Sci. Total Environ.* **2018**, *613–614*, 176–185. https: //doi.org/10.1016/j.scitotenv.2017.09.065.

13 Lunkenheimer, K.; Prescher, D.; Hirte, R.; Geggel, K. Adsorption Properties of Surface Chemically Pure Sodium Perfluoro- N -Alkanoates at the Air/Water Interface: Counterion Effects within Homologous Series of 1:1 Ionic Surfactants. *Langmuir* **2015**, *31* (3), 970–981. https: //doi.org/10.1021/la503450k.

14 Reth, M.; Berger, U.; Broman, D.; Cousins, I. T.; Nilsson, E. D.; McLachlan, M. S. Water-to-Air Transfer of Perfluorinated Carboxylates and Sulfonates in a Sea Spray Simulator. *Environ. Chem.* **2011**, *8* (4), 381–388. https: //doi.org/10.1071/EN11007.

15 Brusseau, M. L.; Van Glubt, S. The Influence of Surfactant and Solution Composition on PFAS Adsorption at Fluid-Fluid Interfaces. *Water Res.* **2019**, *161*, 17–26. https: //doi.org/10.1016/j.watres.2019.05.095.

16 Xiao, X.; Ulrich, B. A.; Chen, B.; Higgins, C. P. Sorption of Poly- and Perfluoroalkyl Substances (PFAS) Relevant to Aqueous Film-Forming Foam (AFFF)-Impacted Groundwater by Biochars and Activated Carbon. *Environ. Sci. Technol.* **2017**, *51* (11), 6342–6351. https: //doi.org/10.1021/acs.est.7b00970.

17) Schaefer, C. E.; DiCarlo, D. A.; Blunt, M. J. Experimental Measurement of Air-Water Interfacial Area during Gravity Drainage and Secondary Imbibition in Porous Media. *Water Resour. Res.* **2000**, *36* (4), 885–890. https: //doi.org/10.1029/2000WR900007.

18 El Ouni, A.; Guo, B.; Zhong, H.; Brusseau, M. L. Testing the Validity of the Miscible-Displacement Interfacial Tracer Method for Measuring Air-Water Interfacial Area: Independent Benchmarking and Mathematical Modeling. *Chemosphere* **2021**, *263*, 128193. https: //doi.org/10.1016/j.chemosphere.2020.128193.

19 Stults, J.; Illangasekare, T.; Higgins, C. P. The Mass Transfer Index (MTI): A Semi-Empirical Approach for Quantifying Transport of Solutes in Variably Saturated Porous Media. *J. Contam. Hydrol.* **2021**, *242*. https: //doi.org/10.1016/j.jconhyd.2021.103842.

20 Runkel, R. L. Solution of the Advection-Dispersion Equation: Continuous Load of Finite Duration. *J. Environ. Eng.* **1996**, *122* (9), 830–832. https: //doi.org/10.1061/(asce)0733-9372(1996)122: 9(830).

21 Shackelford, C. D.; Malusis, M. A.; Majeski, M. J.; Stern, R. T. Electrical Conductivity Breakthrough Curves. *J. Geotech. Geoenvironmental Eng.* **1999**, *125* (4), 260–270. https: //doi.org/10.1061/(asce)1090-0241(1999)125: 4(260).

22 Guelfo, J. L.; Wunsch, A.; McCray, J.; Stults, J. F.; Higgins, C. P. Subsurface Transport Potential of Perfluoroalkyl Acids (PFAAs): Column Experiments and Modeling. *J. Contam. Hydrol.* **2020**, *233* (May), 103661. https: //doi.org/10.1016/j.jconhyd.2020.103661.

23 Brusseau, M. L. Assessing the Potential Contributions of Additional Retention Processes to PFAS Retardation in the Subsurface. *Sci. Total Environ.* **2018**, *613–614*, 176–185. https: //doi.org/10.1016/j.scitotenv.2017.09.065.

24 Kim, H.; Rao, P. S. C.; Annable, M. D. Determination of Effective Air-Water Interfacial Area in Partially Saturated Porous Media Using Surfactant Adsorption. *Water Resour. Res.* **1997**, *33* (12), 2705–2711. https: //doi.org/10.1029/97WR02227.

25 Brusseau, M. L.; Peng, S.; Schnaar, G.; Murao, A. Measuring Air-Water Interfacial Areas with X-Ray Microtomography and Interfacial Partitioning Tracer Tests. *Environ. Sci. Technol.* **2007**, *41* (6), 1956–1961. https: //doi.org/10.1021/es061474m.

26 Araujo, J. B.; Mainhagu, J.; Brusseau, M. L. Measuring Air-Water Interfacial Area for Soils Using the Mass Balance Surfactant-Tracer Method. *Chemosphere* **2015**, *134*, 199–202. https: //doi.org/10.1016/j.chemosphere.2015.04.035.

27 Brusseau, M. L.; Lyu, Y.; Yan, N.; Guo, B. Low-Concentration Tracer Tests to Measure Air-Water Interfacial Area in Porous Media. *Chemosphere* **2020**, *250*, 126305. https: //doi.org/10.1016/j.chemosphere.2020.126305.

28 Brusseau, M. L.; Rao, P. S. C. Sorption Nonideality during Organic Contaminant Transport in Porous Media. *Crit. Rev. Environ. Control* **1989**, *19* (1), 33–99. https: //doi.org/10.1080/10643388909388358.

29 De Gennes, P. G. Hydrodynamic Dispersion in Unsaturated Porous Media. *J. Fluid Mech.* **1983**, *136*, 189–200. https: //doi.org/10.1017/S0022112083002116.

30 Van Genuchten, M. T.; Wierenga, P. J. Mass Transfer Studies in Sorbing Porous Media: II. Experimental Evaluation with Tritium (3H2O). *Soil Sci. Soc. Am. J.* **1977**, *41* (2), 272–278. https: //doi.org/10.2136/sssaj1977.03615995004100020022x.

31 Weber, W. J.; McGinley, P. M.; Katz, L. E. Sorption Phenomena in Subsurface Systems: Concepts, Models and Effects on Contaminant Fate and Transport. *Water Res.* **1991**, *25* (5), 499–528. https: //doi.org/10.1016/0043-1354(91)90125-A.

32 Wierenga, P. J.; Van Genuchten, M. T. Solute Transport Through Small and Large Unsaturated Soil Columns. *Groundwater* **1989**, *27* (1), 35–42. https: //doi.org/10.1111/j.1745-6584.1989.tb00005.x.

33 Padilla, I. Y.; Yeh, T. C. J.; Conklin, M. H. The Effect of Water Content on Solute Transport in Unsaturated Porous Media. *Water Resour. Res.* **1999**, *35* (11), 3303–3313. https: //doi.org/10.1029/1999WR900171.

34 Ghanbarian, B.; Hunt, A. G.; Ewing, R. P.; Sahimi, M. Tortuosity in Porous Media: A Critical Review. *Soil Sci. Soc. Am. J.* **2013**, *77* (5), 1461–1477. https: //doi.org/10.2136/sssaj2012.0435.

35 Hagare, D.; Sivakumar, M.; Bunsri, T. Influence of Dispersion on Transport of Tracer through Unsaturated Porous Media. *J. Appl. Fluid Mech.* **2008**, *1* (02). https: //doi.org/10.36884/jafm.1.02.11846.

36 Hasan, S.; Niasar, V.; Karadimitriou, N. K.; Godinho, J. R. A.; Vo, N. T.; An, S.; Rabbani, A.; Steeb, H. Direct Characterization of Solute Transport in Unsaturated Porous Media Using Fast X-Ray Synchrotron Microtomography. *Proc. Natl. Acad. Sci. U. S. A.* **2020**, *117* (38), 23443–23449. https: //doi.org/10.1073/pnas.2011716117.

37 Hasan, S.; Joekar-Niasar, V.; Karadimitriou, N. K.; Sahimi, M. Saturation Dependence of Non-Fickian Transport in Porous Media. *Water Resour. Res.* **2019**, *55*, 1153–1166. https: //doi.org/10.1029/2018WR023554.

38 Hansen, S. K.; Berkowitz, B. Modeling Non-Fickian Solute Transport Due to Mass Transfer and Physical Heterogeneity on Arbitrary Groundwater Velocity Fields. *Water Resour. Res.* **2020**, *56* (10), 1–19. https: //doi.org/10.1029/2019WR026868.

39 Karadimitriou, N. K.; Joekar-Niasar, V.; Brizuela, O. G. Hydro-Dynamic Solute Transport under Two-Phase Flow Conditions. *Sci. Rep.* **2017**, *7* (1), 1–7. https: //doi.org/10.1038/s41598-017-06748-1.

40 Penman, H. L. Gas and Vapour Movements in the Soil: I. The Diffusion of Vapours through Porous Solids. *J. Agric. Sci.* **1940**, *30* (3), 437–462. https: //doi.org/10.1017/S0021859600048164.

41 Toride, N.; Inoue, M.; Leij, F. J. Hydrodynamic Dispersion in an Unsaturated Dune Sand. *Soil Sci. Soc. Am. J.* **2003**, *67* (3), 703. https: //doi.org/10.2136/sssaj2003.0703.

42 Berkowitz, B.; Cortis, A.; Dentz, M.; Scher, H. Modeling Non-Fickian Transport in Geological Formations as a Continuous Time Random Walk. *Rev. Geophys.* **2006**, *44* (2), 1–49. https: //doi.org/10.1029/2005RG000178.

43 Brusseau, M. L.; Jessup, R. E.; Rao, P. S. C. Modeling the Transport of Solutes Influenced by Multiprocess Nonequilibrium. *Water Resour. Res.* **1989**, *25* (9), 1971–1988. https: //doi.org/10.1029/WR025i009p01971.

44 Haggerty, R.; Gorelick, S. M. Multiple-Rate Mass Transfer for Modeling Diffusion and Surface Reactions in Media with Pore-Scale Heterogeneity. *Water Resour. Res.* **1995**, *31* (10), 2383–2400. https: //doi.org/10.1029/95WR10583.

45 Benson, D. A.; Wheatcraft, S. W.; Meerschaert, M. M. Application of a Fractional Advection-Dispersion Equation. *Water Resour. Res.* **2000**, *36* (6), 1403–1412. https: //doi.org/10.1029/2000WR900031.

46 Van Genuchten, M. T.; Wierenga, P. J. Mass Transfer Studies in Sorbing Porous Media I. Analytical Solutions. *Soil Sci. Soc. Am. J.* **1976**, *40* (4), 473–480. https: //doi.org/10.2136/sssaj1976.03615995004000040011x.

47 Ma, L.; Selim, H. M. Tortuosity, Mean Residence Time, and Deformation of Tritium Breakthroughs from Soil Columns. *Soil Sci. Soc. Am. J.* **1994**, *58* (4), 1076–1085. https: //doi.org/10.2136/sssaj1994.03615995005800040011x.

48 Ezzatabadipour, M.; Zahedi, H. A Novel Method for Streamline-Based Tortuosity Calculation and Investigation of Obstacles Shape Effect on Tortuosity in Porous Media with Random Elliptical Obstacles Using Lattice Boltzmann Method. *Transp. Porous Media* **2021**, *136* (1), 103–124. https: //doi.org/10.1007/s11242-020-01502-0.

49 Moldrup, P.; Olesen, T.; Rolston, D. E.; Yamaguchi, T. Modeling Diffusion and Reaction in Soils: VII. Predicting Gas and Ion Diffusivity in Undisturbed and Sieved Soils. *Soil Sci.* **1997**, *162* (9), 632–640. https: //doi.org/10.1097/00010694-199709000-00004.

50 Millington, R. J.; Quirk, J. . Transport in Porous Media. *Trans. Int. Congr. Soil Sci.* **1961**, *7* (1), 97–106.

51 Brusseau, M. L.; Yan, N.; Van Glubt, S.; Wang, Y.; Chen, W.; Lyu, Y.; Dungan, B.; Carroll, K. C.; Holguin, F. O. Comprehensive Retention Model for PFAS Transport in Subsurface Systems. *Water Res.* **2019**, *148*, 41–50. https: //doi.org/10.1016/j.watres.2018.10.035.

52 Lyu, Y.; Brusseau, M. L. The Influence of Solution Chemistry on Air-Water Interfacial Adsorption and Transport of PFOA in Unsaturated Porous Media. *Sci. Total Environ.* **2020**, *713*, 136744. https: //doi.org/10.1016/j.scitotenv.2020.136744.

53 Schaefer, C. E.; Culina, V.; Nguyen, D.; Field, J. Uptake of Poly- And Perfluoroalkyl Substances at the Air-Water Interface. *Environ. Sci. Technol.* **2019**, *53* (21), 12442–12448. https: //doi.org/10.1021/acs.est.9b04008.

54 Zhou, D.; Brusseau, M. L.; Zhang, Y.; Li, S.; Wei, W.; Sun, H. Simulating PFAS Adsorption Kinetics , Adsorption Isotherms , and Nonideal Transport in Saturated Soil with Tempered One-Sided Stable Density (TOSD) Based Models. *J. Hazard. Mater.* **2021**, *411* (January), 125169. https: //doi.org/10.1016/j.jhazmat.2021.125169.

55 Brusseau, M. L. Examining the Robustness and Concentration Dependency of PFAS Air-Water and NAPL-Water Interfacial Adsorption Coefficients. *Water Res.* **2021**, *190*. https: //doi.org/10.1016/j.watres.2020.116778.

56 Costanza, J.; Abriola, L. M.; Pennell, K. D. Aqueous Film-Forming Foams Exhibit Greater Interfacial Activity than PFOA, PFOS, or FOSA. *Environ. Sci. Technol.* **2020**, *54* (21), 13590–13597. https: //doi.org/10.1021/acs.est.0c03117.

57 Lampic, A.; Parnis, J. M. Property Estimation of Per- and Polyfluoroalkyl Substances: A Comparative Assessment of Estimation Methods. *Environ. Toxicol. Chem.* **2020**, *39* (4), 775–786. https: //doi.org/10.1002/etc.4681.

58 Costanza, J.; Arshadi, M.; Abriola, L. M.; Pennell, K. D. Accumulation of PFOA and PFOS at the Air-Water Interface. *Environ. Sci. Technol. Lett.* **2019**, *6* (8), 487–491. https: //doi.org/10.1021/acs.estlett.9b00355.

59 Arshadi, M.; Costanza, J.; Abriola, L. M.; Pennell, K. D. Comment on "Uptake of Poly- And Perfluoroalkyl Substances at the Air-Water Interface." *Environ. Sci. Technol.* **2020**, *54* (11), 7019–7020. https: //doi.org/10.1021/acs.est.0c01838.

60 Schaefer, C. E.; Nguyen, D.; Field, J. Response to the Comment on "Uptake of Poly- And Perfluoroalkyl Substances at the Air-Water Interface." *Environ. Sci. Technol.* **2020**, *54* (11), 7021–7022. https: //doi.org/10.1021/acs.est.0c02488.

61 Brusseau, M. L.; Guo, B.; Huang, D.; Yan, N.; Lyu, Y. Ideal versus Nonideal Transport of PFAS in Unsaturated Porous Media. *Water Res.* **2021**, *202* (June), 117405. https: //doi.org/10.1016/j.watres.2021.117405.

62 Mcmurdo, C. J.; Ellis, D. A.; Webster, E.; Butler, J.; Christensen, R. D.; Reid, L. K. Aerosol Enrichment of the Surfactant PFO and Mediation of the Water-Air Transport of Gaseous PFOA. *Environ. Sci. Technol.* **2008**, *42* (11), 3969–3974. https: //doi.org/10.1021/es7032026.

63 Johansson, J. H.; Salter, M. E.; Acosta Navarro, J. C.; Leck, C.; Nilsson, E. D.; Cousins, I. T. Global Transport of Perfluoroalkyl Acids via Sea Spray Aerosol. *Environ. Sci. Process. Impacts* **2019**, *21* (4), 635–649. https: //doi.org/10.1039/c8em00525g.

64 Ju, X.; Jin, Y.; Sasaki, K.; Saito, N. Perfluorinated Surfactants in Surface, Subsurface Water and Microlayer from Dalian Coastal Waters in China. *Environ. Sci. Technol.* **2008**, *42* (10), 3538–3542. https: //doi.org/10.1021/es703006d.

65 Wang, Q.; Tsui, M. M. P.; Ruan, Y.; Lin, H.; Zhao, Z.; Ku, J. P. H.; Sun, H.; Lam, P. K. S. Occurrence and Distribution of Per- and Polyfluoroalkyl Substances (PFAS) in the Seawater and Sediment of the South China Sea Coastal Region. *Chemosphere* **2019**, *231*, 468–477. https: //doi.org/10.1016/j.chemosphere.2019.05.162.

66 Li, Z.; Lyu, X.; Gao, B.; Xu, H.; Wu, J.; Sun, Y. Effects of Ionic Strength and Cation Type on the Transport of Perfluorooctanoic Acid (PFOA) in Unsaturated Sand Porous Media. *J. Hazard. Mater.* **2021**, *403* (November 2019). https: //doi.org/10.1016/j.jhazmat.2020.123688.

67 Lyu, X.; Li, Z.; Wang, D.; Zhang, Q.; Gao, B.; Sun, Y.; Wu, J. Transport of Perfluorooctanoic Acid in Unsaturated Porous Media Mediated by SDBS. *J. Hydrol.* **2022**, *607* (June 2021), 127479. https: //doi.org/10.1016/j.jhydrol.2022.127479.

68 Le, S. T.; Gao, Y.; Kibbey, T. C. G.; Glamore, W. C.; O'Carroll, D. M. A New Framework for Modeling the Effect of Salt on Interfacial Adsorption of PFAS in Environmental Systems. *Sci. Total Environ.* **2021**, *796*, 148893. https: //doi.org/10.1016/j.scitotenv.2021.148893.

69 Guédon, G. R.; Hyman, J. D. H.; Inzoli, F.; Riva, M.; Guadagnini, A. Influence of Capillary End Effects on Steady-State Relative Permeability Estimates from Direct Pore-Scale Simulations. *Phys. Fluids* **2017**, *29* (12). https: //doi.org/10.1063/1.5009075.

70 Li, Y.; Wang, S.; Kang, Z.; Yuan, Q.; Xue, X.; Yu, C.; Zhang, X. Research on the Correction Method of the Capillary End Effect of the Relative Permeability Curve of the Steady State. *Energies* **2021**, *14* (15), 1–15. https: //doi.org/10.3390/en14154528.

71 Jiang, Y.; Geng, T.; Li, Q.; Li, G.; Ju, H. Influences of Temperature, PH and Salinity on the Surface Property and Self-Assembly of 1:1 Salt-Free Catanionic Surfactant. *J. Mol. Liq.* **2014**, *199*, 1–6. https: //doi.org/10.1016/j.molliq.2014.07.045.

72 Stults, J. F.; Choi, Y. J.; Schaefer, C. E.; Illangasekare, T. H.; Higgins, C. P. Estimation of Transport Parameters of Perfluoroalkyl Acids (PFAAs) in Unsaturated Porous Media: Critical Experimental and Modeling Improvements. *Environ. Sci. Technol.* **2022**. https: //doi.org/10.1021/acs.est.2c00819.

73 Lebeau, M.; Konrad, J. M. A New Capillary and Thin Film Flow Model for Predicting the Hydraulic Conductivity of Unsaturated Porous Media. *Water Resour. Res.* **2010**, *46* (1), 1–16. https: //doi.org/10.1029/2010WR009092.

74 Ruan, H.; Illangasekare, T. H. Estimation of Relative Hydraulic Conductivity of Sandy Soils Based on a Sheet Flow Model. *J. Hydrol.* **1999**, *219* (1–2), 83–93. https: //doi.org/10.1016/S0022-1694(99)00047-5.

75 Brusseau, M. L.; Peng, S.; Schnaar, G.; Costanza-Robinson, M. S. Relationships among Air-Water Interfacial Area, Capillary Pressure, and Water Saturation for a Sandy Porous Medium. *Water Resour. Res.* **2006**, *42* (3), 1–5. https: //doi.org/10.1029/2005WR004058.

76 Brusseau, M. L.; Peng, S.; Schnaar, G.; Murao, A. Measuring Air-Water Interfacial Areas with X-Ray Microtomography and Interfacial Partitioning Tracer Tests. *Environ. Sci. Technol.* **2007**, *41* (6), 1956–1961. https: //doi.org/10.1021/es061474m.

77 Stammers, W. The Steady State Flow of Water Through Unsaturated Soil In The Low Capillary Potential Region, Oregon State University, 1965.

78 Velásquez-Parra, A.; Aquino, T.; Willmann, M.; Méheust, Y.; Le Borgne, T.; Jiménez-Martínez, J. Sharp Transition to Strongly Anomalous Transport in Unsaturated Porous Media. *Geophys. Res. Lett.* **2022**, *49* (3). https: //doi.org/10.1029/2021gl096280.

79 Pedregosa, F.; Varoquaux, G.; Gramfort, A.; Michel, V.; Thirion, B.; Grisel, O.; Blondel, M.; Prettenhofer, P.; Weiss, R.; Dubourg, V.; et al. Scikit-Learn: Machine Learning in Python. *J. Mach. Learn. Res.* **2011**, *12*, 2825–2830.

80 Le, S. T.; Kibbey, T. C. G.; Weber, K. P.; Glamore, W. C.; O'Carroll, D. M. A Group-Contribution Model for Predicting the Physicochemical Behavior of PFAS Components for Understanding Environmental Fate. *Sci. Total Environ.* **2021**, *764*, 142882. https: //doi.org/10.1016/j.scitotenv.2020.142882.

81 Guo, B.; Zeng, J.; Brusseau, M. L. A Mathematical Model for the Release, Transport, and Retention of Per- and Polyfluoroalkyl Substances (PFAS) in the Vadose Zone. *Water Resour. Res.* **2020**, *56* (2), 1–25. https: //doi.org/10.1029/2019WR026667.

82 Zeng, J.; Guo, B. Multidimensional Simulation of PFAS Transport and Leaching in the Vadose Zone: Impact of Surfactant-Induced Flow and Subsurface Heterogeneities. *Adv. Water Resour.* **2021**, *155* (February), 104015. https: //doi.org/10.1016/j.advwatres.2021.104015.

83 Sprenger, M.; Seeger, S.; Blume, T.; Weiler, M. Travel Times in the Vadose Zone: Variability in Space and Time. *Water Resour. Res.* **2016**, *52* (8), 5727–5754. https: //doi.org/10.1002/2015WR018077.

84 Wittenberg, H.; Aksoy, H.; Miegel, K. Fast Response of Groundwater to Heavy Rainfall. *J. Hydrol.* **2019**, *571* (October 2018), 837–842. https: //doi.org/10.1016/j.jhydrol.2019.02.037.

85 Brusseau, M. L.; Guo, B. Air-Water Interfacial Areas Relevant for Transport of per and Poly-Fluoroalkyl Substances. *Water Res.* **2021**, *207* (July), 117785. https: //doi.org/10.1016/j.watres.2021.117785.

86 Wegrzyńska, J.; Para, G.; Chlebicki, J.; Warszyński, P.; Wilk, K. A. Adsorption of Multiple Ammonium Salts at the Air/Solution Interface. *Langmuir* **2008**, *24* (7), 3171–3180. https: //doi.org/10.1021/la702619a.

87 Schaefer, C. E.; Nguyen, D.; Meng, P.; Fang, Y.; Knappe, D. R. U. Sorption of Perfluoroalkyl Ether Carboxylic Acids (PFECAs) at the Air-Water Interface in Porous Media: Modeling Perspectives. *J. Hazard. Mater. Adv.* **2022**, *3* (4), 100062. https: //doi.org/10.1016/j.hazadv.2022.100062.

88 Schaefer, C. E.; Lavorgna, G. M.; Lippincott, D. R.; Nguyen, D.; Christie, E.; Shea, S.; O'Hare, S.; Lemes, M. C. S.; Higgins, C. P.; Field, J. A Field Study to Assess the Role of Air-Water Interfacial Sorption on PFAS Leaching in an AFFF Source Area. *J. Contam. Hydrol.* **2022**, 104001. https: //doi.org/10.1016/j.jconhyd.2022.104001.

List of Publications

Schaefer, C., Culina, V., Nguyen, D., and Field, J. **2019**. Uptake of Poly- and Perfluoroalkyl Substances at the Air-Water Interface. *Environmental Science & Technology*, 53 (21): 12442-12448. DOI: https: //doi.org/10.1021/acs.est.9b04008.

Kostarelos, K., Sharma, P., Christie, E., Wanzek, T., and J. Field. **2021**. Viscous Microemulsions of Aqueous Film Forming Foam (AFFF) and Jet Fuel A Inhibit Infiltration and Subsurface Transport. *Environmental Science & Technology Letters,* 8 (2): 142-147 DOI: 10.1021/acs.estlett.0c00868

Stultz, J, Illangasakare, T., and C.P. Higgins. **2021**. The Mass Transfer Index (MTI): A Semi-Empirical Approach for Quantifying Transport of Solutes in Variably Saturated Porous Media. *Journal of Contaminant Hydrology, 242,* DOI: 10.1016/j.jconhyd.2021.103842

Stults, J., Choi, Y.J., Schaefer, C., Illangasekare, T., Higgins, C. **2022**. Estimation of Transport Parameters of Per- and Polyfluorinated Alkyl Substances (PFASs) in Unsaturated Porous Media: Critical Experimental and Modelling Improvements, *Environmental Science Technology* 2022, 56, 12, 7963–7975. https://doi.org/10.1021/acs.est.2c00819

Stults, J., Choi, Y.J., Rockwell, C., Schaefer, C., Nguyen, D., Knappe, D., Illangasekare, T., Higgins, C. Submitted Predicting Concentration and Electrolyte Dependent Air-Water Interfacial Partitioning Parameters of PFASs Using Quantitative Structural Property Relationships (QSPRs) *Environ. Sci. Technol.*

Stults, J., Choi, Y.J., Illangasekare, T., Higgins, C. *(In Preparation)* Non-Fickian Transport Induces Rate-Limited Air-Water Interfacial Partitioning of PFAAs in the Vadose Zone

Wanzek, T., Stults, J. F., Johnson, M.G., Field, J.A.. and Kleber, M. (*In preparation*) Predicting PFAS retention in AFFF impacted soil requires joint consideration of sorbate and matrix properties.

Conference or Symposium Abstracts

Stults, J., Illangasekare, T., Higgins, C (2019, Dec. 9th-13th). "The Study of PFAS mobility and retention in unsaturated soils using column tests with x-ray attenuation and liquid chromatography quadrupole time-of-flight mass spectrometry (LC QTOF-MS)." Presented at the American Geophysical Union Conference. https://ui.adsabs.harvard.edu/abs/2019AGUFMGH11B1039S/abstract

Pushpesh Sharma, Konstantinos Kostarelos, Thomas Wanzek, Emerson Christie, and Jennifer Field. "CMC, Foaming, and Phase Behavior Properties of AFFFs: Implications for PFAS Fate and Transport". Battelle **2020** Chlorinated Conference. Abstract Accepted. Note: conference was postponed until 2021 due to COVID 19, and then cancelled.

Stults, J., Illangasekare, T., Higgins, C. (2022, Mar. 20th-24th). "Predicting Concentration Dependent Air-Water Interfacial Partitioning Parameters of PFASs with Multiparametric Computational Models." Presented at The American Chemical Society Spring Meeting. https://acs.digitellinc.com/acs/sessions/446721/view

Stults, J., Illangasekare, T., Higgins, C. (2022, Oct. 4th-6th). "Development of a Quasi-Saturated Column Method for Measuring the Multi-Phase Partitioning of PFASs Absent Non-Fickian Transport Effects." Presented at the RemTec & Emerging Contaminants Summit.

Wanzek, T., Field, J.A., and Kleber, M. PFAS Summit (April 2022) "Identifying the Mechanisms of PFAS (anionic and zwitterionic) sorption to soil horizons" PFAS Summit, Tubeingen Germany [InvitedSpeaker]

Wanzek, T and Field, J.A. SERDP 2022 (July 2022*) Mechanistic Understanding of PFAS in Source Zonesm, San Pedro, CA*

Wanzek, T. and Field, J.A. SERDP Webinar August 2022 "Mechanistic Understanding of PFAS in Source Zones"

Pushpesh Sharma; Konstantinos Kostarelos, Thomas Wanzek, Emerson Christie, and Jennifer Field. "Unlocking PFAS retention mechanisms: LPME and LPmix formation provides a key". Abstract submitted to 9th International Congress on Environmental Geotechnics. (ICEG2023-284; under review).

Pushpesh Sharma, Konstantinos Kostarelos, and Jennifer Field. "CMC, Foaming, and Phase Behavior Properties of AFFFs: Implications for PFAS Fate and Transport". Abstract submitted to 9th International Congress on Environmental Geotechnics. (ICEG2023-283; under review).

—END OF DOCUMENT—